Symmetry-Informed Geometric Representation for Molecules, Proteins, and Crystalline Materials

Shengchao Liu[1,2], **Weitao Du**[3], **Yanjing Li**[4], **Zhuoxinran Li**[5], **Zhiling Zheng**[6], **Chenru Duan**[7], **Zhiming Ma**[3], **Omar Yaghi**[6], **Anima Anandkumar**[8], **Christian Borgs**[6], **Jennifer Chayes**[6], **Hongyu Guo**[9], **Jian Tang**[1,10,11]

[1]Mila - Québec Artificial Intelligence Institute [2]Université de Montréal
[3]University of Chinese Academy of Sciences [4]Carnegie Mellon University
[5]University of Toronto [6]University of California, Berkeley [7]Massachusetts Institute of Technology
[8]California Institute of Technology [9]National Research Council Canada
[10]HEC Montréal [11]CIFAR AI Chair
[#]Correspondence: *shengchao.liu@umontreal.ca, jian.tang@hec.ca*

Abstract

Artificial intelligence for scientific discovery has recently generated significant interest within the machine learning and scientific communities, particularly in the domains of chemistry, biology, and material discovery. For these scientific problems, molecules serve as the fundamental building blocks, and machine learning has emerged as a highly effective and powerful tool for modeling their geometric structures. Nevertheless, due to the rapidly evolving process of the field and the knowledge gap between science (*e.g.*, physics, chemistry, & biology) and machine learning communities, a benchmarking study on geometrical representation for such data has not been conducted. To address such an issue, in this paper, we first provide a unified view of the current symmetry-informed geometric methods, classifying them into three main categories: invariance, equivariance with spherical frame basis, and equivariance with vector frame basis. Then we propose a platform, coined Geom3D, which enables benchmarking the effectiveness of geometric strategies. Geom3D contains 16 advanced symmetry-informed geometric representation models and 14 geometric pretraining methods over 52 diverse tasks, including small molecules, proteins, and crystalline materials. We hope that Geom3D can, on the one hand, eliminate barriers for machine learning researchers interested in exploring scientific problems; and, on the other hand, provide valuable guidance for researchers in computational chemistry, structural biology, and materials science, aiding in the informed selection of representation techniques for specific applications. The source code is available on the GitHub repository.

1 Introduction

Artificial intelligence (AI) for molecule discovery has recently seen many developments, including small molecular property prediction [13, 17, 23, 38, 66, 78, 101, 103, 104, 119, 130, 132, 135], small molecule design and optimization [6, 54, 57, 85, 137], small molecule reaction and retrosynthesis [40, 111, 116], protein property prediction [27, 141], protein folding and inverse folding [48, 64, 92], protein design [15, 41, 46, 88, 91], and crystalline material design [33, 125, 128]. One of the most fundamental building blocks for these tasks is the geometric structure of molecules. Exploring effective methods for robust representation learning to leverage such geometric information fully remains an open challenge that interests both machine learning (ML) and science researchers.

To this end, symmetry-informed geometric representation [1] has emerged as a promising approach. By leveraging physical principles (*i.e.*, group theory for depicting symmetric particles) into spatial

37th Conference on Neural Information Processing Systems (NeurIPS 2023) Track on Datasets and Benchmarks.

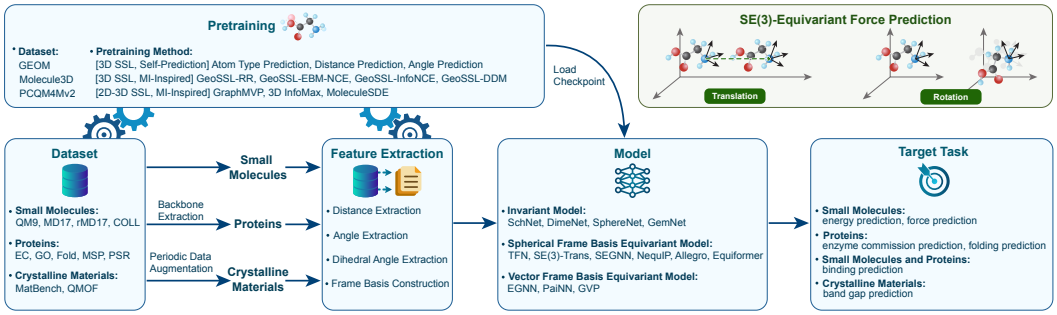

Figure 1: Pipeline for Geom3D, including dataset preprocessing, feature extraction, geometric preetraining and representation, and target tasks. We additionally demonstrate the **SE(3)-equivariant force prediction task**.

representation, they facilitate a more robust representation of small molecules, proteins, and crystalline materials. Nevertheless, pursuing geometric learning research is still challenging due to its evolving nature and the knowledge gap between science (*e.g.*, physics) and machine learning communities. These factors contribute to a substantial barrier for machine learning researchers to investigate scientific problems and hinder efforts to reproduce results consistently. To overcome this, we introduce Geom3D, a benchmarking of the geometric representation with four advantages, as follows. [1]

(1) A unified and novel aspect in understanding symmetry-informed geometric models. The molecule geometry needs to satisfy certain physical constraints regarding the 3D Euclidean space. For instance, the molecules' force needs to be equivariant to translation and rotation (see SE(3)-equivariance in Fig. 1). In this work, we classify the geometric methods into three categories: *invariant* model, SE(3)-equivariant model with *spherical frame basis* and *vector frame basis*. The invariant models only consider features that are constant w.r.t. the SE(3) group, while the two families of equivariant models can be further unified using the *frame basis* to capture equivariant symmetry. An illustration of three categories is in Fig. 2. Building equivariant models on the *frame basis* provides a novel and unified view of understanding geometric models and paves the way for intriguing more ML researchers to explore scientific problems.

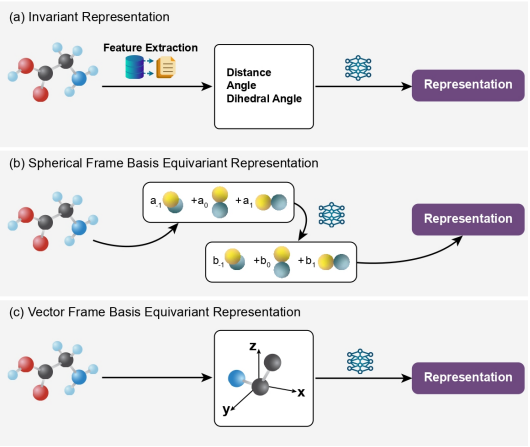

Figure 2: Three categories of geometric modules. (a) Invariant models only consider type-0 features. Equivariant models use either (b) spherical harmonics frames or (c) vector frames by projecting the coordinate vectors.

(2) A unified platform for various scientific domains. There exist multiple platforms and tools for molecule discovery, but they are (1) mainly focusing on molecule's 2D graph representation [77, 102, 145]; (2) using 3D geometry with customized data structures or APIs [3, 105]; or (3) covering only a few geometric models [76]. Thus, it is necessary to have a platform benchmarking the geometric models, especially for researchers interested in solving scientific problems. In this work, we propose Geom3D, a geometric modeling framework based on PyTorch Geometric (PyG) [31], one of the most widely-used platforms for graph representation learning. Geom3D benchmarks 16 geometric models on solving 52 scientific tasks, and these tasks include the three most fundamental molecule types: small molecules, proteins, and crystalline materials. Each of them requires distinct domain-specific preprocessing steps, *e.g.*, crystalline materials molecules possess periodic structures and thus need a particular periodic data augmentation. By leveraging such a unified framework, Geom3D serves as a comprehensive benchmarking tool, facilitating effective and consistent analysis components to interpret the existing geometric representation functions in a fair and convenient comparison setting.

(3) A framework for a wider range of ML tasks. The geometric models in Geom3D can serve as a building block for exploring extensive ML tasks, including but not limited to studying the molecule dynamic simulation and scrutinizing the transfer learning effect on molecule geometry. For example, pre-

[1] In what follows, we may use "molecule" to refer to "small molecule" for brevity.

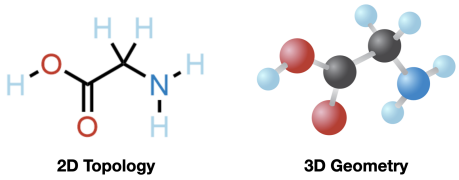

(a) An example of small molecule structure.

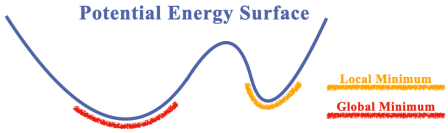

(b) An illustration of the potential energy surface.

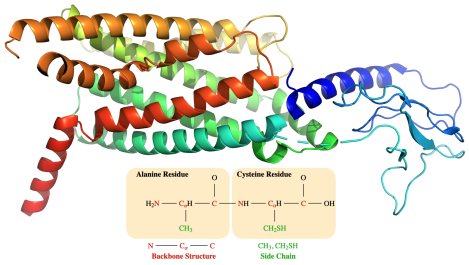

(c) An example of protein sequence and structure.

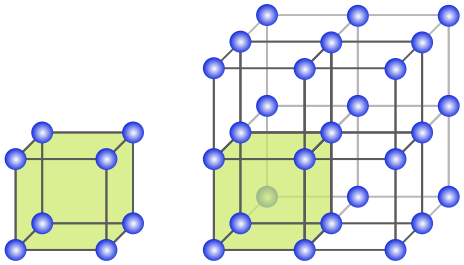

(d) An example of crystalline material.

Figure 3: Fig. 3(a) illustrates 2D topology and 3D conformation for molecule Glycine. Fig. 3(c) displays the 3D structure of protein. Fig. 3(d) shows a simple cubic crystal of the element Po. Fig. 3(b) is a demo of PES.

training is an important strategy to quickly transfer knowledge to target tasks, and recent works explore geometric pretraining on 3D conformations (including supervised and self-supervised) [59, 80, 136] and multi-modality pretraining on 2D topology and 3D geometry [30, 79, 86]. Other transfer learning venues include multi-task learning [82, 84] and out-of-distribution or domain adaptation [58, 133, 134], yet no geometry information has been utilized. All of these directions are promising for future exploration, and Geom3D serves as an auxiliary tool to accomplish them. For example, as will be shown in Sec. 4, we leverage Geom3D to effectively evaluate 14 pretraining methods with benchmarks.

(4) A framework for exploring data preprocessing and optimization tricks. When comparing different symmetry-informed geometric models, we find that in addition to the model architecture, there are two important factors affecting the performance: the data preprocessing (*e.g.*, energy and force rescaling and shift) and optimization methods (*e.g.*, learning rate, learning rate schedule, number of epochs, random seeds). In this work, we explore the effect of four preprocessing tricks and around 2-10 optimization hyperparameters for each model and task. In general, we observe that each model may benefit differently in different tasks regarding the preprocessing and optimization tricks. However, data normalization is found to help improve performance hugely in most cases. We believe that Geom3D is an effective tool for exploring and understanding various engineering tricks.

2 Data Structures for Geometric Data

Small molecule 3D conformation. Molecules are sets of points in the 3D Euclidean space, and they move in a dynamic motion, as known as the potential energy surface (PES). The region with the lowest energy corresponds to the most stable state for molecules, and molecules at these positions are called **conformations**, as illustrated in Fig. 3(b). For notation, we mark each 3D molecular graph as $\boldsymbol{g} = (\boldsymbol{X}, \boldsymbol{R})$, where $\boldsymbol{X}$ and $\boldsymbol{R}$ are for the atom types and positions, respectively.

Crystalline material with periodic structure. The crystalline materials or extended chemical structures possess a characteristic known as periodicity: their atomic or molecular arrangement repeats in a predictable and consistent pattern across all three spatial dimensions. This is the key aspect that differentiates them from small molecules. In Fig. 3(d), we show an original unit cell (marked in green) that can repeatedly compose the crystal structure along the lattice. To model such a periodic structure, we adopt the data augmentation from CGCNN [129]: for each original unit cell, we shift it along the lattice in three dimensions and connect edges within a cutoff value (hyperparameter). For more details on the two augmentation variants, please check Appendix A.

Protein with backbone structure. Protein structures can be classified into four primary levels, and the primary structure represents the linear arrangement of *amino acids*, and each amino acid is a molecule consisting of atoms. Geometric methods mainly focus on the tertiary structure, *i.e.*, the 3D geometry of each atom, encompassing the complete organization of a single protein. However,

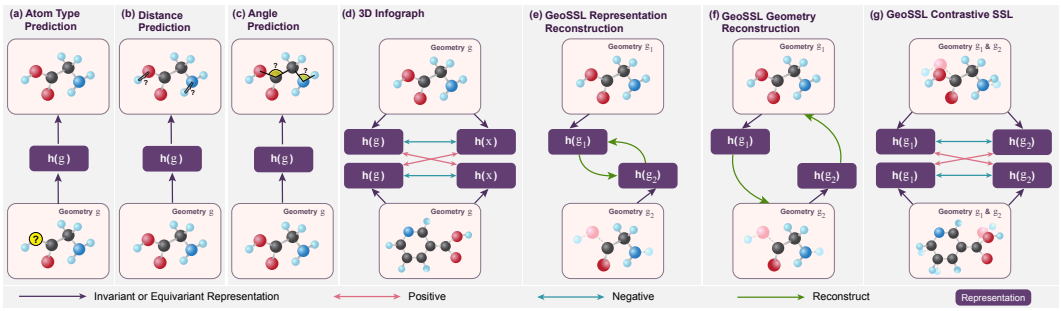

Figure 4: Pipelines for seven single-modal geometric pretraining methods. (a-c) conduct self-prediction. (d) maximizes the MI between nodes and graphs. (e-g) are GeoSSL, maximizing the MI between views $\boldsymbol{g}_1$ and $\boldsymbol{g}_2$.

atom-level modeling for proteins is consuming due to the large volume of atoms and the GPU memory limit. One solution is modeling each amino acid's *backbone structure*. The backbone structure of each amino acid is $N - C_\alpha - C$, and the C_α is bonded to the side chain. 20 common types of side chains corresponding to 20 amino acids, as illustrated in Fig. 3(c). Thus, modeling the backbone structure can balance the computational efficiency and the key geometric information.

3 Symmetry-Informed Geometric Representation

3.1 Group Symmetry and Equivariance

Symmetry means the object remains invariant after certain transformations [127], and it is everywhere on Earth, such as in animals, plants, and molecules. Formally, the set of all symmetric transformations satisfies the axioms of a group. Therefore, the group theory and its representation theory are common tools to depict such physical symmetry. **Group** is a set G equipped with a group product $\times$ satisfying:

$$(1)\ \exists \boldsymbol{e} \in G,\ \boldsymbol{a} \times \boldsymbol{e} = \boldsymbol{e} \times \boldsymbol{a}, \forall \boldsymbol{a} \in G; \quad (2)\ \boldsymbol{a} \times \boldsymbol{a}^{-1} = \boldsymbol{a}^{-1} \times \boldsymbol{a} = \boldsymbol{e}; \quad (3)\ \boldsymbol{a} \times (\boldsymbol{b} \times \boldsymbol{c}) = \boldsymbol{a} \times \boldsymbol{b} \times \boldsymbol{c}. \tag{1}$$

Group representation is a mapping from the group G to the group of linear transformations of a vector space X with dimension d (see [138] for more rigorous definition):

$$\rho_X(\cdot) : G \to \mathbb{R}^{d \times d} \qquad \text{s.t.} \quad \rho(\boldsymbol{e}) = 1 \ \wedge \ \rho_X(\boldsymbol{a})\rho_X(\boldsymbol{b}) = \rho_X(\boldsymbol{a} \times \boldsymbol{b}),\ \forall \boldsymbol{a}, \boldsymbol{b} \in G. \tag{2}$$

During modeling, the X space can be the input 3D Euclidean space, the equivariant vector space in the intermediate layers, or the output force space. This enables the definition of equivariance as below.

Equivariance is the property for the geometric modeling function $f : X \to Y$ as:

$$f(\rho_X(\boldsymbol{a})\boldsymbol{x}) = \rho_Y(\boldsymbol{a})f(\boldsymbol{x}),\ \ \forall \boldsymbol{a} \in G, \boldsymbol{x} \in X. \tag{3}$$

As displayed in Fig. 1, for molecule geometric modeling, the property should be rotation-equivariant and translation-equivariant (*i.e.*, SE(3)-equivariant). More concretely, $\rho_X(\boldsymbol{a})$ and $\rho_Y(\boldsymbol{a})$ are the SE(3) group representations on the input (*e.g.*, atom coordinates) and output space (*e.g.*, force space), respectively. SE(3)-equivariant modeling in Eq. (3) is essentially saying that the designed deep learning model f is modeling the whole transformation trajectory on the molecule conformations, and the output is the transformed $\hat{y}$ accordingly. Further, we want to highlight that, in addition to the network architecture or representation function, the input features can also be represented as an equivariant feature mapping from the 3D mesh to $\mathbb{R}^{\tilde{d}}$ [11], where $\tilde{d}$ depends on input data, *e.g.*, $\tilde{d}$ = 1 (for atom type dimension) + 3 (for atom coordinate dimension) on small molecules. Such features are called steerable features in [5, 11] when only considering the subgroup SO(3)-equivariance.

Invariance is a special type of equivariance, defined as:

$$f(\rho_X(\boldsymbol{a})\boldsymbol{x}) = f(\boldsymbol{x}),\ \ \forall \boldsymbol{a} \in G, \boldsymbol{x} \in X, \tag{4}$$

with $\rho_Y(\boldsymbol{a})$ as the identity $\forall \boldsymbol{a} \in G$. The group representation helps define the equivariance condition for f to follow. Then, the question boils down to how to design such an equivariant f. In the following, we will discuss geometric modelings from a novel and unified perspective using the frame. In the next sections, we will provide a novel and unified aspect of understanding the advanced geometric representation and pretraining methods using the frame basis (details in Appendix H).

3.2 Invariant Geometric Representation Learning

One simple way of achieving SE(3) group symmetry is invariant modeling. It means the geometric model only considers the type-0 features [112], *i.e.*, features that are invariant with respect to rotation and translation. Existing works have been adopting the invariant features for modeling, including pairwise distance (SchNet [109]), bond angles (DimeNet [68]), and torsion angles (SphereNet [89] and GemNet [67]). Note that the torsion angles are angles between two planes defined by pairwise bonds.

3.3 Equivariant Geometric Representation Learning

Invariant modeling only captures the type-0 features. However, equivariant modeling of higher-order particles may bring in extra expressiveness. For example, the elementary particles in high energy physics [98] inherit higher order symmetries in the sense of SO(3) representation theory, which makes the equivariant modeling necessary. Such higher-order particles include type-1 features like coordinates and forces in molecular conformation. There are many approaches to design such SE(3)-equivariant model satisfying Eq. (3). There are two main venues, as will be discussed below.

Spherical Frame Basis. This research line utilizes the irreducible representations [37] for building SO(3)-equivariant representations, and the first work is TFN [112]. Its main idea is to project the 3D Euclidean coordinates into the spherical harmonics space, which transforms equivariantly according to the irreducible representations of SO(3), and the translation-equivariant can be trivially guaranteed using the relative coordinates. Following this, there have been variants combining it with the attention module (Equiformer [73]) or with more expressive network architectures (SEGNN [4], Allegro [95]).

Vector Frame Basis. An alternative philosophy of equivariant modeling utilizes the vector (in physics) frame basis. It constructs three vectors bases, serving as a reference frame to help locate the vectors in each corresponding local environment. Works along this line for molecule discovery include DeePMD [140] for dynamics simulation, 3D-EMGP [59] and MoleculeSDE [79] for geometric pretraining, and ClofNet [20] for conformation generation. For macromolecules like protein, the equivariant vector frame has been used for protein design (StructTrans [53]) and protein folding (AlphaFold2 [64]). We also want to highlight that, from a mathematical perspective, equivariance and invariance can be transformed to each other by the scalarization technique. Please check [49] for details.

The spherical frame basis can be easily extended to higher-order particles, yet it may suffer from the high computational cost. On the other hand, the vector frame basis is specifically designed for the 3D point clouds; thus, it is more efficient but cannot generalize to higher-order particles. Meanwhile, we would like to acknowledge other equivariant modeling paradigms, including using orbital features [99] and elevating 3D Euclidean space to SE(3) group [32, 52]. Please check Appendix F for details.

3.4 Geometric Pretraining

Recent studies have started to explore **single-modal of geometric pretraining** on molecules. The GeoSSL paper [80] covers a wide range of geometric pretraining algorithms. The type prediction, distance prediction, and angle prediction predict the masked atom type, pairwise distance, and bond angle, respectively. The 3D InfoGraph predicts whether the node- and graph-level 3D representation are for the same molecule. GeoSSL is a novel geometric pretraining paradigm that maximizes the mutual information (MI) between the original conformation $\boldsymbol{g}_1$ and augmented conformation $\boldsymbol{g}_2$, where $\boldsymbol{g}_2$ is obtained by adding small perturbations to $\boldsymbol{g}_1$. RR, InfoNCE, and EBM-NCE optimize the objective in the latent representation space, either generative or contrastive. GeoSSL-DDM [80, 136] optimizes the same objective function using denoising score matching. 3D-EMGP [60] has the same strategy and utilizes an equivariant module to denoise the 3D noise directly. Another research line is the **multi-modal of topological and geometric pretraining**. GraphMVP [86] first proposes one contrastive objective (EBM-NCE) and one generative objective (VRR) to optimize the MI between the 2D topologies and 3D geometries in the representation space. 3D InfoMax [114] is a special case of GraphMVP, with the contrastive part only. MoleculeSDE [79] extends GraphMVP by introducing two SDE models for solving the 2D and 3D reconstruction. We illustrate these algorithms in Figs. 4 and 8.

3.5 Discussion: Reflection-antisymmetric in Geometric Learning

Till now, we have discussed the SE(3)-equivariance, *i.e.*, the translation and rotation equivariance. As highlighted in the recent work [61, 79], the molecules needlessly satisfy the reflection-equivariant,

Table 1: Results of 26 models on 12 quantum mechanics prediction tasks in QM9, with 110K for training, 10K for validation, and 11K for testing. The task unit is specified, and the evaluation is the mean absolute error (MAE).

Featurization	Model	$\alpha \downarrow$ a_0^3	$\nabla\mathcal{E} \downarrow$ meV	$\mathcal{E}_{\text{HOMO}} \downarrow$ meV	$\mathcal{E}_{\text{LUMO}} \downarrow$ meV	$\mu \downarrow$ D	$C_v \downarrow$ $\frac{cal}{mol \cdot K}$	$G \downarrow$ meV	$H \downarrow$ meV	$R^2 \downarrow$ a_0^2	$U \downarrow$ meV	$U_0 \downarrow$ meV	ZPVE $\downarrow$ meV
1D FPs	MLP	2.231	196.72	131.27	164.94	0.526	0.919	2158.64	2358.23	68.621	2340.61	2314.77	155.921
	RF	3.801	207.02	165.72	183.04	0.534	1.485	3391.79	3729.94	94.512	3705.75	3678.25	253.132
	XGB	2.748	199.71	139.88	165.43	0.516	1.062	2563.93	2804.27	82.959	2786.28	2769.29	180.989
1D SMILES	CNN	0.364	165.22	124.65	114.81	0.566	0.173	156.66	170.59	20.403	166.18	169.89	10.070
	BERT	0.313	117.50	84.93	98.88	0.446	0.176	170.01	183.43	18.002	183.84	188.60	13.410
1D SELFIES	CNN	0.345	157.04	115.51	113.00	0.499	0.168	136.42	146.56	20.080	143.00	140.01	10.149
	BERT	0.348	123.11	91.15	90.80	0.461	0.203	168.20	187.50	19.125	204.93	195.98	17.328
2D Graph	GCN	1.338	145.82	96.21	106.66	0.434	0.526	1198.12	1291.57	37.585	1281.03	1303.39	85.103
	ENN-S2S	1.401	270.59	129.18	132.84	0.577	0.760	1487.21	955.24	34.609	1800.79	1521.32	51.226
	GraphSAGE	1.601	131.45	88.78	93.21	0.402	0.544	1473.42	1617.73	38.112	1553.01	1565.65	95.344
	GAT	1.132	135.90	94.70	98.52	0.406	0.291	911.82	991.31	26.583	1161.29	592.67	55.061
	GIN	1.165	175.82	90.66	110.74	0.539	0.691	848.24	1090.36	35.110	1498.23	1364.18	108.331
	D-MPNN	0.568	118.42	85.01	86.20	0.441	0.241	423.14	458.39	24.816	470.01	445.91	29.291
	PNA	0.681	148.88	88.72	97.31	0.361	0.409	664.98	692.74	23.855	616.70	694.92	57.217
	Graphormer	2.836	79.27	54.24	52.42	0.330	0.080	2066.28	2546.01	131.158	2229.88	2525.51	144.595
	AWARE	0.297	144.91	133.89	98.86	0.602	0.129	86.62	94.47	22.180	93.59	95.73	5.275
	GraphGPS	0.209	75.98	54.75	54.53	0.288	0.089	528.50	693.19	12.488	296.00	411.16	49.888
3D Graph	SchNet	0.060	44.13	27.64	22.55	0.028	0.031	14.19	14.05	0.133	13.93	13.27	1.749
	DimeNet++	0.044	36.22	20.01	16.66	0.028	**0.022**	**7.45**	**6.14**	0.323	**6.33**	7.18	**1.118**
	SE(3)-Trans	0.137	56.52	34.65	34.41	0.050	0.063	65.28	70.70	1.747	68.92	68.88	5.428
	EGNN	0.062	49.56	30.08	24.98	0.029	0.030	10.01	9.14	**0.089**	9.28	9.08	1.519
	PaiNN	0.049	42.73	24.46	20.16	0.016	0.025	8.43	7.88	0.169	8.18	7.63	1.419
	GemNet-T	**0.041**	35.46	17.85	**15.86**	0.021	0.023	7.61	7.08	0.271	6.42	**5.88**	1.232
	SphereNet	0.047	38.93	21.45	18.25	0.027	0.025	8.16	13.68	0.288	6.77	7.43	1.295
	SEGNN	0.048	33.61	**17.66**	17.01	0.021	0.026	11.60	12.45	0.404	11.29	12.20	1.590
	Allegro	0.097	102.44	61.86	63.17	0.176	0.032	42.08	44.96	1.977	44.64	44.43	2.949
	NequIP	0.066	61.94	42.00	31.64	0.036	0.028	22.08	23.36	0.415	23.23	23.02	1.899
	Equiformer	0.051	**33.46**	17.93	16.85	**0.015**	0.023	14.49	14.60	0.433	14.88	13.78	2.342

but instead, they should be reflection-antisymmetric [79]. One classic example is that the energy of small molecules is reflection-antisymmetric in a binding system. Each of the two equivariant categories discussed in Sec. 3.3 can solve this problem easily. The spherical frame basis can achieve this by adding the reflection into the Wigner-D matrix [4], and the vector frame basis can accomplish this using the cross-product during frame construction [79].

4 Geometric Datasets and Benchmarks

In Sec. 3, we introduce a novel aspect for understanding symmetry-informed geometric models. In this section, we discuss utilizing Geom3D framework for benchmarking 16 geometric models over 52 tasks. For the detailed dataset acquisitions and task specifications (*e.g.*, *dataset size*, *splitting*, and *task unit*), please check Appendix B. Geom3D also covers 7 1D models and 10 2D graph neural networks (GNNs) and benchmarks the 14 pretraining algorithms to learn a robust geometric representation. Additionally, we want to highlight Geom3D enables exploration of important data preprocessing and optimization tricks for performance improvement, as will be introduced next.

4.1 Small Molecules: QM9

QM9 [100] is a dataset consisting of 134K molecules, each with up to 9 heavy atoms. It includes 12 tasks that are related to the quantum properties. For example, U0 and U298 are the internal energies at temperatures of 0K and 298.15K, respectively. On the QM9 dataset, we can easily get the 1D descriptors (Fingerprints/FPs [106], SMILES [126], SELFIES [70]), 2D topology, and 3D conformation. This enables us to build models on each of them respectively: (1) We benchmark 7 models on 1D descriptors, including multi-layer perception (MLP), random forest (RF), XGBoost (SGB), convolution neural networks (CNN), and BERT [18]. (2) We benchmark 10 2D GNN models on the molecular topology, including GCN [23, 66], ENN-S2S [38], GraphSAGE [43], GAT [119], GIN [130], D-MPNN [132], PNA [13], Graphormer [135], AWARE [17], GraphGPS [101]. (3) We benchmark 11 3D geometric models on the molecular conformation, including SchNet [109], DimeNet++ [68], SE(3)-Trans [35], EGNN [108], PaiNN [110], GemNet-T [67], SphereNet [89], SEGNN [4], Allegro [95], NequIP [3], Equiformer [73]. The evaluation metric is the mean absolute error.

The results of these 28 models are in Table 1, and two important insights are observed: (1) There is no one universally best geometric model, yet DimeNet++, PaiNN, GemNet, and Equiformer perform well in most tasks. However, PaiNN takes less than 20 GPU hours, and the other three models take up to 5 GPU days per task. (2) The geometric conformation is important for quantum property prediction. The performance of 3D models is better than all the 1D and 2D models *by orders of magnitudes*.

Table 2: Results on 6 energy ($\frac{kcal}{mol}$) and force ($\frac{kcal}{mol \cdot Å}$) prediction tasks in MD17 and rMD17 (w/o normalization), and the metric is the mean absolute error (MAE). The data split and complete results are in Appendices B and I.

Model	Energy /Force	MD17						rMD17					
		Aspirin ↓	Ethanol ↓	Malonaldehyde ↓	Naphthalene ↓	Salicylic ↓	Toluene ↓	Aspirin ↓	Ethanol ↓	Malonaldehyde ↓	Naphthalene ↓	Salicylic ↓	Toluene ↓
SchNet	Energy	0.475	0.109	0.300	0.167	0.212	0.149	0.534	1.757	0.260	0.124	2.618	0.119
	Force	1.203	0.386	0.794	0.587	0.826	0.568	1.243	0.449	0.862	0.587	0.878	0.574
DimeNet++	Energy	4.168	1.238	1.385	1.846	2.445	1.484	2.438	1.456	2.317	1.648	1.555	1.210
	Force	7.212	0.753	1.842	8.515	1.752	1.037	2.009	1.213	7.029	0.629	0.934	0.921
EGNN	Energy	17.892	0.436	0.896	12.177	6.964	4.051	17.35	0.402	0.534	12.164	7.794	15.021
	Force	3.042	0.924	1.566	1.136	1.177	1.202	3.825	0.989	1.334	1.183	1.571	1.165
PaiNN	Energy	27.626	**0.063**	**0.102**	0.622	0.371	0.165	30.156	1.17	**0.070**	5.297	5.219	0.045
	Force	0.572	0.230	0.338	0.132	0.288	0.141	0.573	0.316	0.377	0.161	0.321	0.231
GemNet-T	Energy	0.684	4.598	4.966	0.482	**0.128**	**0.098**	5.389	1.615	9.496	0.031	21.411	959.745
	Force	0.558	0.219	0.433	0.212	0.326	0.174	0.555	0.233	0.337	0.154	0.371	0.400
SphereNet	Energy	**0.244**	1.603	1.559	0.167	0.188	0.113	**0.304**	0.072	0.138	0.093	0.771	20.479
	Force	0.546	0.168	0.667	0.315	0.479	0.194	0.622	0.217	0.500	0.279	2.088	0.254
SEGNN	Energy	17.774	0.151	0.247	0.655	2.173	0.624	15.721	0.13	0.182	1.11	1.494	0.814
	Force	9.003	0.893	1.249	0.895	2.220	1.138	8.549	0.846	1.185	0.926	2.056	1.241
NequIP	Energy	8.333	0.971	2.293	1.032	2.952	1.303	9.618	0.936	2.313	2.089	3.302	1.306
	Force	23.769	5.832	12.099	5.247	14.048	6.8	22.904	6.027	12.372	5.529	15.693	7.094
Allegro	Energy	1.138	0.258	1.33	0.824	1.114	0.441	1.366	1.002	0.417	1.756	1.035	0.437
	Force	3.405	1.412	4.191	3.743	4.934	1.968	3.186	2.799	2.125	3.815	4.781	2.048
Equiformer	Energy	0.308	0.096	0.183	**0.097**	0.189	0.209	0.375	0.064	0.085	**0.069**	**0.143**	**0.104**
	Force	**0.286**	**0.142**	**0.230**	**0.068**	**0.200**	**0.080**	**0.305**	**0.162**	**0.240**	**0.070**	**0.218**	**0.077**

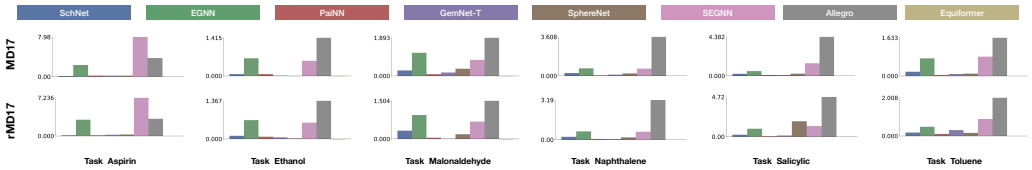

Figure 5: Ablation study on the effect of data normalization. Here are visualizations on performance differences on 6 tasks and 2 datasets, with MAE(force pred w/o normalization) - MAE(force pred w/ normalization).

4.2 Small Molecules: MD17 and rMD17

MD17 [8] is a dataset of molecular dynamics simulation. It has 8 tasks corresponding to eight organic molecules, and each task includes the molecule positions along the PES (see Fig. 3(b)). The goal is to predict each atom's energy and interatomic forces for each molecule's position. We follow the literature [68, 89, 109, 110] of using 8 subtasks, 1K for training and 1K for validation, while the test set (from 48K to 991K) is much larger. However, the MD17 dataset contains non-negligible numerical noises [9], and it is corrected by the revised MD17 (rMD17) dataset [10]. 100K structures were randomly chosen for each task/molecule in MD17, and the single-point force and energy calculations were performed for each structure using the PBE/def2-SVP level of theory. The calculations were conducted with tight SCF convergence and a dense DFT integration grid, significantly minimizing the computational noises.

The results on MD17 and rMD17 are in Table 2. We select 12 tasks for illustration, and more comprehensive results can be found in Appendix I. We can observe that, in general, PaiNN, GemNet and Equiformer perform well on MD17 and rMD17 tasks. We also report **ablation study on data normalization**. NequIP [3] and Allegro [95] introduce a normalization trick: multiplying the predicted energy with the mean of ground-truth force (reproduced results in Appendix J). We plot the performance gap, MAE(w/o normalization) - MAE(w/ normalization), in Fig. 5, and observe most of the gaps are positive, meaning that adding data normalization can lead to generally better performance.

4.3 Small Molecules: COLL

The COLL dataset [36] comprises energy and force data for 140K random snapshots obtained from molecular dynamics simulations of molecular collisions. These simulations were conducted using the semiempirical GFN2-xTB method. To obtain the data, DFT calculations were performed utilizing the revPBE functional and def2-TZVP basis set, which also incorporated D3 dispersion corrections. The task is to predict the energy and force for each atom in the molecule, and we consider 10 advanced geometric models for benchmarking. The results are in Table 3, and GemNet, SphereNet, and Equiformer reach more optimal performance.

Table 3: Results on energy and force prediction in COLL. 120k for training, 10k for val, 9.48k for test. The metric is the mean absolute error (MAE).

Model	Energy (eV) ↓	Force (eV/Å) ↓
SchNet	0.178	0.130
DimeNet++	0.036	0.049
EGNN	1.808	0.234
PaiNN	0.030	0.052
GemNet-T	**0.017**	**0.028**
SphereNet	0.032	0.047
SEGNN	7.085	0.642
NequIP	0.120	0.113
Allegro	0.161	0.130
Equiformer	0.036	0.030

Table 4: Results on 2 binding affinity prediction tasks. We select three evaluation metrics for LBA: the root mean squared error (RMSD), the Pearson correlation (R_p) and the Spearman correlation (R_S). LEP is a binary classification task, and we use the area under the curve for receiver operating characteristics (ROC) and precision-recall (PR) for evaluation. We run cross-validation with 5 seeds, and the mean and std are reported.

Model	LBA			LEP	
	RMSD ↓	R_P ↑	R_C ↑	ROC ↑	PR ↑
SchNet	1.521 ± 0.02	0.474 ± 0.01	0.452 ± 0.01	0.450 ± 0.03	0.379 ± 0.03
DimeNet++	1.672 ± 0.09	0.550 ± 0.01	0.556 ± 0.01	0.590 ± 0.06	0.496 ± 0.05
EGNN	1.494 ± 0.04	0.503 ± 0.04	0.483 ± 0.05	**0.657 ± 0.05**	**0.559 ± 0.05**
PaiNN	**1.434 ± 0.02**	0.583 ± 0.02	**0.580 ± 0.02**	0.585 ± 0.02	0.432 ± 0.03
GemNet-T	–	–	–	0.659 ± 0.05	0.506 ± 0.05
SphereNet	1.581 ± 0.02	0.538 ± 0.01	0.529 ± 0.01	0.523 ± 0.04	0.432 ± 0.05
SEGNN	1.416 ± 0.03	0.566 ± 0.02	0.550 ± 0.02	0.574 ± 0.03	0.485 ± 0.03
NequIP	1.606 ± 0.02	0.537 ± 0.01	0.520 ± 0.01	0.538 ± 0.12	0.481 ± 0.07
Allegro	1.567 ± 0.02	0.547 ± 0.00	0.534 ± 0.00	0.627 ± 0.04	0.525 ± 0.03
Equiformer	1.392 ± 0.03	**0.598 ± 0.02**	0.578 ± 0.02	0.618 ± 0.06	0.510 ± 0.05

Table 5: Results on 10 protein tasks from six datasets: ECSingle, ECMultiple, Fold (Fold, Sup., Fam.), GO (MF, BP, CC), MSP, and PSR. The evaluation metrics are Accuracy (ACC, %), F_{max} (definition in Appendix B), ACC, F_{max}, receiver operating characteristics (ROC), and Spearman's ρ, respectively.

	ECSingle	ECMultiple	Fold			GO			MSP	PSR	
			Fold	Sup.	Fam.	MF	BP	CC			
	ACC ↑	F_{max} ↑	ACC ↑	ACC ↑	ACC ↑	F_{max} ↑	F_{max} ↑	F_{max} ↑	ROC ↑	Global ρ ↑	Mean ρ ↑
IEConv	–	–	45.0	69.7	98.9	–	–	–	–	–	–
GVP-GNN	65.5	0.712	34.8	52.7	95.0	0.476	0.312	0.389	0.574	0.744	0.302
GearNet	78.8	0.799	29.1	43.1	95.9	0.477	0.283	0.373	–	–	–
ProNet	86.4	0.823	52.7	70.3	99.3	0.559	0.367	0.414	0.634	**0.818**	0.462
CDConv	**86.9**	**0.862**	**60.0**	**79.9**	**99.5**	**0.649**	**0.435**	**0.450**	**0.717**	0.817	**0.500**

4.4 Small Molecules & Proteins Binding: LBA & LEP

The binding affinity measures the strength of the binding interaction between a small molecule (ligand) to the target protein. In Geom3D, we consider modeling both the ligands and proteins with their 3D structures. During binding, a cavity in a protein can potentially possess suitable properties for binding a small molecule, and it is called a pocket [113]. Due to the large volume of protein, Geom3D follows existing works [118] by only taking the binding pocket instead of the whole protein structure. Specifically, Geom3D models up to 600 atoms for each ligand and protein pair. For the benchmarking, we consider two binding affinity tasks. (1) The first task is ligand binding affinity (LBA) [123]. It is gathered from [124], and the task is to predict the binding affinity strength between a ligand and a protein pocket. (2) The second task is ligand efficacy prediction (LEP) [34]. The input is a ligand and both the active and inactive conformers of a protein, and the goal is to classify whether or not the ligand can activate the protein's function. The results on two binding tasks are in Table 4, and we can observe that PaiNN, SEGNN, and Equiformer are generally outstanding on the two tasks.

4.5 Proteins: ECSingle, ECMultiple, Fold, GO, MSP, and PSR

ECSingle is a classification task [45] that classifies 37K proteins into 384 four-level Enzyme Commission (EC) types. This task aims to recognize the fundamental role of proteins as bio-catalysts or enzymes, which are essential in facilitating biological reactions. The EC numbering system [63] serves as a comprehensive numerical classification scheme, systematically organizing the varied functionalities of enzymes and providing a structured approach to understanding their biological roles.

ECMultiple is a multi-label classification task proposed by Gligorijevic et al. [39], where 19K proteins are associated with 538 distinct EC categories, including both three-level and four-level types and a single protein can be concurrently labeled with several three-level or four-level EC numbers.

Fold is a task classifying 16K proteins into 1,195 fold patterns [47, 74]. It is an important biological task in predicting the 3D structures from 1D amino acid sequences. We further consider three testsets (Fold, Superfamily, and Family) based on the sequence and structure similarity [94].

GO (Gene Ontology) is a dataset [39] with 36K proteins for GO term classification, where the GO term provides a consistent description of gene product attributes across species and databases [12]. Concretely, each protein contains up to three types of GO terms, corresponding to three types of classification tasks: (1) Molecular Function (MF) has 489 classes; (2) Biological Process (BP) has 1,943

Table 6: Results on the 8 tasks from MatBench and 1 task from QMOF (with optimal DA). The data split and task unit are in Appendix B, and the metric is the mean absolute error (MAE).

Model	MatBench								QMOF
	Per. $E_{\text{form}}\downarrow$ 18,928	Dielectric $\downarrow$ 4,764	$log_{10}G\downarrow$ 10,987	$log_{10}K\downarrow$ 10,987	$E_{\text{exfo}}\downarrow$ 636	Phonons $\downarrow$ 1,265	Band Gap $\downarrow$ 106,113	$E_{\text{form}}\downarrow$ 132,752	Band Gap $\downarrow$ 20,425
SchNet	0.040	0.334	0.081	0.060	65.201	42.586	0.327	0.026	0.236
DimeNet++	**0.037**	0.357	0.081	0.058	68.685	38.339	**0.208**	0.025	0.234
EGNN	0.038	0.331	0.087	0.064	78.015	74.846	0.211	0.026	0.256
PaiNN	0.038	0.317	**0.080**	**0.053**	67.752	44.602	**0.022**	0.190	0.207
GemNet-T	0.042	0.325	0.088	0.061	68.425	48.986	0.186	0.026	**0.207**
SphereNet	0.043	0.388	0.087	0.061	72.987	36.300	0.217	0.029	0.251
SEGNN	0.046	0.360	0.087	0.059	65.052	43.638	0.330	0.047	0.330
Equiformer	0.046	**0.280**	0.087	0.057	**62.977**	**37.381**	0.202	0.027	0.234

classes; and (3) Cellular Component (CC) has 320 classes. Notice that each protein can be associated with multiple GO terms in each GO term type, thus all three tasks are multi-label classifications.

MSP & PSR are two protein tasks from a collection of benchmark datasets for machine learning in structural biology [118]. MSP (Mutation Stability Prediction) aims to predict whether the stability of a protein increases after mutation. The dataset is a mutation dataset containing 4K proteins. It is constructed by incorporating single-point mutations given in the SKEMPI database [56]. PSR (Protein Structure Ranking) is a regression task based on the Critical Assessment of Structure Prediction (CASP) [71]. In CASP, a protein structure is predicted and a quality score, the global distance test (GDT_TS), is calculated between the predicted structure and experimentally determined structure. This task aims to predict this score for 44K proteins.

The results of 5 models are in Table 5. CDConv [29] outperforms other models by a large margin on almost all 10 tasks, while ProNet [122] performs second well in general, and reaches the best result on the PSR task with global ρ metric. Notice that certain entries in the table are temporarily left blank due to memory constraints encountered. More detailed dataset specifications are in Appendix B.

4.6 Crystalline Materials: MatBench and QMOF

MatBench [21] is explicitly created to evaluate the performance of machine learning models in predicting properties of inorganic bulk materials covering mechanical, electronic, and thermodynamic material properties [21]. Here we consider 8 regression tasks with crystal structures, including predicting the formation energy (Perovskites, E_{form}), exfoliation energies (E_{exfo}), band gap, shear and bulk modulus ($log_{10}G$ and $log_{10}K$), etc. Please check Appendix B for more details.

Quantum MOF (QMOF) [107] is a dataset of over 20K metal-organic frameworks (MOFs) and coordination polymers derived from DFT. The task is to predict the band gap, the energy gap between the valence band and the conduction band. The results of 8 geometric models on 8 MatBench tasks and 1 QMOF task are in Table 6, and we can observe that the performance of all the models is very close, while DimeNet++, PaiNN, GemNet-T, and Equiformer are slightly better.

We also conduct **ablation study on periodic data augmentation** on crystal materials. We note that there are two data augmentation (DA) methods: gathered and expanded. Gathered DA means that we shift the original unit cell along three dimensions, and the translated unit cells will have the *same* node indices as the original unit cell, *i.e.*, a multi-edge graph. However, expanded DA will assume the translated unit cells have different node indices from the original unit cell. (A visual demonstration is in Appendix A). We conduct an ablation study on the effect of these two DAs, and we plot MAE(expanded DA) - MAE(gathered DA) on six tasks in Fig. 6. It reveals that for most of the models (except EGNN), using gathered DA can lead to consistently better performance, and thus it is preferred. For more qualitative analysis, please check Appendix J.

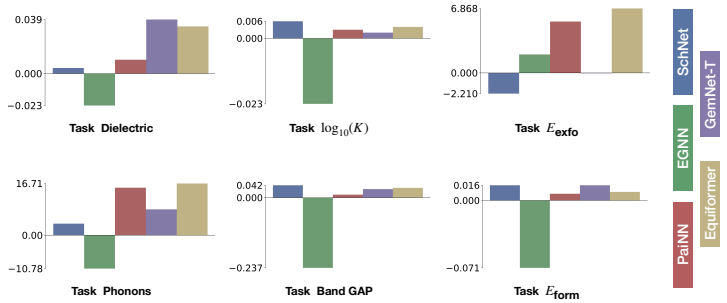

Figure 6: Ablation study on the performance gap with data augmentation (DA): MAE(expanded DA) - MAE(gathered DA).

Table 7: QM9 downstream results after pretraining, and the backbone model is SchNet. We take 110K for training, 10K for validation, and 11K for testing. The evaluation metric is the mean absolute error (MAE).

Pretraining	$\alpha \downarrow$	$\nabla\mathcal{E} \downarrow$	$\mathcal{E}_{\text{HOMO}} \downarrow$	$\mathcal{E}_{\text{LUMO}} \downarrow$	$\mu \downarrow$	$C_v \downarrow$	$G \downarrow$	$H \downarrow$	$R^2 \downarrow$	$U \downarrow$	$U_0 \downarrow$	ZPVE $\downarrow$
– (random init)	0.060	44.13	27.64	22.55	0.028	0.031	14.19	14.05	0.133	13.93	13.27	1.749
Supervised	0.062	40.31	25.57	21.69	0.030	0.030	14.36	14.68	0.308	15.21	16.13	1.638
Type Prediction	0.073	45.38	28.76	24.83	0.036	0.032	16.66	16.28	0.275	15.56	14.66	2.094
Distance Prediction	0.065	45.87	27.61	23.34	0.031	0.033	14.83	15.81	0.248	15.07	15.01	1.837
Angle Prediction	0.066	48.45	29.02	24.40	0.034	0.031	14.13	13.77	0.214	13.50	13.47	1.861
3D InfoGraph	0.062	45.96	29.29	24.60	0.028	0.030	13.93	13.97	0.133	13.55	13.47	1.644
GeoSSL-RR	0.060	43.71	27.71	22.84	0.028	0.031	14.54	13.70	0.122	13.81	13.75	1.694
GeoSSL-InfoNCE	0.061	44.38	27.67	22.85	0.027	0.030	13.38	13.36	**0.116**	13.05	13.00	1.643
GeoSSL-EBM-NCE	0.057	43.75	27.05	22.75	0.028	0.030	12.87	12.65	0.123	13.44	12.64	1.652
3D InfoMax	0.057	42.09	25.90	21.60	0.028	0.030	13.73	13.62	0.141	13.81	13.30	1.670
GraphMVP	0.056	41.99	25.75	21.58	0.027	0.029	13.43	13.31	0.136	13.03	13.07	1.609
GeoSSL-DDM-1L	0.058	42.64	26.32	21.87	0.028	0.030	12.61	12.81	0.173	12.45	12.12	1.696
GeoSSL-DDM	0.056	42.29	**25.61**	21.88	0.027	0.029	11.54	11.14	0.168	11.06	**10.96**	1.660
MoleculeSDE (VE)	0.056	41.84	25.79	21.63	0.027	0.029	**11.47**	**10.71**	0.233	**11.04**	10.95	**1.474**
MoleculeSDE (VP)	**0.054**	**41.77**	25.74	**21.41**	**0.026**	**0.028**	13.07	12.05	0.151	12.54	12.04	1.587

4.7 Geometric Pretraining on Small Molecules

We run 14 pretraining algorithms, including one supervised pretraining: the pretraining dataset (*e.g.*, PCQM4Mv2 [51]) possess the energy or energy gap label for each conformation, which can be naturally adopted for pretraining. The benchmark results of using SchNet as the backbone model pretrained on PCQM4Mv2 and fine-tuning on QM9 tasks are in Table 7. We observe that MoleculeSDE and GeoSSL-DDM utilizing the geometric denoising diffusion models outperform other pretraining methods in most cases. On the other hand, supervised pretraining (pretrained on energy gap $\nabla\mathcal{E}$) reaches outstanding performance on $\nabla\mathcal{E}$ downstream task, yet the generalization to other tasks is modest. Please check Appendix I for more pretraining results with different backbone models.

5 Conclusion and Future Directions

Geom3D provides a unified view on the SE(3)-equivariant models, together with the implementations. Indeed these can serve as the building blocks to various tasks, such as geometric pretraining (as displayed in Sec. 4.7) and the conformation generation (ClofNet [20], MoleculeSDE [79]), paving the way for building more foundational models and solving more challenging tasks.

Limitations on models and tasks. Geom3D includes 10 topological models, 16 geometric models, 14 geometric pretraining methods, and 52 diverse tasks. We would also like to acknowledge there exist many more tasks (*e.g.*, Atom3D [118], Molecule3D [131], OC20 [7]) and more geometric models (*e.g.*, OrbNet [99], MACE [2], Uni-Mol [144], and LieTransformer [52]). The continual updating may necessitate the collective efforts of our entire community, exemplifying our collaborative endeavors.

Foundation model as future exploration. Recently, there have been certain explorations on building the foundation models for molecule discovery, especially by incorporating textual data on the molecule's functionalities [25, 26, 83, 87, 88, 115, 139, 143]. However, existing works mainly focus on the 1D sequence or 2D topology, while the 3D geometric structure of molecules is rarely considered. We believe that Geom3D can offer essential support for future explorations along this direction.

Reproducibility and Tutorials

The codes of Geom3D have been released on this GitHub repository. Both the raw and preprocessed datasets have been released on this HuggingFace link. The checkpoints of all models have been released on this HuggingFace link. We further added four tutorials on using Geom3D on customized data, energy prediction, force prediction, and geometric pretraining. These tutorials can sufficiently demonstrate how users can inject new methods into Geom3D platform, showcasing its potential as a fundamental building block for tackling a wide range of machine learning tasks.

Acknowledgement

The authors would like to thank Zichao Rong, Chengpeng Wang, Jiarui Lu, Farzaneh Heidari, Zuobai Zhang, Limei Wang, and Hanchen Wang for their helpful discussions. This project is supported by the Natural Sciences and Engineering Research Council (NSERC) Discovery Grant, the Canada CIFAR AI Chair Program, collaboration grants between Microsoft Research and Mila, Samsung Electronics Co., Ltd., Amazon Faculty Research Award, Tencent AI Lab Rhino-Bird Gift Fund, and a National Research Council of Canada (NRC) Collaborative R&D Project. This project was also partially funded by IVADO Fundamental Research Project grant PRF-2019-3583139727.

References

[1] Kenneth Atz, Francesca Grisoni, and Gisbert Schneider. Geometric deep learning on molecular representations. *Nature Machine Intelligence*, 3(12):1023–1032, 2021. 1

[2] Ilyes Batatia, Simon Batzner, Dávid Péter Kovács, Albert Musaelian, Gregor N. C. Simm, Ralf Drautz, Christoph Ortner, Boris Kozinsky, and Gábor Csányi. The design space of e(3)-equivariant atom-centered interatomic potentials, 2022. 10

[3] Simon Batzner, Albert Musaelian, Lixin Sun, Mario Geiger, Jonathan P Mailoa, Mordechai Kornbluth, Nicola Molinari, Tess E Smidt, and Boris Kozinsky. E(3)-equivariant graph neural networks for data-efficient and accurate interatomic potentials. *Nature communications*, 13(1):1–11, 2022. 2, 6, 7, 34, 36, 45, 48, 51

[4] Johannes Brandstetter, Rob Hesselink, Elise van der Pol, Erik Bekkers, and Max Welling. Geometric and physical quantities improve e(3) equivariant message passing. *arXiv preprint arXiv:2110.02905*, 2021. 5, 6, 34, 51

[5] Michael M Bronstein, Joan Bruna, Taco Cohen, and Petar Veličković. Geometric deep learning: Grids, groups, graphs, geodesics, and gauges. *arXiv preprint arXiv:2104.13478*, 2021. 4, 32

[6] Nathan Brown, Marco Fiscato, Marwin HS Segler, and Alain C Vaucher. Guacamol: benchmarking models for de novo molecular design. *Journal of chemical information and modeling*, 59(3):1096–1108, 2019. 1

[7] Lowik Chanussot*, Abhishek Das*, Siddharth Goyal*, Thibaut Lavril*, Muhammed Shuaibi*, Morgane Riviere, Kevin Tran, Javier Heras-Domingo, Caleb Ho, Weihua Hu, Aini Palizhati, Anuroop Sriram, Brandon Wood, Junwoong Yoon, Devi Parikh, C. Lawrence Zitnick, and Zachary Ulissi. Open catalyst 2020 (oc20) dataset and community challenges. *ACS Catalysis*, 2021. 10

[8] Stefan Chmiela, Alexandre Tkatchenko, Huziel E Sauceda, Igor Poltavsky, Kristof T Schütt, and Klaus-Robert Müller. Machine learning of accurate energy-conserving molecular force fields. *Science advances*, 3(5):e1603015, 2017. 7, 23

[9] Anders Christensen and O. Anatole von Lilienfeld. Revised md17 dataset. *Materials Cloud Archive*, 2020. 7

[10] Anders S Christensen and O Anatole von Lilienfeld. On the role of gradients for machine learning of molecular energies and forces. *arXiv.org*, 2020. 7, 23

[11] Taco S Cohen and Max Welling. Steerable cnns. *arXiv preprint arXiv:1612.08498*, 2016. 4

[12] Gene Ontology Consortium. The gene ontology (go) database and informatics resource. *Nucleic acids research*, 32(suppl_1):D258–D261, 2004. 8, 26

[13] Gabriele Corso, Luca Cavalleri, Dominique Beaini, Pietro Liò, and Petar Veličković. Principal neighbourhood aggregation for graph nets. *Advances in Neural Information Processing Systems*, 33:13260–13271, 2020. 1, 6, 21

[14] Jose M Dana, Aleksandras Gutmanas, Nidhi Tyagi, Guoying Qi, Claire O'Donovan, Maria Martin, and Sameer Velankar. Sifts: updated structure integration with function, taxonomy and sequences resource allows 40-fold increase in coverage of structure-based annotations for proteins. *Nucleic acids research*, 47(D1):D482–D489, 2019. 24

[15] Justas Dauparas, Ivan Anishchenko, Nathaniel Bennett, Hua Bai, Robert J Ragotte, Lukas F Milles, Basile IM Wicky, Alexis Courbet, Rob J de Haas, Neville Bethel, et al. Robust deep learning–based protein sequence design using proteinmpnn. *Science*, 378(6615):49–56, 2022. 1

[16] Pierre-Paul De Breuck, Matthew L Evans, and Gian-Marco Rignanese. Robust model benchmarking and bias-imbalance in data-driven materials science: a case study on modnet. *Journal of Physics: Condensed Matter*, 33(40):404002, 2021. 27

[17] Mehmet F Demirel, Shengchao Liu, Siddhant Garg, Zhenmei Shi, and Yingyu Liang. Attentive walk-aggregating graph neural networks. *TMLR*, 2022. 1, 6, 21

[18] Jacob Devlin, Ming-Wei Chang, Kenton Lee, and Kristina Toutanova. Bert: Pre-training of deep bidirectional transformers for language understanding. *arXiv preprint arXiv:1810.04805*, 2018. 6

[19] Weitao Du, Yuanqi Du, Limei Wang, Dieqiao Feng, Guifeng Wang, Shuiwang Ji, Carla Gomes, and Zhi-Ming Ma. A new perspective on building efficient and expressive 3d equivariant graph neural networks, 2023. 29, 32, 33, 37

[20] Weitao Du, He Zhang, Yuanqi Du, Qi Meng, Wei Chen, Nanning Zheng, Bin Shao, and Tie-Yan Liu. Se (3) equivariant graph neural networks with complete local frames. In *International Conference on Machine Learning*, pages 5583–5608. PMLR, 2022. 5, 10, 29, 31, 32, 33

[21] Alexander Dunn, Qi Wang, Alex Ganose, Daniel Dopp, and Anubhav Jain. Benchmarking materials property prediction methods: the matbench test set and automatminer reference algorithm. *arXiv.org*, 6, 2020. 9, 27, 51

[22] Alexander Dunn, Qi Wang, Alex Ganose, Daniel Dopp, and Anubhav Jain. Benchmarking materials property prediction methods: the matbench test set and automatminer reference algorithm. *npj Computational Materials*, 6(1):138, 2020. 27, 48

[23] David Duvenaud, Dougal Maclaurin, Jorge Aguilera-Iparraguirre, Rafael Gómez-Bombarelli, Timothy Hirzel, Alán Aspuru-Guzik, and Ryan P Adams. Convolutional networks on graphs for learning molecular fingerprints. *arXiv preprint arXiv:1509.09292*, 2015. 1, 6, 21

[24] Nadav Dym and Haggai Maron. On the universality of rotation equivariant point cloud networks. *arXiv preprint arXiv:2010.02449*, 2020. 33

[25] Carl Edwards, Tuan Lai, Kevin Ros, Garrett Honke, and Heng Ji. Translation between molecules and natural language. *arXiv preprint arXiv:2204.11817*, 2022. 10

[26] Carl Edwards, ChengXiang Zhai, and Heng Ji. Text2mol: Cross-modal molecule retrieval with natural language queries. In *Proceedings of the 2021 Conference on Empirical Methods in Natural Language Processing*, pages 595–607, 2021. 10

[27] Ahmed Elnaggar, Michael Heinzinger, Christian Dallago, Ghalia Rehawi, Wang Yu, Llion Jones, Tom Gibbs, Tamas Feher, Christoph Angerer, Martin Steinegger, Debsindhu Bhowmik, and Burkhard Rost. Prottrans: Towards cracking the language of lifes code through self-supervised deep learning and high performance computing. *IEEE Transactions on Pattern Analysis and Machine Intelligence*, pages 1–1, 2021. 1

[28] Thomas Engel and Johann Gasteiger. *Applied chemoinformatics: achievements and future opportunities*. John Wiley & Sons, 2018. 50

[29] Hehe Fan, Zhangyang Wang, Yi Yang, and Mohan Kankanhalli. Continuous-discrete convolution for geometry-sequence modeling in proteins. In *The Eleventh International Conference on Learning Representations*, 2023. 9, 31, 34, 37, 50, 51

[30] Xiaomin Fang, Lihang Liu, Jieqiong Lei, Donglong He, Shanzhuo Zhang, Jingbo Zhou, Fan Wang, Hua Wu, and Haifeng Wang. Chemrl-gem: Geometry enhanced molecular representation learning for property prediction. *arXiv preprint arXiv:2106.06130*, 2021. 3

[31] Matthias Fey and Jan E. Lenssen. Fast graph representation learning with PyTorch Geometric. In *ICLR Workshop on Representation Learning on Graphs and Manifolds*, 2019. 2

[32] Marc Finzi, Samuel Stanton, Pavel Izmailov, and Andrew Gordon Wilson. Generalizing convolutional neural networks for equivariance to lie groups on arbitrary continuous data. In *International Conference on Machine Learning*, pages 3165–3176. PMLR, 2020. 5, 32

[33] Daniel Flam-Shepherd and Alán Aspuru-Guzik. Language models can generate molecules, materials, and protein binding sites directly in three dimensions as xyz, cif, and pdb files. *arXiv preprint arXiv:2305.05708*, 2023. 1, 32

[34] Richard A Friesner, Jay L Banks, Robert B Murphy, Thomas A Halgren, Jasna J Klicic, Daniel T Mainz, Matthew P Repasky, Eric H Knoll, Mee Shelley, Jason K Perry, et al. Glide: a new approach for rapid, accurate docking and scoring. 1. method and assessment of docking accuracy. *Journal of medicinal chemistry*, 47(7):1739–1749, 2004. 8, 24

[35] Fabian B Fuchs, Daniel E Worrall, Volker Fischer, and Max Welling. Se(3)-transformers: 3d roto-translation equivariant attention networks. *arXiv preprint arXiv:2006.10503*, 2020. 6, 34, 36, 51

[36] Johannes Gasteiger, Shankari Giri, Johannes T Margraf, and Stephan Günnemann. Fast and uncertainty-aware directional message passing for non-equilibrium molecules. 2020. 7, 24

[37] Mario Geiger and Tess Smidt. e3nn: Euclidean neural networks. *arXiv preprint arXiv:2207.09453*, 2022. 5, 30, 33, 34, 51

[38] Justin Gilmer, Samuel S Schoenholz, Patrick F Riley, Oriol Vinyals, and George E Dahl. Neural message passing for quantum chemistry. In *International conference on machine learning*, pages 1263–1272. PMLR, 2017. 1, 6, 21, 30

[39] Vladimir Gligorijević, P Douglas Renfrew, Tomasz Kosciolek, Julia Koehler Leman, Daniel Berenberg, Tommi Vatanen, Chris Chandler, Bryn C Taylor, Ian M Fisk, Hera Vlamakis, et al. Structure-based protein function prediction using graph convolutional networks. *Nature communications*, 12(1):3168, 2021. 8, 25

[40] Sai Krishna Gottipati, Boris Sattarov, Sufeng Niu, Yashaswi Pathak, Haoran Wei, Shengchao Liu, Simon Blackburn, Karam Thomas, Connor Coley, Jian Tang, et al. Learning to navigate the synthetically accessible chemical space using reinforcement learning. In *International Conference on Machine Learning*, pages 3668–3679. PMLR, 2020. 1

[41] Nate Gruver, Samuel Stanton, Nathan C Frey, Tim GJ Rudner, Isidro Hotzel, Julien Lafrance-Vanasse, Arvind Rajpal, Kyunghyun Cho, and Andrew Gordon Wilson. Protein design with guided discrete diffusion. *arXiv preprint arXiv:2305.20009*, 2023. 1

[42] Thomas A Halgren. Merck molecular force field. i. basis, form, scope, parameterization, and performance of mmff94. *Journal of computational chemistry*, 17(5-6):490–519, 1996. 50

[43] Will Hamilton, Zhitao Ying, and Jure Leskovec. Inductive representation learning on large graphs. *Advances in neural information processing systems*, 30, 2017. 6, 21

[44] Kaiming He, Xiangyu Zhang, Shaoqing Ren, and Jian Sun. Deep residual learning for image recognition. In *Proceedings of the IEEE conference on computer vision and pattern recognition*, pages 770–778, 2016. 36

[45] Pedro Hermosilla, Marco Schäfer, Matěj Lang, Gloria Fackelmann, Pere Pau Vázquez, Barbora Kozlíková, Michael Krone, Tobias Ritschel, and Timo Ropinski. Intrinsic-extrinsic convolution and pooling for learning on 3d protein structures. 2020. 8, 24, 34, 51

[46] Brian L Hie, Varun R Shanker, Duo Xu, Theodora UJ Bruun, Payton A Weidenbacher, Shaogeng Tang, Wesley Wu, John E Pak, and Peter S Kim. Efficient evolution of human antibodies from general protein language models. *Nature Biotechnology*, 2023. 1

[47] Jie Hou, Badri Adhikari, and Jianlin Cheng. Deepsf: deep convolutional neural network for mapping protein sequences to folds. *Bioinformatics*, 34, 2018. 8, 25, 26

[48] Chloe Hsu, Robert Verkuil, Jason Liu, Zeming Lin, Brian Hie, Tom Sercu, Adam Lerer, and Alexander Rives. Learning inverse folding from millions of predicted structures. *bioRxiv*, 2022. 1

[49] Elton P Hsu. *Stochastic analysis on manifolds*. Number 38. American Mathematical Soc., 2002. 5, 29

[50] Qian-Nan Hu, Hui Zhu, Xiaobing Li, Manman Zhang, Zhe Deng, Xiaoyan Yang, and Zixin Deng. Assignment of ec numbers to enzymatic reactions with reaction difference fingerprints. *PloS one*, 7(12):e52901–e52901, 2012. 24

[51] Weihua Hu, Matthias Fey, Marinka Zitnik, Yuxiao Dong, Hongyu Ren, Bowen Liu, Michele Catasta, and Jure Leskovec. Open graph benchmark: Datasets for machine learning on graphs. *arXiv preprint arXiv:2005.00687*, 2020. 10

[52] Michael J Hutchinson, Charline Le Lan, Sheheryar Zaidi, Emilien Dupont, Yee Whye Teh, and Hyunjik Kim. Lietransformer: Equivariant self-attention for lie groups. In *International Conference on Machine Learning*, pages 4533–4543. PMLR, 2021. 5, 10, 32

[53] John Ingraham, Vikas Garg, Regina Barzilay, and Tommi Jaakkola. Generative models for graph-based protein design. *Advances in neural information processing systems*, 32, 2019. 5, 31

[54] Clemens Isert, Kenneth Atz, and Gisbert Schneider. Structure-based drug design with geometric deep learning. *Current Opinion in Structural Biology*, 79:102548, 2023. 1

[55] Anubhav Jain, Shyue Ping Ong, Geoffroy Hautier, Wei Chen, William Davidson Richards, Stephen Dacek, Shreyas Cholia, Dan Gunter, David Skinner, Gerbrand Ceder, et al. Commentary: The materials project: A materials genome approach to accelerating materials innovation. *APL materials*, 1(1):011002, 2013. 27, 51

[56] Justina Jankauskaitė, Brian Jiménez-García, Justas Dapkūnas, Juan Fernández-Recio, and Iain H Moal. Skempi 2.0: an updated benchmark of changes in protein–protein binding energy, kinetics and thermodynamics upon mutation. *Bioinformatics*, 35(3):462–469, 2019. 9, 26

[57] Jan H Jensen. A graph-based genetic algorithm and generative model/monte carlo tree search for the exploration of chemical space. *Chemical science*, 10(12):3567–3572, 2019. 1

[58] Yuanfeng Ji, Lu Zhang, Jiaxiang Wu, Bingzhe Wu, Long-Kai Huang, Tingyang Xu, Yu Rong, Lanqing Li, Jie Ren, Ding Xue, et al. Drugood: Out-of-distribution (ood) dataset curator and benchmark for ai-aided drug discovery–a focus on affinity prediction problems with noise annotations. *arXiv preprint arXiv:2201.09637*, 2022. 3

[59] Rui Jiao, Jiaqi Han, Wenbing Huang, Yu Rong, and Yang Liu. 3d equivariant molecular graph pretraining. *arXiv preprint arXiv:2207.08824*, 2022. 3, 5, 34, 52

[60] Rui Jiao, Jiaqi Han, Wenbing Huang, Yu Rong, and Yang Liu. Energy-motivated equivariant pretraining for 3d molecular graphs. *arXiv preprint arXiv:2207.08824*, 2022. 5, 39

[61] Bowen Jing, Gabriele Corso, Jeffrey Chang, Regina Barzilay, and Tommi Jaakkola. Torsional diffusion for molecular conformer generation. *arXiv preprint arXiv:2206.01729*, 2022. 5

[62] Bowen Jing, Stephan Eismann, Patricia Suriana, Raphael J. L Townshend, and Ron Dror. Learning from protein structure with geometric vector perceptrons. 2020. 34, 51

[63] J.M. Enzyme nomenclature: prepared by edwin c. webb, academic press, 1992. £34.00 (xiii + 862 pages) isbn 0 12 227165 3. *Trends in biochemical sciences (Amsterdam. Regular ed.)*, 18, 1993. 8

[64] John Jumper, Richard Evans, Alexander Pritzel, Tim Green, Michael Figurnov, Olaf Ronneberger, Kathryn Tunyasuvunakool, Russ Bates, Augustin Žídek, Anna Potapenko, et al. Highly accurate protein structure prediction with alphafold. *Nature*, 596(7873):583–589, 2021. 1, 5

[65] Nicolas Keriven and Gabriel Peyré. Universal invariant and equivariant graph neural networks, 2019. 33

[66] Thomas N Kipf and Max Welling. Semi-supervised classification with graph convolutional networks. *arXiv preprint arXiv:1609.02907*, 2016. 1, 6, 21

[67] Johannes Klicpera, Florian Becker, and Stephan Günnemann. Gemnet: Universal directional graph neural networks for molecules. In *Conference on Neural Information Processing Systems (NeurIPS)*, 2021. 5, 6, 34, 35, 51

[68] Johannes Klicpera, Shankari Giri, Johannes T Margraf, and Stephan Günnemann. Fast and uncertainty-aware directional message passing for non-equilibrium molecules. *arXiv preprint arXiv:2011.14115*, 2020. 5, 6, 7, 23, 34, 51

[69] Johannes Klicpera, Janek Groß, and Stephan Günnemann. Directional message passing for molecular graphs. *arXiv preprint arXiv:2003.03123*, 2020. 35

[70] Mario Krenn, Florian H"ase, AkshatKumar Nigam, Pascal Friederich, and Alan Aspuru-Guzik. Self-referencing embedded strings (selfies): A 100% robust molecular string representation. *Machine Learning: Science and Technology*, 1(4):045024, 2020. 6, 21

[71] Andriy Kryshtafovych, Torsten Schwede, Maya Topf, Krzysztof Fidelis, and John Moult. Critical assessment of methods of protein structure prediction (casp)—round xiii. *Proteins: Structure, Function, and Bioinformatics*, 87(12):1011–1020, 2019. 9, 26

[72] Greg Landrum et al. RDKit: A software suite for cheminformatics, computational chemistry, and predictive modeling, 2013. 50

[73] Yi-Lun Liao and Tess Smidt. Equiformer: Equivariant graph attention transformer for 3d atomistic graphs. *arXiv preprint arXiv:2206.11990*, 2022. 5, 6, 33, 34, 36, 51

[74] Chen Lin, Ying Zou, Ji Qin, Xiangrong Liu, Yi Jiang, Caihuan Ke, and Quan Zou. Hierarchical classification of protein folds using a novel ensemble classifier. *PloS one*, 8(2):e56499, 2013. 8

[75] Chen Lin, Ying Zou, Ji Qin, Xiangrong Liu, Yi Jiang, Caihuan Ke, and Quan Zou. Hierarchical classification of protein folds using a novel ensemble classifier. *PloS one*, 8(2):e56499–e56499, 2013. 25

[76] Meng Liu, Youzhi Luo, Limei Wang, Yaochen Xie, Hao Yuan, Shurui Gui, Haiyang Yu, Zhao Xu, Jingtun Zhang, Yi Liu, et al. Dig: A turnkey library for diving into graph deep learning research. *The Journal of Machine Learning Research*, 22(1):10873–10881, 2021. 2

[77] Meng Liu, Youzhi Luo, Limei Wang, Yaochen Xie, Hao Yuan, Shurui Gui, Haiyang Yu, Zhao Xu, Jingtun Zhang, Yi Liu, Keqiang Yan, Haoran Liu, Cong Fu, Bora M Oztekin, Xuan Zhang, and Shuiwang Ji. DIG: A turnkey library for diving into graph deep learning research. *Journal of Machine Learning Research*, 22(240):1–9, 2021. 2

[78] Shengchao Liu, Mehmet F Demirel, and Yingyu Liang. N-gram graph: Simple unsupervised representation for graphs, with applications to molecules. *NeurIPS*, 32, 2019. 1, 21

[79] Shengchao Liu, Weitao Du, Zhiming Ma, Hongyu Guo, and Jian Tang. A group symmetric stochastic differential equation model for molecule multi-modal pretraining. In *International Conference on Machine Learning*, 2023. 3, 5, 6, 10, 31, 34, 39, 52

[80] Shengchao Liu, Hongyu Guo, and Jian Tang. Molecular geometry pretraining with se (3)-invariant denoising distance matching. *arXiv preprint arXiv:2206.13602*, 2022. 3, 5, 39

[81] Shengchao Liu, Hongyu Guo, and Jian Tang. Molecular geometry pretraining with SE(3)-invariant denoising distance matching. In *ICLR*, 2023. 34, 52

[82] Shengchao Liu, Yingyu Liang, and Anthony Gitter. Loss-balanced task weighting to reduce negative transfer in multi-task learning. In *Proceedings of the AAAI conference on artificial intelligence*, volume 33, pages 9977–9978, 2019. 3

[83] Shengchao Liu, Weili Nie, Chengpeng Wang, Jiarui Lu, Zhuoran Qiao, Ling Liu, Jian Tang, Chaowei Xiao, and Anima Anandkumar. Multi-modal molecule structure-text model for text-based retrieval and editing. *arXiv preprint arXiv:2212.10789*, 2022. 10

[84] Shengchao Liu, Meng Qu, Zuobai Zhang, Huiyu Cai, and Jian Tang. Structured multi-task learning for molecular property prediction. In *International Conference on Artificial Intelligence and Statistics*, pages 8906–8920. PMLR, 2022. 3

[85] Shengchao Liu, Chengpeng Wang, Weili Nie, Hanchen Wang, Jiarui Lu, Bolei Zhou, and Jian Tang. Graphcg: Unsupervised discovery of steerable factors in graphs, 2023. 1

[86] Shengchao Liu, Hanchen Wang, Weiyang Liu, Joan Lasenby, Hongyu Guo, and Jian Tang. Pre-training molecular graph representation with 3d geometry. *arXiv preprint arXiv:2110.07728*, 2021. 3, 5, 34, 39, 52

[87] Shengchao Liu, Jiongxiao Wang, Yijin Yang, Chengpeng Wang, Ling Liu, Hongyu Guo, and Chaowei Xiao. Chatgpt-powered conversational drug editing using retrieval and domain feedback. *arXiv preprint arXiv:2305.18090*, 2023. 10

[88] Shengchao Liu, Yutao Zhu, Jiarui Lu, Zhao Xu, Weili Nie, Anthony Gitter, Chaowei Xiao, Jian Tang, Hongyu Guo, and Anima Anandkumar. A text-guided protein design framework. *arXiv preprint arXiv:2302.04611*, 2023. 1, 10

[89] Yi Liu, Limei Wang, Meng Liu, Xuan Zhang, Bora Oztekin, and Shuiwang Ji. Spherical message passing for 3d graph networks. *arXiv preprint arXiv:2102.05013*, 2021. 5, 6, 7, 23, 34, 35, 51

[90] Ilya Loshchilov and Frank Hutter. Sgdr: Stochastic gradient descent with warm restarts. *arXiv preprint arXiv:1608.03983*, 2016. 23

[91] Ali Madani, Bryan McCann, Nikhil Naik, Nitish Shirish Keskar, Namrata Anand, Raphael R Eguchi, Po-Ssu Huang, and Richard Socher. Progen: Language modeling for protein generation. *arXiv preprint arXiv:2004.03497*, 2020. 1

[92] Joshua Meier, Roshan Rao, Robert Verkuil, Jason Liu, Tom Sercu, and Alexander Rives. Language models enable zero-shot prediction of the effects of mutations on protein function. *bioRxiv*, 2021. 1

[93] Jan Mostowski and Joanna Pietraszewicz. Quantum versus classical angular momentum. 2019. 33

[94] Alexey G. Murzin, Steven E. Brenner, Tim Hubbard, and Cyrus Chothia. Scop: A structural classification of proteins database for the investigation of sequences and structures. *Journal of molecular biology*, 247(4):536–540, 1995. 8, 25

[95] Albert Musaelian, Simon Batzner, Anders Johansson, Lixin Sun, Cameron J Owen, Mordechai Kornbluth, and Boris Kozinsky. Learning local equivariant representations for large-scale atomistic dynamics. *arXiv preprint arXiv:2204.05249*, 2022. 5, 6, 7, 34, 36, 45, 48, 51

[96] Emmy Noether and M. A. Tavel. Invariant variation problems. 2005. 28

[97] Shyue Ping Ong, William Davidson Richards, Anubhav Jain, Geoffroy Hautier, Michael Kocher, Shreyas Cholia, Dan Gunter, Vincent L Chevrier, Kristin A Persson, and Gerbrand Ceder. Python materials genomics (pymatgen): A robust, open-source python library for materials analysis. *Computational Materials Science*, 68:314–319, 2013. 22

[98] Donald H Perkins. *Introduction to high energy physics*. CAMBRIDGE university press, 2000. 5

[99] Zhuoran Qiao, Matthew Welborn, Animashree Anandkumar, Frederick R Manby, and Thomas F Miller. Orbnet: Deep learning for quantum chemistry using symmetry-adapted atomic-orbital features. *The Journal of chemical physics*, 153(12), 2020. 5, 10, 32

[100] Raghunathan Ramakrishnan, Pavlo O Dral, Matthias Rupp, and O Anatole Von Lilienfeld. Quantum chemistry structures and properties of 134 kilo molecules. *Scientific data*, 1(1):1–7, 2014. 6, 23

[101] Ladislav Rampášek, Mikhail Galkin, Vijay Prakash Dwivedi, Anh Tuan Luu, Guy Wolf, and Dominique Beaini. Recipe for a General, Powerful, Scalable Graph Transformer. *Advances in Neural Information Processing Systems*, 35, 2022. 1, 6, 21

[102] Bharath Ramsundar, Peter Eastman, Patrick Walters, Vijay Pande, Karl Leswing, and Zhenqin Wu. *Deep Learning for the Life Sciences*. O'Reilly Media, 2019. https://www.amazon.com/Deep-Learning-Life-Sciences-Microscopy/dp/1492039837. 2

[103] Roshan Rao, Jason Liu, Robert Verkuil, Joshua Meier, John F. Canny, Pieter Abbeel, Tom Sercu, and Alexander Rives. Msa transformer. *bioRxiv*, 2021. 1

[104] Roshan M Rao, Joshua Meier, Tom Sercu, Sergey Ovchinnikov, and Alexander Rives. Transformer protein language models are unsupervised structure learners. *bioRxiv*, 2020. 1

[105] Patrick Reiser, Andre Eberhard, and Pascal Friederich. Graph neural networks in tensorflow-keras with raggedtensor representation (kgcnn). *Software Impacts*, page 100095, 2021. 2, 48, 51

[106] David Rogers and Mathew Hahn. Extended-connectivity fingerprints. *Journal of chemical information and modeling*, 50(5):742–754, 2010. 6, 21

[107] Andrew S Rosen, Shaelyn M Iyer, Debmalya Ray, Zhenpeng Yao, Alan Aspuru-Guzik, Laura Gagliardi, Justin M Notestein, and Randall Q Snurr. Machine learning the quantum-chemical properties of metal–organic frameworks for accelerated materials discovery. *Matter*, 4(5):1578–1597, 2021. 9, 27

[108] Victor Garcia Satorras, Emiel Hoogeboom, and Max Welling. E(n) equivariant graph neural networks. *arXiv preprint arXiv:2102.09844*, 2021. 6, 34, 36, 51

[109] Kristof T Schütt, Huziel E Sauceda, P-J Kindermans, Alexandre Tkatchenko, and K-R Müller. Schnet–a deep learning architecture for molecules and materials. *The Journal of Chemical Physics*, 148(24):241722, 2018. 5, 6, 7, 23, 34, 35, 51

[110] Kristof T Schütt, Oliver T Unke, and Michael Gastegger. Equivariant message passing for the prediction of tensorial properties and molecular spectra. *arXiv preprint arXiv:2102.03150*, 2021. 6, 7, 23, 33, 34, 37, 51

[111] Chence Shi, Minkai Xu, Hongyu Guo, Ming Zhang, and Jian Tang. A graph to graphs framework for retrosynthesis prediction. In *International Conference on Machine Learning*, pages 8818–8827. PMLR, 2020. 1

[112] Tess Smidt, Nathaniel Thomas, Steven Kearnes, Lusann Yang, Li Li, Kai Kohlhoff, and Patrick Riley. Tensor field networks: Rotation-and translation-equivariant neural networks for 3d point clouds. *arXiv preprint arXiv:1802.08219*, 2018. 5, 30, 35, 51

[113] Antonia Stank, Daria B Kokh, Jonathan C Fuller, and Rebecca C Wade. Protein binding pocket dynamics. *Accounts of chemical research*, 49(5):809–815, 2016. 8, 24

[114] Hannes Stärk, Dominique Beaini, Gabriele Corso, Prudencio Tossou, Christian Dallago, Stephan Günnemann, and Pietro Liò. 3d infomax improves gnns for molecular property prediction. In *International Conference on Machine Learning*, pages 20479–20502. PMLR, 2022. 5, 34, 39, 52

[115] Bing Su, Dazhao Du, Zhao Yang, Yujie Zhou, Jiangmeng Li, Anyi Rao, Hao Sun, Zhiwu Lu, and Ji-Rong Wen. A molecular multimodal foundation model associating molecule graphs with natural language. *arXiv preprint arXiv:2209.05481*, 2022. 10

[116] Ruoxi Sun, Hanjun Dai, Li Li, Steven Kearnes, and Bo Dai. Energy-based view of retrosynthesis. *arXiv preprint arXiv:2007.13437*, 2020. 1

[117] Ruoxi Sun, Hanjun Dai, and Adams Wei Yu. Rethinking of graph pretraining on molecular representation. 2022. 42

[118] Raphael JL Townshend, Martin Vögele, Patricia Suriana, Alexander Derry, Alexander Powers, Yianni Laloudakis, Sidhika Balachandar, Brandon Anderson, Stephan Eismann, Risi Kondor, et al. Atom3d: Tasks on molecules in three dimensions. *arXiv preprint arXiv:2012.04035*, 2020. 8, 9, 10, 24, 26

[119] Petar Veličković, Guillem Cucurull, Arantxa Casanova, Adriana Romero, Pietro Lio, and Yoshua Bengio. Graph attention networks. *arXiv preprint arXiv:1710.10903*, 2017. 1, 6, 21

[120] Soledad Villar, David W. Hogg, Kate Storey-Fisher, Weichi Yao, and Ben Blum-Smith. Scalars are universal: Equivariant machine learning, structured like classical physics. 2021. 33

[121] Hanchen Wang, Jean Kaddour, Shengchao Liu, Jian Tang, Matt Kusner, Joan Lasenby, and Qi Liu. Evaluating self-supervised learning for molecular graph embeddings. *arXiv preprint arXiv:2206.08005*, 2022. 42

[122] Limei Wang, Haoran Liu, Yi Liu, Jerry Kurtin, and Shuiwang Ji. Learning hierarchical protein representations via complete 3d graph networks. 2022. 9, 34, 35, 51

[123] Renxiao Wang, Xueliang Fang, Yipin Lu, and Shaomeng Wang. The pdbbind database: Collection of binding affinities for protein- ligand complexes with known three-dimensional structures. *Journal of medicinal chemistry*, 47(12):2977–2980, 2004. 8, 24

[124] Renxiao Wang, Xueliang Fang, Yipin Lu, Chao-Yie Yang, and Shaomeng Wang. The pdbbind database: methodologies and updates. *Journal of medicinal chemistry*, 48(12):4111–4119, 2005. 8, 24

[125] Shiyu Wang, Xiaojie Guo, and Liang Zhao. Deep generative model for periodic graphs. *arXiv preprint arXiv:2201.11932*, 2022. 1

[126] David Weininger. Smiles, a chemical language and information system. 1. introduction to methodology and encoding rules. *Journal of chemical information and computer sciences*, 28(1):31–36, 1988. 6, 21

[127] Hermann Weyl. *Symmetry*, volume 47. Princeton University Press, 2015. 4

[128] Tian Xie, Xiang Fu, Octavian-Eugen Ganea, Regina Barzilay, and Tommi Jaakkola. Crystal diffusion variational autoencoder for periodic material generation. *arXiv preprint arXiv:2110.06197*, 2021. 1

[129] Tian Xie and Jeffrey C Grossman. Crystal graph convolutional neural networks for an accurate and interpretable prediction of material properties. *Physical review letters*, 120(14):145301, 2018. 3, 22

[130] Keyulu Xu, Weihua Hu, Jure Leskovec, and Stefanie Jegelka. How powerful are graph neural networks? *arXiv preprint arXiv:1810.00826*, 2018. 1, 6, 21

[131] Zhao Xu, Youzhi Luo, Xuan Zhang, Xinyi Xu, Yaochen Xie, Meng Liu, Kaleb Andrew Dickerson, Cheng Deng, Maho Nakata, and Shuiwang Ji. Molecule3d: A benchmark for predicting 3d geometries from molecular graphs, 2021. 10

[132] Kevin Yang, Kyle Swanson, Wengong Jin, Connor Coley, Philipp Eiden, Hua Gao, Angel Guzman-Perez, Timothy Hopper, Brian Kelley, Miriam Mathea, et al. Analyzing learned molecular representations for property prediction. *Journal of chemical information and modeling*, 59(8):3370–3388, 2019. 1, 6, 21, 35

[133] Huaxiu Yao, Ying Wei, Long-Kai Huang, Ding Xue, Junzhou Huang, and Zhenhui Jessie Li. Functionally regionalized knowledge transfer for low-resource drug discovery. *Advances in Neural Information Processing Systems*, 34:8256–8268, 2021. 3

[134] Huaxiu Yao, Xinyu Yang, Xinyi Pan, Shengchao Liu, Pang Wei Koh, and Chelsea Finn. Leveraging domain relations for domain generalization. *arXiv preprint arXiv:2302.02609*, 2023. 3

[135] Chengxuan Ying, Tianle Cai, Shengjie Luo, Shuxin Zheng, Guolin Ke, Di He, Yanming Shen, and Tie-Yan Liu. Do transformers really perform badly for graph representation? *Advances in Neural Information Processing Systems*, 34:28877–28888, 2021. 1, 6, 21

[136] Sheheryar Zaidi, Michael Schaarschmidt, James Martens, Hyunjik Kim, Yee Whye Teh, Alvaro Sanchez-Gonzalez, Peter Battaglia, Razvan Pascanu, and Jonathan Godwin. Pre-training via denoising for molecular property prediction. *arXiv preprint arXiv:2206.00133*, 2022. 3, 5, 34, 39, 52

[137] Chengxi Zang and Fei Wang. Moflow: an invertible flow model for generating molecular graphs. In *Proceedings of the 26th ACM SIGKDD International Conference on Knowledge Discovery & Data Mining*, pages 617–626, 2020. 1

[138] Anthony Zee. *Group theory in a nutshell for physicists*, volume 17. Princeton University Press, 2016. 4, 28

[139] Zheni Zeng, Yuan Yao, Zhiyuan Liu, and Maosong Sun. A deep-learning system bridging molecule structure and biomedical text with comprehension comparable to human professionals. *Nature communications*, 13(1):862, 2022. 10

[140] Linfeng Zhang, Jiequn Han, Han Wang, Roberto Car, and EJPRL Weinan. Deep potential molecular dynamics: a scalable model with the accuracy of quantum mechanics. *Physical review letters*, 120(14):143001, 2018. 5

[141] Ningyu Zhang, Zhen Bi, Xiaozhuan Liang, Siyuan Cheng, Haosen Hong, Shumin Deng, Jiazhang Lian, Qiang Zhang, and Huajun Chen. Ontoprotein: Protein pretraining with gene ontology embedding. *arXiv preprint arXiv:2201.11147*, 2022. 1

[142] Zuobai Zhang, Minghao Xu, Arian Jamasb, Vijil Chenthamarakshan, Aurelie Lozano, Payel Das, and Jian Tang. Protein representation learning by geometric structure pretraining. 2022. 34, 35, 51

[143] Haiteng Zhao, Shengchao Liu, Chang Ma, Hannan Xu, Jie Fu, Zhi-Hong Deng, Lingpeng Kong, and Qi Liu. Gimlet: A unified graph-text model for instruction-based molecule zero-shot learning. *bioRxiv*, pages 2023–05, 2023. 10

[144] Gengmo Zhou, Zhifeng Gao, Qiankun Ding, Hang Zheng, Hongteng Xu, Zhewei Wei, Linfeng Zhang, and Guolin Ke. Uni-mol: A universal 3d molecular representation learning framework. 2023. 10

[145] Zhaocheng Zhu, Chence Shi, Zuobai Zhang, Shengchao Liu, Minghao Xu, Xinyu Yuan, Yangtian Zhang, Junkun Chen, Huiyu Cai, Jiarui Lu, et al. Torchdrug: A powerful and flexible machine learning platform for drug discovery. *arXiv preprint arXiv:2202.08320*, 2022. 2, 51

Checklist

1. For all authors...
   (a) Do the main claims made in the abstract and introduction accurately reflect the paper's contributions and scope? [Yes]
   (b) Did you describe the limitations of your work? [Yes]
   (c) Did you discuss any potential negative societal impacts of your work? [N/A]
   (d) Have you read the ethics review guidelines and ensured that your paper conforms to them? [N/A]
2. If you are including theoretical results...
   (a) Did you state the full set of assumptions of all theoretical results? [N/A]
   (b) Did you include complete proofs of all theoretical results? [N/A]
3. If you ran experiments (e.g. for benchmarks)...
   (a) Did you include the code, data, and instructions needed to reproduce the main experimental results (either in the supplemental material or as a URL)? [Yes]
   (b) Did you specify all the training details (e.g., data splits, hyperparameters, how they were chosen)? [Yes]
   (c) Did you report error bars (e.g., with respect to the random seed after running experiments multiple times)? [Yes]
   (d) Did you include the total amount of compute and the type of resources used (e.g., type of GPUs, internal cluster, or cloud provider)? [Yes]
4. If you are using existing assets (e.g., code, data, models) or curating/releasing new assets...
   (a) If your work uses existing assets, did you cite the creators? [Yes]
   (b) Did you mention the license of the assets? [Yes]
   (c) Did you include any new assets either in the supplemental material or as a URL? [Yes]
   (d) Did you discuss whether and how consent was obtained from people whose data you're using/curating? [Yes]
   (e) Did you discuss whether the data you are using/curating contains personally identifiable information or offensive content? [N/A]
5. If you used crowdsourcing or conducted research with human subjects...
   (a) Did you include the full text of instructions given to participants and screenshots, if applicable? [N/A]
   (b) Did you describe any potential participant risks, with links to Institutional Review Board (IRB) approvals, if applicable? [N/A]
   (c) Did you include the estimated hourly wage paid to participants and the total amount spent on participant compensation? [N/A]

Appendix

Table of Contents

A Data Structure and Data Preprocessing

Recall that as illustrated in Fig. 2, we split existing geometric models into three big venues: invariant modeling, equivariant modeling with spherical frame, and equivariant modeling with vector frame. All these modelings are application-agnostic, *i.e.*, they can be naturally adapted to small molecules, proteins, and crystal materials.

In this section, we would like to scrutinize the key data structure of such three data types. They are critical factors when we design geometric modeling. For instance:

- Small molecules often have <100 atoms in the 3D Euclidean space, and thus they can be easily fed into GPU memory.
- Proteins are macromolecules with tens of thousands of atoms. Thus, geometric models on small molecules cannot be easily adapted. Existing research works are working on modeling the backbone-level and residue-level, *i.e.*, only modeling the most important atoms (e.g., C_α, C, N) in proteins.
- Crystal materials are molecules with periodic structures, and typical solutions consider periodic data augmentation before feeding them into geometric models.

In the next, we will explain in more detail of these three data structures.

A.1 Small Molecules

In the machine learning and computational chemistry domain, existing works are mainly focusing on the molecule 1D description [70, 106, 126] and 2D topology graph [13, 17, 23, 38, 43, 66, 78, 101, 119, 130, 132, 132, 135]. Especially as the 2D graph, where the atoms and bonds are treated as nodes and edges, respectively. To model this graph structure, a message-passing graph neural network model family has been proposed.

Simultaneously, molecules can be naturally treated as 3D point clouds in Euclidean space, where atoms are the 3D points. In geometric modeling, as illustrated in Sec. 2, the inputs are atom types and atom positions, *i.e.*, $\boldsymbol{g} = (\boldsymbol{X}, \boldsymbol{R})$.

In Table 1, we provide a comparison of models on 1D descriptions, 2D topological graphs, and 3D geometric conformations. The observation verifies the necessity of using conformation for quantum property prediction tasks.

A.2 Proteins

Protein structures can be classified into four primary levels. The primary structure represents the linear arrangement of amino acids within a polypeptide chain. Secondary structure arises from local interactions between adjacent amino acids, resulting in the formation of recognizable patterns like alpha helices and beta sheets. The tertiary structure encompasses the complete three-dimensional organization of a single protein, involving additional folding and structural modifications beyond the secondary structure. Quaternary structure emerges when multiple polypeptide chains or subunits interact to form a protein complex.

Specifically for geometric modeling, we are now focusing on the protein tertiary structure, which can be constructed based on different structural levels, namely the all-atom level, backbone level, and residue level. We explain the details below, and you can find an illustration in Fig. 3(c).

- At the all-atom level, the graph nodes represent individual atoms, capturing the fine-grained details of the protein structure.
- At the backbone level, the graph nodes correspond to the backbone atoms ($N - C_\alpha - C$), omitting the side chain information. This level of abstraction focuses on the essential backbone structure of the protein.
- At the residue level, the graph nodes represent amino acid residues. The position of each residue can be represented by the position of its C_α atom or calculated as the average position of the backbone atoms within the residue. This level provides a higher-level representation of the protein structure, grouping atoms into residue units.

A.3 Crystalline Materials

Periodic structure. The crystalline materials or extended chemical structures possess a characteristic known as periodicity: their atomic or molecular arrangement repeats in a predictable and consistent pattern across all three spatial dimensions. This is the key aspect that differentiates them from small molecules. In Fig. 3(d), we

show an original unit cell (marked in green) that can repeatedly compose the crystal structure along the lattice. To model such a periodic structure, we adopt the data augmentation (DA) from CGCNN [129], yet with two variants as explained below.

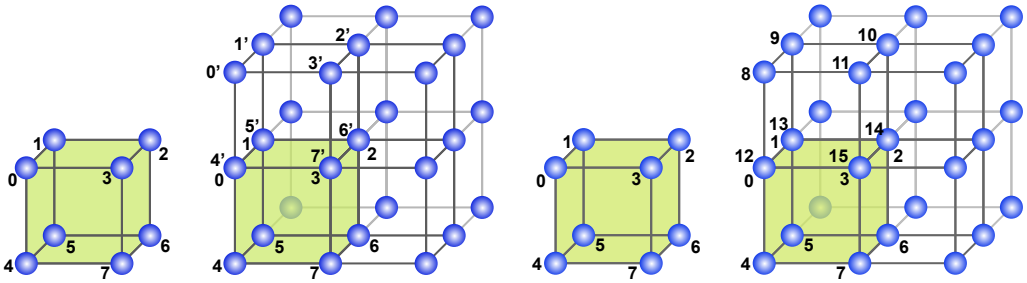

(a) DA: gathered. (b) DA: expanded.

Figure 7: An illustration for crystalline material data augmentation (DA). Notice that in Fig. 7(a), the shifted unit cells and the original unit cells share the same corresponding node indices; for the demonstration clarity, we mark them with $'$, *e.g.*,) 0 and $0'$ are the indices for the same nodes.

Data augmentation 1: Gathered. Gathered DA means that we will shift the original unit cell along three dimensions, and the translated unit cells will have the same node indices as the original unit cell. An example is in Fig. 7(a).

Data augmentation 2: Expanded. Expanded DA refers that we shift the original unit cell in the same way as Gathered, but the translated unit cells have different node indices from the original unit cell. An example is in Fig. 7(b).

Once we have these two augmentations, we have the augmented nodes and corresponding periodic coordinates. The edge connection needs to satisfy three conditions simultaneously:

- The pairwise distance should be larger than 0 and no larger than the threshold τ, *i.e.*, the distance is within $(0, \tau)$.
- At least one of the linked nodes (bonded atoms) belongs to the anchor unit cell.
- No self-loop.

In specific, we give an example of the two DAs below. We take the same simple cubic crystal in Fig. 7 for illustration, and we assume that the edge length in the unit cell is l. The threshold for building the edge is $\tau = l$.

- Gathered DA. $(0, 1)$ satisfies the conditions; $(0, 3')$ violets the condition; $(0, 4')$ violets the conditions; $(0', 1')$ violets the conditions.
- Expanded DA. $(0, 1)$ satisfies the conditions; $(0, 11)$ violets the conditions; $(0, 12)$ violets the condition; $(8, 9)$ violets the conditions.

In terms of implementation, this can be easily achieved by calling the pymatgen [97] package. Such data augmentation is merely one way of handling the periodic data structure in crystalline materials. There could be more potential ways, and we would like to leave them for future exploration.

Thus, after the data augmentation, we can feed the augmented 3D point clouds into the geometric models. This modeling process is the same as that of the small molecules.

B Dataset Acquisition and Preparation & Benchmark Hyperparameters

For the dataset download, please check this GitHub repository for detailed instructions.

B.1 Small Molecules: QM9

Task specification. QM9 [100] is a dataset of 134K molecules, consisting of 9 heavy atoms. It includes 12 tasks that are related to the quantum properties. For example, U0 and U298 are the internal energies at 0K and 298.15K, respectively, and H298 and G298 are the other two energies that can be transferred from U298, respectively. The other 8 tasks are quantum mechanics related to the DFT process.

Task unit. We list the units for 12 QM9 tasks below.

Table 8: Units for 12 tasks in QM9.

α	$\nabla\mathcal{E}$	$\mathcal{E}_{\text{HOMO}}$	$\mathcal{E}_{\text{LUMO}}$	μ	C_v	G	H	R^2	U	U_0	ZPVE
α_0^3	meV	meV	meV	D	$\frac{cal}{mol\cdot K}$	meV	meV	α_0^2	meV	meV	meV

Dataset size and split. There are 133,885 molecules in QM9, where 3,054 are marked as "uncharacterized" and have been filtered out because they are rearranged during geometry optimization. This leads to 130,831 molecules. For data splitting, we use 110K for training, 10K for validation, and 11K for testing.

Others. Current work is using different optimization strategies and different data splits (in terms of the splitting size). During the benchmark, we find that: (1) The performance on QM9 is very robust to either using (i) 110K for training, 10K for validation, 10,831 for test or using (ii) 100K for training, 13,083 for validation and 17,748 for test. (2) The optimization, especially the learning rate scheduler, is very critical. During the benchmarking, we find that using cosine annealing learning rate schedule [90] is generally the most robust.

B.2 Small Molecules: MD17

Task specification. MD17 [8] is a dataset on molecular dynamics simulation. It includes eight tasks, corresponding to eight organic molecules, and each task includes the molecule positions along the potential energy surface (PES), as shown in Fig. 3(b). The goal is to predict the energy-conserving interatomic forces for each atom in each molecule position.

Task unit. The MD17 aims for energy and force prediction. The unit is $\frac{kcal}{mol}$ for energy and $\frac{kcal}{mol\cdot\text{Å}}$ for force.

Dataset size and split. We follow the literature [68, 89, 109, 110] of using 1K for training and 1K for validation, while the test set (from 48K to 991K) is much larger, and we list them below.

Table 9: Dataset size and splits on MD17.

Pretraining	Aspirin	Benzene	Ethanol	Malonaldehyde	Naphthalene	Salicylic	Toluene	Uracil
Train	1K	1K	1K	1K	1K	1K	1K	1K
Validation	1K	1K	1K	1K	1K	1K	1K	1K
Test	209,762	47,863	553,092	991,237	324,250	318,231	440,790	131,770

Others. There are multiple ways to predict the energy, *e.g.*, using the SE(3)-equivariant to predict the forces directly. In Geom3D, we first predict the energy for each position; then, we take the gradient w.r.t. the input position. The Python codes are attached below:

```
from torch.autograd import grad

positions = batch.positions # input positions
energy = model_3D(batch) # energy prediction
force = -grad(outputs=energy, inputs=positions) # force prediction
```

Notice that this holds for all the force prediction tasks, like rMD17 and COLL, which will be introduced below.

Additionally, in Appendix J.2, we will discuss the data normalization for MD prediction.

B.3 Small Molecules: rMD17

Task specification. The revised MD17 (rMD17) dataset [10] is constructed based on the original MD17 dataset. 100K structures were randomly chosen for each type of molecule present in the MD17 dataset. Subsequently, the single-point force and energy calculations were performed for each of these structures using the PBE/def2-SVP

level of theory. The calculations were conducted with tight SCF convergence and a dense DFT integration grid, significantly minimizing noise.

Task unit. The rMD17 aims for energy and force prediction. The unit is $\frac{kcal}{mol}$ for energy and $\frac{kcal}{mol \cdot \text{Å}}$ for force.

Dataset size and split. We use 950 for training, 50 for validation, and 1000 for test.

B.4 Small Molecules: COLL

Task specification. COLL dataset [36] is a collection of configurations obtained from molecular dynamics simulations on molecular collisions. Around 140,000 snapshots were randomly taken from the trajectories of the collision, for each of which the energy and force were calculated using density functional theory (DFT).

Task unit. The rMD17 aims for energy and force prediction. The unit is eV for energy and $eV/\text{Å}$ for force.

Dataset size and split. The published COLL dataset has split the whole data into 120,000 training samples, 10,000 validation samples, and 9,480 testing samples.

B.5 Small Molecules & Proteins Binding: LBA & LEP

Task specification. Ligand-protein binding is formed between a small molecule (ligand) and a target protein. During the binding process, there is a cavity in a protein that can potentially possess suitable properties for binding a small molecule, called pocket [113]. Due to the large volume of protein, Geom3D follows existing works [118] by only taking the binding pocket, where there are no more than 600 atoms for each molecule and protein pair. For the benchmarking, we consider two binding affinity tasks. (1) The first task is ligand binding affinity (LBA) [123]. It is gathered from [124], and the task is to predict the binding affinity strength between a small molecule and a protein pocket. (2) The second task is ligand efficacy prediction (LEP) [34]. We have a molecule bounded to pockets, and the goal is to detect if the same molecule has a higher binding affinity with one pocket compared to the other one.

Task unit. LBA is to predict $pK = -\log(K)$, where K is the binding affinity in Molar units. LEP has no unit since it is a classification task.

Dataset size and split. The dataset size and splitting are listed below.

Table 10: Dataset size and splits on LBA & LEP. For LBA, we use split-by-sequence-identity-30: we split protein-ligand complexes such that no protein in the test dataset has more than 30% sequence identity with any protein in the training dataset. For LEP, we split the complex pairs by protein target.

Pretraining	LBA	LEP
Train	3,507	304
Validation	466	110
Test	490	104
Split	split-by-identity-30	split-by-target

B.6 Proteins: ECSingle

Task specification. The Enzyme Commission(EC) Number is a numerical classification of enzymes according to the catalyzed chemical reactions [50]. Therefore, the functions of enzymes and the chemical reaction type they catalyze can be represented by different EC numbers. An example of EC number is $EC3.1.1.4$: 3 represents Hydrolases (the first number represents enzyme class); 3.1 represents Ester Hydrolases (the second number represents enzyme subclass); 3.1.1 represents Carboxylic-ester Hydrolases (the third number represents enzyme sub-subclass); 3.1.1.4 represents Phospholipases (the fourth number represents the specific enzyme). The EC dataset was constructed by Hermosilla et al. [45] for the protein function prediction task. The enzyme reaction data with Enzyme Committee annotations were originally collected from the SIFTS database [14]. Then, all the protein chains were clustered using a 50% similarity threshold. EC numbers that were annotated for at least five clusters were selected and five proteins with less than 100% similarities were selected from each cluster, annotated by the EC number.

Task unit. No unit is available since it is a classification task.

Dataset size and split. ECSingle contains 37,428 protein chains, which were split into 29,215 for training, 2,562 for validation, and 5,651 for testing.

B.7 Proteins: ECMultiple

Task specification. In a manner analogous to the ECSingle task, the ECMultiple task classifies proteins into various three-level and four-level EC numbers. Given a protein's potential for multifunctionality, it can be associated with multiple three- or four-level EC numbers. As illustrated in the ECSingle task, a three-level EC number is represented as 3.1.1.-, while a four-level number takes the form 3.1.1.4. As [39], the testing set is divided into subsets based on sequence identity relative to proteins in the training set. Specifically, the testing set is segmented for proteins exhibiting less than 30%, 40%, 50%, 70%, and 95% sequence similarity to those in the training set. F_{max} is used as the evaluation metric since it is a multi-label classification task.

F_{max}, or the protein-centric maximum F Score [39], is proposed to evaluate the multi-label classification task, where each label can be considered as a binary classification task. Denote $\lambda \in [0, 1]$ as the threshold for the binary classification, p_i^j as the probability for the i-th protein to be classified as true for class j, and $b_i^j \in 0, 1$ as the label for the i-th protein in the j-th class. Then, for each threshold value λ, we first calculate the precision and recall for the i-th protein:

$$\begin{aligned} \text{precision}_i(\lambda) &= \frac{\sum_j^J ((p_i^j \geq \lambda) \cap b_i^j)}{\sum_j^J (p_i^j \geq \lambda)} \\ \text{recall}_i(\lambda) &= \frac{\sum_j^J (p_i^j \geq \lambda)}{\sum_j^J (b_i^j)}. \end{aligned} \tag{5}$$

Then, we calculate the average precision and recall for each λ over all the proteins. The denominator of the average precision represents the number of proteins with at least one prediction over the threshold:

$$\begin{aligned} \text{precision}(\lambda) &= \frac{\sum_i^N precision_i(\lambda)}{\sum_i^N ((\sum_j^J (p_i^j \geq \lambda)) \geq 1)} \\ \text{recall}(\lambda) &= \frac{\sum_i^N recall_i(\lambda)}{N}. \end{aligned} \tag{6}$$

Finally, F_{max} is the maximum F score for $\lambda \in [0, 1]$:

$$F_{max} = \max_{\lambda \in [0,1]} \frac{2 \cdot precision(\lambda) \cdot recall(\lambda)}{precision(\lambda) + recall(\lambda)}. \tag{7}$$

Task unit. No unit is available since it is a classification task.

Dataset size and split. ECMultiple contains 19,198 protein chains, which are split into 15,550 for training, 1,729 for validation, and 1,919 for testing. The testing set is further split into: 720 for Tesing_<30%, 902 for Tesing_<40%, 1,117 for Tesing_<50%, 1,476 for Tesing_<70%, and 1,919 for Tesing_<95%. Notice that these sub-testing sets can have overlaps.

B.8 Proteins: Fold

Task specification. Proteins can be hierarchically divided into different levels: Family, Superfamily, and Fold based on their sequence similarity, structure similarity, and evolutionary relations [94]. Proteins with (1) $\geq$30% residue identities or (2) lower residue identities but have similar functions are grouped into the same Family. A Superfamily is for families whose proteins have low residue identities but their structural and functional features suggest a possible same evolutionary origin. A Fold is for proteins sharing the same major secondary structures with the same arrangement and topological connections.

Based on the SCOP 1.75 database, all the fold categories can be grouped into seven structural classes with in total of 1195 fold types [75]: (a) all α proteins (primarily formed by $\alpha-$helices, 284 folds), (b) all β proteins (primarily formed by $\beta-$sheets, 174 folds), (c) α/β proteins (α-helices and β-strands interspersed, 147 folds), (d) $\alpha + \beta$ proteins (α-helices and β-strands segregated, 376 folds), (e) multi-domain proteins (66 folds), (f) membrane and cell surface proteins and peptides (58 folds), and (g) small proteins (90 folds). DeepSF [47] proposed a three-level redundancy removal at fold superfamily/family levels, resulting in three subsets for testing.

- **Fold testing set** Firstly, the proteins are split into Fold-level training set and testing set, where the training set and testing set don't share the same superfamily.
- **Superfamily testing set** Then, the Fold-level training set is split into Superfamily-level training set and testing set, where they don't share the same family.
- **Family testing set** Finally, the Superfamily-level training set is split into Family-level training set and testing set, where for proteins in the same family, 80% of them are used for training and 20% of them are used for testing.

Task unit. No unit is available since they are classification tasks.

Dataset size and split. FOLD contains 16,292 proteins, and we follow [47]: 12,312 training samples, 736 validation samples, 3,244 testing samples. The testing samples contain 3 sub testsets: 718 for folding testset, 1,254 for superfamily testset, and 1,272 for family testset.

B.9 Proteins: GO

Task specification. Gene Ontology (GO) categorizes terms into three distinct classifications:

- **Molecular Function (MF)** This describes activities at the molecular level. It captures the broad concept of a function without delving into specifics such as its location, the time it occurs, or the molecular or complex entity executing this function. An exemplar term under this category is "oxidoreductase activity."
- **Biological Process (BP)** This pertains to broader biological objectives achieved through one or more molecular functions. For instance, "cell division" falls under this category.
- **Cellular Component (CC)** This denotes the specific locations within or outside a cell where a gene product is active. It encompasses both subcellular structures and macromolecular complexes, with terms like "cytosolic large ribosomal subunit" being illustrative of this category [12].

For each of these categories, proteins can be affiliated with several GO terms. In the context of the testing set, it is divided based on sequence similarity with the training set proteins, specifically for those with less than 30%, 40%, 50%, 70%, and 95% similarity. Given that this is a multi-label classification task, the evaluation metric employed is F_{max} described before.

Task unit. No unit is available since it is a classification task.

Dataset size and split. GO contains 36,632 protein chains, which were split into 29,894 for training, 3,322 for validation, and 3,416 for testing. The testing set is further split into: 1,717 for Tesing_<30%, 1,937 for Tesing_<40%, 2,199 for Tesing_<50%, 2,733 for Tesing_<70%, and 3,416 for Tesing_<95%. The sub-testing sets can overlap with each other.

B.10 Proteins: MSP

Task specification. The Mutation Stability Prediction (MSP) task, as proposed in [118], aims to predict whether a protein's stability increases following a mutation, categorizing it as a binary classification task. The SKEMPI database, documented in [56], catalogs mutations present in protein–protein interactions along with their effects on binding affinity and various other attributes. To construct the MSP dataset, single-point mutations are modeled on the wild-type protein sequence, thereby producing the mutated protein variant. A single-point mutation refers to instances where a lone base pair is added, removed, or modified, which may subsequently alter the protein sequence. During the training process, the model independently generates representations for both the wild-type protein and its mutated counterpart. The proteins in the testing set have a <30% sequence similarity with proteins in the training set.

Task unit. No unit is available since it is a classification task.

Dataset size and split. MSP contains 4,184 protein chains, which were split into 2,864 for training, 937 for validation, and 347 for testing.

B.11 Proteins: PSR

Task specification. The Critical Assessment of Structure Prediction (CASP) is a prestigious international competition that focuses on 3D protein structure prediction [71]. The Protein Structure Ranking (PSR) dataset has been curated from protein structures submitted to CASP, with the primary objective being the prediction of the Global Distance Test (GDT_TS) score between the predicted and experimentally determined structures. As such, this constitutes a regression task. As outlined on the official CASP website, the computation of the GDT_TS score includes the following steps:

(1) Superimposition of the predicted structure onto the true structure. (2) Calculation of pairwise distances between residues in the predicted structure and their respective counterparts in the true structure post-superimposition. (3) Determination of the percentage of residues that align within four distinct distance thresholds. (4) The GDT_TS score is derived by averaging the percentages obtained in the previous step.

In the CASP competition, participants are typically given an experimentally determined protein structure, along with a set of decoy structures. These decoys are generated using various computational modeling techniques and closely resemble the true protein in terms of structure. In other words, a true protein is associated with a set of decoys. The evaluation process in CASP not only assesses the proximity of predicted protein structures to the true

structure but also involves ranking the predicted structures relative to the decoys, for a more robust assessment. Correspondingly, we include both Global Spearman's ρ and Mean Spearman's ρ in the evaluation metrics. Global Spearman's ρ is simply the correlation between the predicted GDT_TS score and the ground truth by calculating the Spearman's ρ for all samples. In comparison, for Mean Spearman's ρ, we first separately calculate the Spearman's ρ for decoys corresponding to the same protein and then take the average of these Spearman's ρ.

Task unit. GDT_TS has no units.

Dataset size and split. PSR contains 44,214 protein chains, which were split into 25,400 for training, 2,800 for validation, and 16,014 for testing.

B.12 Crystalline Materials: MatBench

Task specification. MatBench [21] is a test suite for benchmarking 13 machine learning model performances for predicting different material properties. The dataset size for these tasks varies from 312 to 132k. The MatBench dataset has been pre-processed to clean up the task-irrelevant and unphysical-computed data. For benchmarking, we take 8 regression tasks with crystal structure data. These tasks are [16, 22, 55] Formation energy per Perovskite cell (Per. E_{form}), Refractive index (Dielectric), Shear modulus ($log_{10}G$), Bulk modulus($log_{10}K$), exfoliation energy (E_{exfo}), frequency at last phonon PhDOS peak (Phonons), band gap (Band Gap), and formation energy (E_{form}). Detailed explanations are as below:

- Perovskites: predicting formation energy from the crystal structure.
- Dielectric: predicting refractive index from the crystal structure.
- $log_{10}G$: predicting DFT log10 VRH-average shear modulus from crystal structure.
- $log_{10}K$: predicting DFT log10 VRH-average bulk modulus from crystal structure.
- E_{exfo}: predicting exfoliation energies from the crystal structure.
- Phonons: predicting vibration properties from the crystal structure.
- Band Gap: predicting DFT PBE band gap from the crystal structure.
- E_{form}: predicting DFT formation energy from the crystal structure.

Task unit. The unit for each task is listed below.

Dataset size and split. The dataset size for each task is listed above. For benchmarking, we take 60%-20%-20% as training-validation-testing for all tasks.

Table 11: Unit, dataset size, and naming specifications for MatBench.

Column in MatBench	Perovskites	Dielectric	log gvrh	log kvrh	jdft2d	Phonons	Band Gap	E Form
Task Name in Table 6	Per. E_{form}	Dielectric	$log_{10}G$	$log_{10}K$	E_{exfo}	Phonons	Band Gap	E_{form}
Size	18,928	4,764	10,987	10,987	636	1,265	106,113	132,752
Unit	eV	–	log_{10} GPa	log_{10} GPa	meV	cm^{-1}	eV	eV/atom

B.13 Crystalline Materials: QMOF

Task specification. QMOF [107] is a database containing 20,425 metal–organic frameworks (MOFs) with quantum-chemical properties generated using density functional theory (DFT) calculations. The task is to predict the band gap, the energy gap between the valence band and the conduction band.

Task unit. The unit for the band gap task is eV.

Dataset size and split. As mentioned above, there are 20,425 MOFs, and we take 80%-10%-10% for training-validation-testing.

C Group Representation and Equivariance

Symmetry is everywhere on Earth, such as in animals, plants, and molecules. The group theory is the most expressive tool to depict such physical symmetry. In this section, we would like to go through certain key concepts in group theory.

Symmetry is the collection of all transformations under which an object is invariant. The readers can easily check that these transformations are automatically invertible and form a group, where the group multiplication is identified with the composition operation of two transformations. From a dynamical system point of view, symmetries are essential for reducing the degree of freedom of a system. For example, Noether's first theorem states that every differentiable symmetry of a physical system with conservative forces has a corresponding conservation law [96]. Therefore, symmetries form an important source of inductive bias that can shed light on the design of neural networks for modeling physical systems.

Type-0, type-1 and higher-order particles are critical concepts in describing physical word. In general, different orders of spherical harmonics exhibit varying degrees of angular variation across the sphere's surface. This variation refers to how quickly the function changes as you move around in different directions on the sphere. Lower-order spherical harmonics have smoother angular patterns with slower rates of change, while higher-order harmonics have more rapid changes in angular directions. In concrete, type-0 features include pairwise distance, and (dihedral) angle information, and type-1 features cover 3D coordinates, velocities, and forces.

C.1 Group

A **group** is a set G equipped with an operator (group product) $\times$, and they need to follow three rules:

1. It contains an identity element $\boldsymbol{e} \in G$, s.t. $\boldsymbol{ae} = \boldsymbol{ea} = \boldsymbol{a}, \forall \boldsymbol{a} \in G$.
2. Associativity rule $(\boldsymbol{ab})\boldsymbol{c} = \boldsymbol{a}(\boldsymbol{bc})$.
3. Each element has an inverse $\boldsymbol{a}\boldsymbol{a}^{-1} = \boldsymbol{a}^{-1}\boldsymbol{a} = \boldsymbol{e}$.

Below we list several well-known groups:

- **O(n)** is an n-dimensional **orthogonal group** that consists of rotation and reflections.
- **SO(n)** is a **special orthogonal group** that only consists of rotations.
- **E(n)** is an n-dimensional **Euclidean group** that consists of rotations, translations, and reflections.
- **SE(n)** is an n-dimensional **special Euclidean group**, which comprises arbitrary combinations of rotations and translations (no reflections).
- **Lie Group** is a group whose elements form a differentiable manifold. All the groups above are specific examples of the Lie Group.

C.2 Group Representation and Irreducible Group Representation

Group representation is a mapping from the group G to the group of linear transformations of a vector space X with dimension d (see [138] for more rigorous definition):

$$\rho_X(\cdot) : G \to \mathbb{R}^{d\times d} \qquad \text{s.t.} \quad \rho(\boldsymbol{e}) = 1 \ \ \wedge \ \ \rho_X(\boldsymbol{a})\rho_X(\boldsymbol{b}) = \rho_X(\boldsymbol{a}\times\boldsymbol{b}),\ \forall \boldsymbol{a}, \boldsymbol{b} \in G. \tag{8}$$

During modeling, the X space can be the input 3D Euclidean space, the equivariant vector space in the intermediate layers, or the output force space. This enables the definition of equivariance as in Appendix C.3.

Group representation of SO(3) can be applied to any n-dimensional vector space. If we map SO(3) to the 3D Euclidean space (*i.e.*, $n = 3$), the group representation has the same formula as the rotation matrix.

Irreducible representations of rotations The irreducible representations (irreps) of SO(3) are indexed by the integers 0, 1, 2, ..., and we call this index l. The l-irrep is of dimension $2l + 1$. $l = 0$ (dimension 1) corresponds to scalars and $l = 1$ (dimension 3) corresponds to vectors.

C.3 Equivariance and Invariance

Equivariance is the property for the geometric modeling function $f : X \to Y$, and we want to design a function f that is equivariant as:

$$f(\rho_X(\boldsymbol{a})\boldsymbol{x}) = \rho_Y(\boldsymbol{a})f(\boldsymbol{x}), \ \ \forall \boldsymbol{a} \in G, \boldsymbol{x} \in X. \tag{9}$$

How to understand this in the molecule discovery scenarios? $\rho_X(g)$ is the group representation on the input space, like atom coordinates; and $\rho_Y(g)$ is the group representation on the output space $Y = f(X)$, *e.g.*, the force field space. Equivariance modeling in Eq. (9) is essentially saying that the designed deep learning model f is modeling the whole transformation trajectory (*e.g.*, rotation for SO(3)-group) on the molecule conformations, and the output is the transformed $\hat{y}$ accordingly.

Note that in deep learning, a function with learned parameters can be abstracted as $f : W \times X \to Y$, where $w \in W$ is a choice of learned parameters (or weights). The parameters are scalars, *i.e.*, they don't transform

under a transformation of E(3)/SE(3). This implies that weights are scalars and are invariant under any choice of coordinate system.

Invariance is a special type of equivariance where

$$f(\rho_X(\boldsymbol{a})\boldsymbol{x}) = f(\boldsymbol{x}), \quad \forall \boldsymbol{a} \in G, \boldsymbol{x} \in X, \tag{10}$$

with $\rho_Y(g)$ as the identity $\forall g \in G$.

Thus, group and group representation help define the equivariance condition for f to follow. Then, the question turns to how to design such invariant or equivariant f.

- In Sec. 3.2, we introduced the invariant geometric models.
- In Sec. 3.3, we briefly discussed two main categories of equivariant geometric models: the spherical frame basis model and the vector frame basis model. In the following, we will introduce both in more detail in Appendices D and E, respectively.

Through lifting from the original geometric space to its frame bundle (see [49] for the precise definition), equivariant operations like covariant derivatives are realized in an invariant way. From a practical perspective, the lifting operation can be alternatively replaced by scalarization by equivariant frames. See [19, 20] for an illustration. Therefore, invariance and equivariance are just two equivariant descriptions of characterizing symmetry that can be transformed into each other through frames.

One thing we want to highlight is that convolutional neural networks (CNNs) on images are translation-equivariant on $\mathbb{R}^2$, which demonstrates the power of encoding symmetry into the deep neural network architectures.

D Equivariance with Spherical Frame Basis

First, we would like to give a high-level idea of this basis:

- It introduces the spherical harmonics as the basis and maps all the points into such a space.
- The mapping from 3D Euclidean space to the spherical harmonics space satisfies the E(3)/SE(3)-equivariance property as defined Eq. (9).
- Based on such basis, we can design a message-passing framework to learn the desired properties.

Then, we would like to refer to Figure 2 in SEGNN ArXiv version v3. It nicely illustrates how the equivariance works in the spherical harmonics space.

Spherical Harmonics The spherical harmonics are functions from points on the sphere to vectors, or more rigoriously:

Definition 1. *The spherical harmonics are a family o functions Y^l from the unit sphere to the irrep D^l. For each $l = 0, 1, 2...$, the spherical harmonics can be seen as a vector of $2l+1$ functions $Y^l(\vec{x}) = \big(Y^l_{-l}(\vec{x}), Y^l_{-l+1}(\vec{x}), ..., Y^l_l(\vec{x})\big)$. Each Y^l is equivariant to SO(3) with respect to the irrep of the same order,* i.e.*,*

$$Y^l_m(R\vec{x}) = \sum_{n=-1}^{l} D^l(R)_{mn} Y^l_n(\vec{x}), \tag{11}$$

where R is any rotation matrix and D^l are the irreducible representation of SO(3). They are normalized $\|Y^l(\vec{x})\| = 1$ when evaluated on the sphere $\|\vec{x}\| = 1$.

According to Eq. (9), Eq. (11) satisfies the equivariance property: the input space X is the 3D Euclidean space, and the output space Y is the Spherical Harmonics space.

Some key points we would like to highlight:

- Sphere $\mathbb{S}^2$ is not a group, but it is a homogeneous space of SO(3).
- The decomposition into the irreducible group representations makes it steerable.
- The parameter l is named the **rotation order**.

Model Design With the spherical basis, we can design our own geometric models. Notice that during the modeling process, all the variables are tensors.

For instance, we can take the vector $\boldsymbol{r}_j - \boldsymbol{r}_i$ as the vector in $Y^l_m(\frac{\boldsymbol{r}_j - \boldsymbol{r}_i}{\|\boldsymbol{r}_j - \boldsymbol{r}_i\|})$. As shown in Eq. (11), this is rotation-equivariant. And we can easily see $\boldsymbol{r}_j - \boldsymbol{r}_i$ is translation-equivariant.

This term can be naturally adopted for the edge embedding under the message passing framework [38], and we can parameterize it with a radial term [112] as[2]:

$$\boldsymbol{h}_{i,j} = \text{Radial}(\|\boldsymbol{r}_j - \boldsymbol{r}_i\|) Y^l_m(\frac{\boldsymbol{r}_j - \boldsymbol{r}_i}{\|\boldsymbol{r}_j - \boldsymbol{r}_i\|}), \tag{12}$$

where the radial function is invariant with the pairwise distance as the input. This is for the message function. Then generally, for the update and aggregate function of node-level tensor $\boldsymbol{v}_i$, we have two options:

$$\boldsymbol{v}_i = \begin{cases} \boldsymbol{v}_i + \sum_{j \in \mathcal{N}(i)} \boldsymbol{h}_{i,j} + \boldsymbol{v}_j \\ \boldsymbol{v}_i + \sum_{j \in \mathcal{N}(i)} \boldsymbol{h}_{i,j} \otimes \boldsymbol{v}_j, \end{cases} \tag{13}$$

where the update can be done either with plus or multiplication. Note that $\otimes$ is the tensor product, which can be calculated using the *Clebsch-Gordan coefficients*. Please refer to [37] for more details.

[2] Notice that the index of angular momentum in the spherical frame is very important, yet we ignore them here for brevity. Please refer to the papers for more rigorous definitions.

E Equivariance with Vector Frame Basis

In physics, the vector frame is equivalent to the coordinate system. For example, we may assign a frame to all observers, although different observers may collect different data under different frames, the underlying physics law should be the same. In other words, denote the physics law by f, then f should be an equivariant function.

Since there are three orthogonal directions in $\mathbf{R}^3$, a vector frame in $\mathbf{R}^3$ consists of three orthogonal vectors:

$$F = (\boldsymbol{e}_1, \boldsymbol{e}_2, \boldsymbol{e}_3).$$

Once equipped with a vector frame (coordinate system), we can project all geometric quantities to this vector frame. For example, an abstract vector $\boldsymbol{r} \in \mathbf{R}^3$ can be written as $\boldsymbol{r} = (r_1, r_2, r_3)$ under vector frame F, if: $\boldsymbol{r} = r_1\boldsymbol{e}_1 + r_2\boldsymbol{e}_2 + r_3\boldsymbol{e}_3$. An equivariant vector frame further requires the three orthonormal vectors in $(\boldsymbol{e}_1, \boldsymbol{e}_2, \boldsymbol{e}_3)$ to be equivariant. Intuitively, an equivariant vector frame will transform according to the global rotation or translation of the whole system. Once equipped with an equivariant vector frame, we can project equivariant vectors into this vector frame:

$$\boldsymbol{r} = \tilde{r}_1\boldsymbol{e}_1 + \tilde{r}_2\boldsymbol{e}_2 + \tilde{r}_3\boldsymbol{e}_3. \tag{14}$$

We call the process of $\boldsymbol{r} \to \tilde{r} := (\tilde{r}_1, \tilde{r}_2, \tilde{r}_3)$ the **projection** operation. Since $\tilde{r}_i = \boldsymbol{e}_i \cdot \boldsymbol{r}_i$ is expressed as an inner product between equivariant vectors, we know that $\tilde{r}$ consists of scalars.

We assign an equivariant vector frame to each node/edge to incorporate equivariant frames with graph message passing. Therefore, we call them the local frames. For example, consider node i and one of its neighbors j with positions $\boldsymbol{x}_i$ and $\boldsymbol{x}_j$, respectively. One way to construct the equivariant frame is the orthonormal frame using the Gram-Schmidt, like Clofnet [20] and MoleculeSDE [79]. The vector frame $\mathcal{F}_{ij} := (\boldsymbol{e}_1^{ij}, \boldsymbol{e}_2^{ij}, \boldsymbol{e}_3^{ij})$ is defined with respect to $\boldsymbol{x}_i$ and $\boldsymbol{x}_j$ as follows:

$$\left(\frac{\boldsymbol{x}_i - \boldsymbol{x}_j}{\|\boldsymbol{x}_i - \boldsymbol{x}_j\|}, \frac{\boldsymbol{x}_i \times \boldsymbol{x}_j}{\|\boldsymbol{x}_i \times \boldsymbol{x}_j\|}, \frac{\boldsymbol{x}_i - \boldsymbol{x}_j}{\|\boldsymbol{x}_i - \boldsymbol{x}_j\|} \times \frac{\boldsymbol{x}_i \times \boldsymbol{x}_j}{\|\boldsymbol{x}_i \times \boldsymbol{x}_j\|}\right). \tag{15}$$

The Gram-Schmidt orthogonalization makes sure that the Local-Frame$(\boldsymbol{r}_i, \boldsymbol{r}_j)$ is orthonormal. However, there also exist other ways to construct the vector frames, like using the protein backbone structures [29, 53]. Finally, it's worth mentioning that global frames can be built by pooling local frames. For example, a graph-level equivariant frame is obtained by aggregating node frames and implementing the Gram-Schmidt orthogonalization. However, the Newton dynamics experiments in [20] demonstrated that the global frame's performance is worse than edge local frames. Therefore, although edge-, node-, and global- frames are equal in terms of equivariance, the optimization properties of different equivariant frames depend varies according to different scientific datasets.

F Other Geometric Modeling (Featurization and Lie Group)

We also want to acknowledge other equivariant modeling methods.

Featurization. OrbNet [99] models the atomic orbital, the description of the location and wave-like behavior of electrons in atoms. This possesses a finer-grained featurization level than other methods. Voxel means that we discretize the 3D Euclidean space into bins, and recent work [33] empirically shows that this also applies to geometry learning tasks.

Equivariance modeling with Lie group. In previous sections, equivariant algorithms are viewed as mappings from a 3D point cloud (which discretizes the 3D Euclidean space) to another 3D point cloud, or as mappings to invariant quantities. From this point of view, the symmetry group $E(3)/SE(3)$ manifests itself as a group action transforming the Euclidean space. However, it is worth noting that this action is transitive in the sense that any two points in 3D Euclidean space can be transformed from one to the other through a combination of translation and rotation. In mathematical terms, the 3D Euclidean space is a **homogeneous space** of the group $E(3)$. Exploiting this observation, LieConv [32] and LieTransformer [52] elevate the 3D point cloud to the $E(3)$ group and perform parameterized group convolution (and attention) operations, ensuring equivariance, to obtain an equivariant embedding on the group $E(3)$. Finally, by projecting the result back to $\mathbf{R}^3$ (taking the quotient), an equivariant map from $\mathbf{R}^3$ to the output space is obtained. The main limitation of Lie group modeling lies in the convolution operation, which often involves high-dimensional integration and requires approximation for most groups. For more in-depth insights into the properties of convolution on groups, we refer readers to [5]. Another lifting of $\mathbf{R}^3$ is to lift it to the SO(3) frame bundle, such that the SO(3) group transforms one orthonormal frame to another orthonormal frame transitively. This lifting also inspires the design of [19, 20].

G Expressive Power: from Invariance to Equivariance

Equivariant neural networks are constructed for equivariant tasks. That is, to approximate an equivariant function. Compared with ordinary neural networks, a natural question arises: *Does an equivariant neural network have the universal approximation property whiten the equivariant function class?* By the novel D-spanning concept [24], this question is partially answered. The author further proposed two types of equivariant architectures that can enjoy the D-spanning property: 1. the G-equivariant polynomials enhanced TFN; 2. the minimal universal architecture constructed by tensor products. Therefore, at least in terms of universal approximation, an equivariant neural network doesn't necessarily require irreducible representations and Clebsch-Gordan decomposition. The reader can check [20] for how to realize the minimal universal architecture in an invariant way through equivariant frames and tensorized graph neural networks (*e.g.*, [65]). Informally, we conclude that an invariant graph neural network equipped with a powerful message-passing mechanism can achieve the universal approximation property. Another proof strategy of the universality of invariant scalars that doesn't rely on theories of tensorized graph neural networks can be found in [120].

However, the mainstream GNN is usually based on a 1-hop message passing mechanism (although tensorized graph neural networks have empirically shown competitive performances in molecular tasks) for computational efficiency. For 1-hop message passing mechanisms (including node-based transformers), our previous conclusion no longer holds, and vector (or higher order tensors) updates are necessary for enhancing the expressiveness power. The reader can consult the concrete example from PaiNN [110] to illustrate this point.

More precisely, We denote the nodes in Figure 1 of [110] as $\{a : white, b : blue, c : red, d : white\}$, and we consider whether the message of b and c received from their 1-hop neighbors can discriminate the two different geometric structures. For node b, the invariant geometric information we can get from 1-hop neighbors are the relative distance d_{ab} and d_{bc} and their intersection angle α_1. Since the relative distances of the two structures remain equal, only the angle information is useful. Similarly, for node c, we have the intersection angle α_2. Unfortunately, the intersection angles α_1 and α_2 of the two structures are still the same, and we conclude that invariant features are insufficient for discriminating the two different structures. On the other hand, [110] showed that by introducing directional vector features (type-1 equivariant steerable features), we are able to solve the problem in this special case, which proves the superiority of 'equivariance' over 'invariance' within 1-hop message passing mechanisms. Another invariant way of filling in this type of expressiveness gaps systematically is to introduce the information of frame transitions **FTE**, as was demonstrated in [19].

Vector update is just a special case of the more general higher-order tensor updates. To merge general equivariant tensors into our GNN, we can either utilize tensor products of vector frames [19], or introduce the concepts of spherical harmonics, which form a complete basis in the sense of irreducible representations of group $SO(3)$ and $O(3)$. However, to express the output of the tensor product between spherical harmonics as a combination of spherical harmonics is nontrivial. Fortunately, this procedure has been studied by quantum physicists, which is named after the Clebsch-Gordan decomposition (coefficients) [93]. Combining these blocks, we can build convolution or attention-based equivariant graph neural networks, see [37, 73] for detailed constructions.

H Architecture for Geometric Representation

In this section, we are going to give a brief review of certain advanced geometric models, and a summary of more methods can be found in Table 12. Meanwhile, we will keep updating more advanced models.

We include all the hyperparameters in this GitHub repository. We are sure that we won't be able to tune all the hyperparameters, yet we want to claim that our reported results are reproducible using the hyperparameters listed above. In the future, we appreciate any contribution to do more searching on this.

Table 12: Categorization on geometric methods. For pretraining methods, the categorization is based on the pretraining algorithms and backbone models are not considered.

	Model	Invariance	Equivariance	
			Spherical Frame	Vector Frame
Representation	SchNet [109]	✓		
	DimeNet [68]	✓		
	SphereNet [89]	✓		
	GemNet [67]	✓		
	IEConv [45]	✓		
	GearNet [142]	✓		
	ProNet [122]	✓		
	TFN [35]		✓	
	SEGNN [4]		✓	
	SE(3)-Trans [35]		✓	
	NequIP [3]		✓	
	Allegro [95]		✓	
	Equiformer [73]		✓	
	PaiNN [110]			✓
	GVP-GNN [62]			✓
	CDConv [29]			✓
	EGNN [108]		✓	✓
Pretraining	GraphMVP [86]	✓		
	3D InfoMax [114]	✓		
	GeoSSL-RR [81]	✓		
	GeoSSL-EBM-NCE [81]	✓		
	GeoSSL-InfoNCE [81]	✓		
	GeoSSL-DDM [81]	✓		
	GeoSSL-DDM-1L [136]	✓		
	3D-EMGP [59]			✓
	MoleculeSDE [79]			✓

Generally, all the algorithms can be classified into two categories: SE(3)-invariant and SE(3)-equivariant. Note that, rigorously, SE(3)-invariant is also SE(3)-equivariant. Here we follow the definition in [37][3]:

- SE(3)-invariant models only operate on scalars ($l = 0$) which interact thought simple scalar multiplication. These scalars include pairwise distance, triplet-wise angle, etc, that will not change under rotation. In other words, the SE(3)-invariant pre-compute the invariant features and throw away the coordinate system.
- SE(3)-equivariant models keep the coordinate system and if the coordinate system changes, the outputs change accordingly. These models have been believed to empower larger model capacity [3, 37] with $l > 0$ quantities.

There are other variants, like the activation functions, the number of layers, normalization layers, etc. In this section, we will stick to the key module, *i.e.*, the SE(3)-invariant and SE(3)-equivariant modules for each backbone model.

The aggregation function is the same as:

$$h_i' = \text{aggregate}_{j \in \mathcal{N}(i)}(m_{ij}). \tag{16}$$

In the following, we will be mainly discussing the message-passing function as below.

[3] Also a video by Tess et al, link is here.

H.1 Invariant Models

SchNet SchNet [109] simply handles a molecule by feeding in the pairwise distance and throws them into the message-passing style GNN.

$$m_{ij} = \text{MLP}(h_j, \mathbf{RBF}(d_{ij})). \tag{17}$$

where $\mathbf{RBF}(\cdot)$ is the RBF kernel.

DimeNet The directional message passing neural network (DimeNet and DimeNet++) [69]. The message passing function in DimeNet is two-hop instead of one-hop. Such message-passing step is similar to directed message-passing neural network (D-MPNN) [132], and it can reduce the redundancy during the message passing process.

$$m_{ji}^{l+1} = \sum_{k \in \mathcal{N}_j \setminus \{i\}} \text{MLP}(m_{ji}^{l}, \mathbf{RBF}(d_{ji}), \mathbf{SBF}(d_{kj}, \alpha_{\angle kij})), \tag{18}$$

where $\text{SBF}_{ln}(d_{kj}, \alpha_{\angle kij}) = \sqrt{\frac{2}{c^3 j_{l+1}^2(z_{ln})}} j_l(\frac{z_{ln}}{c} d_{kj}) Y_l^0(\alpha)$ is the spherical Fourier-Bessel (spherical harmonics) basis, a joint 2D basis for distance d_{kj} and angle $\alpha_{\angle kij}$.

SphereNet SphereNet [89] is an extension of DimeNet by further modeling the dihedral angle. It first adopts the spherical Fourier-Bessel (spherical harmonics) basis for dihedral angle modeling, namely

$$\text{SBF}(d, \theta, \phi) = j_l(\frac{\beta_{l_n}}{c} d) Y_l^m(\theta, \phi). \tag{19}$$

In addition, the basic operation of SphereNet is based on the quadruplets: r, s, q_1, and these three nodes formulate a reference plan to provide the polar angle to the point q_2. However, SphereNet provides an acceleration module, by projecting all the neighborhoods of s, in an anticlockwise direction, and the reference plan for each node q_i is determined by r, s and q_{i-1}. Thus, the computational complexity is reduced by one order of magnitude. SphereNet further considers the following for distance and angle modeling:

$$\text{CBF}_{ln}(d_{kj}, \alpha_{\angle kij}) = \sqrt{\frac{2}{c^3 j_{l+1}^2(z_{ln})}} j_l(\frac{z_{ln}}{c} d_{kj}) Y_l^0(\alpha), \qquad \text{RBF}_{ln}(d_{kj}) = \sqrt{\frac{2}{c}} \frac{\sin(\frac{n\pi}{c} d)}{d}. \tag{20}$$

GemNet GemNet [67] further extends DimeNet and SphereNet. It explicitly models the dihedral angle. Notice that both GemNet and SphereNet are using the SBF for dihedral angle modeling, yet the difference is that GemNet is using edge-based 2-hop information, *i.e.*, the torsion angle, while SphereNet is using the edge-based 1-hop information. Thus, GemNet is expected to possess richer information, while the trade-off is the larger computational efficiency (by one order of magnitude): GemNet has the complexity of $O(nk^3)$ while SphereNet is $O(nk^2)$.

GearNet and ProNet for Macromolecules The invariant modeling for macromolecules follows the same strategy as the previous geometric models. The only difference, as illustrated in Appendix A, is that the modeling particles are the protein backbones ($N - C_\alpha - C$) or residues (C_α). GearNet [142] and ProNet [122] are modeling the pairwise distance and dihedral angles at different scales.

H.2 Equivariant Models with Spherical Frame Basis

TFN Tensor field network (TFN) [112] first introduces using the SE(3)-equivariance group symmetry for modeling the geometric molecule data. As will be introduced later, the translation-equivariance can be easily achieved by considering the relative coordinates, *i.e.*, $\vec{\boldsymbol{r}} = \boldsymbol{r}_i - \boldsymbol{r}_j$. Then the problem is simplified to design an SO(3)-equivariant model. To handle this, TFN first proposes a general **framework** by using the spherical harmonics as the basis satisfying the following for all $\boldsymbol{a} \in SO(3)$ and $\hat{\boldsymbol{r}}$:

$$Y_m^l(R(\boldsymbol{a})\hat{\boldsymbol{r}}) = \sum_{m'=-l}^{l} D_{mm'}^{(l)}(\boldsymbol{a}) Y_{m'}^{(l)}(\hat{\boldsymbol{r}}), \tag{21}$$

where $\hat{\boldsymbol{r}} = \vec{\boldsymbol{r}}/\|\vec{\boldsymbol{r}}\|$, and D^l is the irreducible representations of SO(3) to $(2l+1) \times (2l+1)$-dim matrices (*i.e.*, the Wigner-D matrices). This is one design criterion for SE(3)-equivariant neural networks with the spherical harmonics frame. In specific, to design an SE(3)-equivariant network, we take the following form:

$$F(\vec{\boldsymbol{r}}) = W(\boldsymbol{r}) Y(\hat{\boldsymbol{r}}), \tag{22}$$

where $\boldsymbol{r} = \|\vec{\boldsymbol{r}}\|$, $W(\cdot)$ is the learnable function. Thus we are separating the spherical harmonics basis and the radial signal. For modeling, we only need to learn the $W(\cdot)$ on the radial. Then we use the Clebsch-Gordan tensor product for message passing on node i, which is:

$$\boldsymbol{v}_i = \boldsymbol{v}_i + \sum_{j \in \mathcal{N}(i)} F(\vec{\boldsymbol{r}}_{ij}) \otimes \boldsymbol{v}_j, \tag{23}$$

where $\otimes$ is the Clebsch-Gordan tensor product. **Note** that for brevity and to give the audience a high-level idea of the spherical frame basis modeling, we omit the **rotation order** and the **channel index** in Eqs. (22) and (23). First, we want to acknowledge that the rotation order is the key to conducting the message passing along tensors, and please refer to the original paper for details. Then for the channel or depth of the message passing layers (notation c in the TFN paper), they are important to expand the model capacity.

To sum up, by far, we can observe that TFN only considers the pairwise information (*i.e.*, 1-hop neighborhood) for SE(3)-equivariance.

SE(3)-Transformer SE(3)-Transformer [35] extends the TFN by introducing an attention score, *i.e.*,

$$\boldsymbol{v}_i = \boldsymbol{v}_i + \sum_{j \in \mathcal{N}(i)} \alpha_{ij} F(\vec{\boldsymbol{r}}_{ij}) \otimes \boldsymbol{v}_j, \tag{24}$$

where α_{ij} is the attention score.

To calculate the attention score, first, we need to define the following:

$$\boldsymbol{q}_i = \bigoplus_{l \geq 0} \sum_{k \geq 0} W_Q^{lk} \boldsymbol{v}_i^k, \qquad \boldsymbol{k}_{ij} = \bigoplus_{l \geq 0} \sum_{k \geq 0} F_K^{lk}(\boldsymbol{r}_j - \boldsymbol{r}_i) \otimes \boldsymbol{v}_j^k, \tag{25}$$

where k and l correspond to the rotation order of the input and output tensor, W_Q is a learnable linear matrix, F_K follows the same formation as Eq. (22), and $\bigoplus$ is the direct sum. Then we can obtain the attention coefficients with dot product as:

$$\alpha_{ij} = \frac{\exp(\boldsymbol{q}_i^T \boldsymbol{k}_{ij})}{\sum_{j' \in \mathcal{N}_i \setminus i} \exp(\boldsymbol{q}_i^T \boldsymbol{k}_{ij'})} \tag{26}$$

Equiformer SE(3)-Trans adopts the dot product attention, and Equiformer [73] extends this with an MLP attention and with higher efficiency. We also want to mention that during modeling, Equiformer has an option of adding extra atom and bond information, and we set this hyperparameter as False for a fair comparison when comparing with other geometric models.

NequIP Neural Equivariant Interatomic Potentials (NequIP) [3] is a follow-up of TFN, which mainly focuses on improving the force prediction. Originally, TFN was directly predicting the $l = 1$ tensor for the force prediction. In NequIP, the output only includes the $l = 1$ tensor, while the force is obtained by taking the gradient with respect to the energy.

There are also other minor architecture design updates, such as adding the skip-connection [44]. Please refer [3] for more details.

Allegro Allegro [95] is a follow-up of NequIP by further modeling a local frame around each atom. In specific, the standard message-passing framework is based on the nodes (or atoms here), while Allegro focuses on the edge-level information.

Difference with Spherical Harmonics in Invariant Modeling As you may notice, the invariant models also adopt the spherical harmonics (or spherical Fourier-Bessel), *e.g.*, Eq. (18) in DimeNet and Eq. (19) in SphereNet and GemNet. However, their usage of the spherical harmonics is different from the spherical frame models discussed in this section.

- In invariant models, the spherical harmonics are used for embedding the angle information, either bond angles or dihedral angles. Such angles are type-0 features, and they are invariant w.r.t. the SO(3) group. Note that this embedding is related to quantum mechanics since the spherical harmonics appear as general solutions of the Schrödinger equations.
- In the spherical frame models, the spherical harmonics are used to serve as the basis for transforming the relative coordinates into tensors, utilizing the fact that spherical harmonics are equivariant functions with respect to the SO(3) group.

Thus, they may follow the same numerical calculation, but their physical meanings are different.

H.3 Equivariant Models with Vector Frame Basis

From a very high-level view, we can view this as first constructing the tensor and then conducting the message-passing between the type-0 tensor and type-1 tensor.

EGNN E(n)-equivariant graph neural network (EGNN) [108] has a very neat design to achieve the E(n)-equivariance property. It constructs the message update function for both the atom positions and atom attributes

simultaneously. Concretely, for edge embedding $\boldsymbol{e}$, input node embedding $\boldsymbol{h}$ and coordinate $\boldsymbol{v} = \boldsymbol{r}$, the l-th layer updates are:

$$\begin{aligned}
\boldsymbol{m}_{ij} &= W_e\big(\boldsymbol{h}_i^l, \boldsymbol{h}_j^l, \|\boldsymbol{v}_i^l - \boldsymbol{v}_j^l\|, \boldsymbol{e}_{ij}\big) \\
\boldsymbol{v}_i^{l+1} &= \boldsymbol{v}_i^l + \sum_{j \neq i} (\boldsymbol{v}_i^l - \boldsymbol{v}_j^l), W_v(\boldsymbol{m}_{ij}) \\
\boldsymbol{m}_i &= \sum_{j \neq i} \boldsymbol{m}_{ij} \\
h_i^{l+1} &= W_h(\boldsymbol{h}_i^l, \boldsymbol{m}_i),
\end{aligned} \tag{27}$$

where W_e, W_v, W_h are learnable parameters. The equivariance can be proved easily and with good efficiency. However, one inherent limitation of EGNN is that it is essentially a global vector frame model and utilizes only one projection (scalarization) dimension, and it does not satisfy the reflection-antisymmetric condition for certain tasks like binding.

PaiNN Polarizable atom interaction neural network (PaiNN) [110] utilizes a multi-channel vector aggregation method, which contains more expressive equivariant vector information than Eq. (27). More precisely, each node of PaiNN maintains a multi-channel vector: $\boldsymbol{v}_i \in \mathbf{R}^{F\times 3}$, where F denotes the channel number. Comparing with Eq. (27), the $\boldsymbol{v}_i \in \mathbf{R}^{1\times 3}$ of EGNN restricted the expressiveness power. [19] provides a geometric explanation of the updating method of PaiNN ((9) of [110]) by the frame transition functions between local vector frames.

CDConv for Macromolecules CDConv [29] models the residue-level information of proteins. In specific, it utilizes the 3D coordinates of C_α as the surrogates to the residue coordinates. Then it builds an orthogonal frame based on the 1D residue sequence. The experimental results show that it can reach promising results on protein structure tasks.

I Complete Results

In the main body, due to space limitations, we cannot provide the results on certain tasks. Here we would like to provide more comprehensive results.

For the results not listed either in the main body or in this section, there are two possible reasons for us to exclude them: (1) We cannot reproduce them using the reported hyperparameters in the original paper, and we may need to do more hyperparameter tuning as the next steps. (2) Some models are too large to fit in the GPU memory, even with batch-size=1.

I.1 Small Molecules: MD17 and rMD17

In Table 2, we select 6 subtasks in MD17 and 6 subtasks in rMD17. Next we will show the complete results of MD17 and rMD17 are in Tables 13 and 14.

Table 13: Results on 8 energy ($\frac{kcal}{mol}$) and force ($\frac{kcal}{mol \cdot \text{Å}}$) prediction tasks in MD17. The evaluation is the mean absolute error. No data normalization is used.

Model	Energy/Force	Aspirin ↓	Benzene ↓	Ethanol ↓	Malonaldehyde ↓	Naphthalene ↓	Salicylic ↓	Toluene ↓	Uracil ↓
SchNet	Energy	0.475	0.117	0.109	0.300	0.167	0.212	0.149	0.170
	Force	1.203	0.380	0.386	0.794	0.587	0.826	0.568	0.773
DimeNet++	Energy	4.168	0.893	1.238	1.385	1.846	2.445	1.484	1.522
	Force	7.212	0.603	0.753	1.842	8.515	1.752	1.037	1.632
EGNN	Energy	17.892	1.142	0.436	0.896	12.177	6.964	4.051	0.854
	Force	3.042	0.736	0.924	1.566	1.136	1.177	1.202	1.367
PaiNN	Energy	27.626	0.095	0.063	0.102	0.622	0.371	0.165	0.111
	Force	0.572	0.053	0.230	0.338	0.132	0.288	0.141	0.201
GemNet-T	Energy	0.684	0.097	4.598	4.966	0.482	0.128	0.098	1.349
	Force	0.558	0.089	0.219	0.433	0.212	0.326	0.174	486.612
SphereNet	Energy	0.244	0.107	1.603	1.559	0.167	0.188	0.113	7.115
	Force	0.546	0.135	0.168	0.667	0.315	0.479	0.194	0.442
SEGNN	Energy	17.774	0.086	0.151	0.247	0.655	2.173	0.624	0.259
	Force	9.003	0.265	0.893	1.249	0.895	2.220	1.138	0.948
NequIP	Energy	8.333	0.355	0.971	2.293	1.032	2.952	1.303	1.266
	Force	23.769	2.383	5.832	12.099	5.247	14.048	6.800	8.060
Allegro	Energy	1.138	0.154	0.258	1.330	0.824	1.114	0.441	0.613
	Force	3.405	0.823	1.412	4.191	3.743	4.934	1.968	3.544
Equiformer	Energy	0.308	0.075	0.096	0.183	0.097	0.189	0.209	0.106
	Force	0.286	0.045	0.142	0.230	0.068	0.200	0.080	0.141

Table 14: Results on 10 energy ($\frac{kcal}{mol}$) and force ($\frac{kcal}{mol \cdot \text{Å}}$) prediction tasks in rMD17. The evaluation is the mean absolute error. Data normalization is used.

Model	Energy/Force	Aspirin ↓	Azobenzene ↓	Benzene ↓	Ethanol ↓	Malonaldehyde ↓	Naphthalene ↓	Paracetamol ↓	Salicylic ↓	Toluene ↓	Uracil ↓
SchNet	Energy	0.534	1.818	0.111	1.757	0.260	0.124	8.138	2.618	0.119	7.029
	Force	1.243	3.596	0.233	0.449	0.862	0.587	2.320	0.878	0.574	0.762
DimeNet++	Energy	2.438	3.955	0.741	1.456	2.317	1.648	2.261	1.555	1.210	2.320
	Force	2.009	1.243	0.340	1.213	7.029	0.629	1.047	0.934	0.921	3.181
EGNN	Energy	17.350	21.333	0.315	0.402	0.534	12.164	26.902	7.794	15.021	1.669
	Force	3.825	2.330	0.529	0.989	1.334	1.183	2.313	1.571	1.165	1.323
PaiNN	Energy	30.156	0.107	0.010	1.170	0.070	5.297	0.117	5.219	0.045	2.478
	Force	0.573	0.326	0.032	0.316	0.377	0.161	0.440	0.321	0.231	0.235
GemNet-T	Energy	5.389	7.770	0.007	1.615	9.496	0.031	2.173	21.411	959.745	994.036
	Force	0.555	0.347	0.033	0.233	0.337	0.154	0.388	0.371	0.400	1.165
SphereNet	Energy	0.304	0.257	0.052	0.072	0.138	0.093	0.183	0.771	20.479	12.211
	Force	0.622	0.532	0.076	0.217	0.500	0.279	0.482	2.088	0.254	0.959
SEGNN	Energy	15.721	3.474	0.270	0.130	0.182	1.110	4.197	1.494	0.814	1.115
	Force	8.549	2.579	0.174	0.846	1.185	0.926	3.191	2.056	1.241	0.966
NequIP	Energy	9.618	1.993	3.048	0.936	2.313	2.089	5.136	3.302	1.306	1.738
	Force	22.904	6.406	1.523	6.027	12.372	5.529	17.574	15.693	7.094	10.220
Allegro	Energy	1.366	0.872	0.029	1.002	0.417	1.756	0.944	1.035	0.437	0.387
	Force	3.186	2.763	0.237	2.799	2.125	3.815	3.081	4.781	2.048	1.939
Equiformer	Energy	0.375	0.127	0.027	0.064	0.085	0.069	0.215	0.143	0.104	0.200
	Force	0.305	0.132	0.020	0.162	0.240	0.070	0.258	0.218	0.077	0.149

I.2 Geometric Pretraining

Single-modal Pretraining. Recent studies have started to explore **single-modal geometric pretraining** on molecules. The GeoSSL paper [80] covers a wide range of geometric pretraining algorithms. The type prediction, distance prediction, and angle prediction predict the masked atom type, pairwise distance, and bond angle, respectively. The 3D InfoGraph predicts whether the node- and graph-level 3D representation are for the same molecule. GeoSSL is a novel geometric pretraining paradigm that maximizes the mutual information (MI) between the original conformation $\boldsymbol{g}_1$ and augmented conformation $\boldsymbol{g}_2$, where $\boldsymbol{g}_2$ is obtained by adding small perturbations to $\boldsymbol{g}_1$. RR, InfoNCE, and EBM-NCE optimize the objective in the latent representation space, either generative or contrastive. GeoSSL-DDM [80] optimizes the same objective function using denoising score matching. GeoSSL-DDM-1L [136] is a special case of GeoSSL-DDM with one layer of denoising. 3D-EMGP [60] geometric pretraining is specifically built on equivariant models, and the goal is to denoise the 3D coordinates directly using a diffusion model. We illustrate these seven algorithms in Fig. 4.

2D-3D Multi-modal Pretraining. Another promising direction is the **multi-modal pretraining on topology and geometry**. GraphMVP [86] first proposes one contrastive objective (EBM-NCE) and one generative objective (variational representation reconstruction, VRR) to optimize the mutual information between the 2D and 3D modalities. Specifically, VRR does the 2D and 3D reconstruction in the latent space. 3D InfoMax [114] is a special case of GraphMVP, with the contrastive part only. MoleculeSDE [79] extends GraphMVP by introducing two SDE models for solving the 2D and 3D reconstruction. An illustration of them is in Fig. 8.

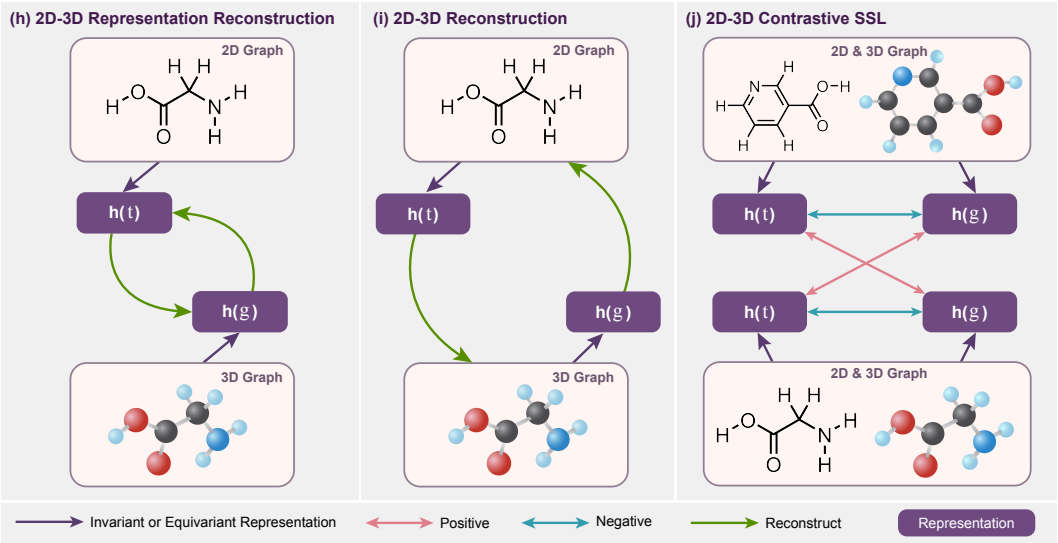

Figure 8: Pipelines for three multi-modal geometric pretraining methods.

In Table 7, we show the pretraining results of using **SchNet as the backbone** and fine-tuning on QM9. The pretraining results of using **SchNet as the backbone** and fine-tuning on MD17 are in Table 15. The pretraining results of using **PaiNN as the backbone** and fine-tuning on QM9 and MD17 are in Tables 16 and 17. For MD17, as will be discussed in Appendix J, we do not consider the data normalization trick. Notice that some pretraining results are skipped due to the collapsed performance.

Table 15: Pretraining results on eight force prediction tasks from MD17, and the backbone model is SchNet. We take 1K for training, 1K for validation, and 48K to 991K molecules for the test concerning different tasks. The evaluation is mean absolute error, and the best results are marked in **bold** and **bold**, respectively.

Pretraining	Aspirin ↓	Benzene ↓	Ethanol ↓	Malonaldehyde ↓	Naphthalene ↓	Salicylic ↓	Toluene ↓	Uracil ↓
– (random init)	1.203	0.380	0.386	0.794	0.587	0.826	0.568	0.773
Supervised	1.867	0.434	0.566	1.106	0.637	13.037	0.607	0.759
Type Prediction	1.383	0.402	0.450	0.879	0.622	1.028	0.662	0.840
Distance Prediction	1.427	0.396	0.434	0.818	0.793	0.952	0.509	1.567
Angle Prediction	1.542	0.447	0.669	1.022	0.680	1.032	0.623	0.768
3D InfoGraph	1.610	0.415	0.560	0.900	0.788	1.278	0.768	1.110
GeoSSL-RR	1.215	0.393	0.514	1.092	0.596	0.847	0.570	0.711
GeoSSL-InfoNCE	1.132	0.395	0.466	0.888	0.542	0.831	0.554	0.664
GeoSSL-EBM-NCE	1.251	0.373	0.457	0.829	0.512	0.990	0.560	0.742
3D InfoMax	1.142	0.388	0.469	0.731	0.785	0.798	0.516	0.640
GraphMVP	1.126	0.377	0.430	0.726	0.498	0.740	0.508	0.620
GeoSSL-DDM-1L	1.364	0.391	0.432	0.830	0.599	0.817	0.628	0.607
GeoSSL-DDM	**1.107**	0.360	0.357	0.737	0.568	0.902	0.484	0.502
MoleculeSDE (VE)	**1.112**	**0.304**	**0.282**	**0.520**	**0.455**	**0.725**	**0.515**	**0.447**
MoleculeSDE (VP)	1.244	**0.315**	**0.338**	**0.488**	**0.432**	**0.712**	**0.478**	**0.468**

Table 16: Pretraining results on 12 quantum mechanics prediction tasks from QM9, and the backbone model is PaiNN. We take 110K for training, 10K for validation, and 11K for testing. The evaluation is mean absolute error, and the best and the second best results are marked in **bold** and **bold**, respectively.

Pretraining	$\alpha \downarrow$	$\nabla\mathcal{E} \downarrow$	$\mathcal{E}_{\text{HOMO}} \downarrow$	$\mathcal{E}_{\text{LUMO}} \downarrow$	$\mu \downarrow$	$C_v \downarrow$	$G \downarrow$	$H \downarrow$	$R^2 \downarrow$	$U \downarrow$	$U_0 \downarrow$	ZPVE ↓
–	0.049	42.73	24.46	20.16	0.016	0.025	8.43	7.88	0.169	8.18	7.63	1.419
Supervised	0.161	64.30	23.41	19.31	0.015	0.024	9.01	9.53	0.152	16.17	9.43	1.470
Distance Prediction	0.049	37.23	22.75	18.26	0.014	0.030	9.31	9.35	0.143	9.85	9.07	1.566
3D InfoGraph	0.047	44.25	24.06	18.54	0.015	0.052	8.81	7.97	0.143	8.68	8.08	1.416
GeoSSL-RR	0.046	41.20	23.93	19.36	0.016	0.025	8.32	8.17	0.174	7.99	8.20	1.438
GeoSSL-InfoNCE	0.045	39.29	23.23	18.40	0.015	0.024	8.34	8.37	**0.127**	7.45	8.34	1.356
GeoSSL-EBM-NCE	0.045	38.87	22.71	17.89	0.014	0.082	8.28	7.35	0.130	7.85	7.68	1.338
3D InfoMax	0.046	36.97	21.31	17.69	0.014	0.024	8.38	7.36	0.135	8.60	7.99	1.453
GraphMVP	0.044	36.03	20.71	17.02	0.014	0.024	8.31	7.36	0.132	7.57	7.34	1.337
GeoSSL-DDM-1L	0.045	36.13	20.59	17.26	0.014	0.024	9.45	8.43	0.128	8.88	8.16	1.380
GeoSSL-DDM	**0.043**	35.55	20.57	**16.95**	0.014	0.024	8.25	7.42	**0.127**	7.36	7.34	1.334
3D-EMGP (Gaussian)	0.277	40.56	21.25	23.99	0.014	0.039	9.16	9.14	0.340	9.31	8.59	1.433
MoleculeSDE (VE)	0.044	**34.67**	**20.14**	17.05	**0.013**	**0.023**	**7.64**	**7.05**	0.139	**6.88**	**6.79**	**1.273**
MoleculeSDE (VP)	**0.042**	**35.09**	**20.14**	**16.78**	**0.013**	**0.023**	**8.17**	**7.01**	0.133	**7.30**	**7.05**	**1.315**

Table 17: Results on eight force prediction tasks from MD17, and the backbone model is PaiNN. We take 1K for training, 1K for validation, and 48K to 991K molecules for the test concerning different tasks. The evaluation is mean absolute error, and the best results are marked in **bold** and **bold**, respectively.

Pretraining	Aspirin ↓	Benzene ↓	Ethanol ↓	Malonaldehyde ↓	Naphthalene ↓	Salicylic ↓	Toluene ↓	Uracil ↓
–	0.572	0.053	0.230	0.338	0.132	0.288	0.141	0.201
Supervised	0.509	0.056	0.181	0.330	–	0.284	0.163	–
Distance Prediction	0.480	0.053	0.200	0.296	0.131	0.265	0.171	0.168
3D InfoGraph	0.554	0.067	0.249	0.353	0.177	0.331	0.179	0.213
GeoSSL-RR	0.559	0.051	0.262	0.368	0.146	0.303	0.154	0.202
GeoSSL-InfoNCE	0.428	0.051	0.197	0.337	0.127	0.247	0.136	0.169
GeoSSL-EBM-NCE	0.435	0.048	0.198	**0.295**	0.143	0.245	0.132	0.172
3D InfoMax	0.479	0.052	0.220	0.344	0.138	0.267	0.155	0.174
GraphMVP	0.465	0.050	0.205	0.316	**0.119**	0.242	0.136	0.168
GeoSSL-DDM-1L	0.436	0.048	0.209	0.320	**0.119**	0.249	0.132	0.177
GeoSSL-DDM	**0.427**	0.047	**0.188**	0.313	0.120	**0.240**	**0.129**	0.167
3D-EMGP (Gaussian)	0.487	0.048	0.217	0.329	0.151	0.299	0.141	0.182
MoleculeSDE (VE)	**0.421**	**0.043**	0.195	**0.284**	**0.105**	**0.236**	**0.123**	**0.158**
MoleculeSDE (VP)	0.443	**0.045**	**0.191**	0.301	0.131	0.261	0.140	**0.159**

J Ablation Studies

We have the following challenges in the literature: (1) Different data preprocessors, including data augmentations and normalization strategies. (2) Different data splits, *i.e.*, with different seeds or different train-valid-test sizes. (3) Different running epochs. (4) Different optimizers (SGD, Adam, or EMA) and learning rate schedulers (cosine annealing or cyclic). These factors can significantly affect performance, and Geom3D is a useful tool for careful scrutinization. In this section, we are mainly focusing on the first point, *i.e.*, the tricks that are mainly related to the specific applications. For the following factors, we adopt a fixed setting, *i.e.*, the same seeds for tasks if using random splits, fixed epochs for most of the geometric modelings, Adam as the optimizer, and cosine annealing learning rate scheduler. We would like to acknowledge that the EMA optimizer and cyclic learning rate scheduler can be beneficial for certain geometric models, yet this is more related to the optimization process and is beyond the scope of this work. We will explore this in future work.

J.1 Ablation Studies on the Effect of Latent Dimension d

Recent works [117, 121] have found that the latent dimensions play an important role in molecule pretraining, and here we list the comparison between latent dimension $d = 128$ and latent dimension $d = 300$.

- The performance comparison for QM9 is in Table 18, and we visually plot the performance gap MAE($d = 128$) - MAE($d = 300$) in Fig. 9. The results with $d = 300$ are reported in Table 1.
- The performance **(w/ normalization)** comparison for MD17 and rMD17 is in Tables 19 to 22. The results with $d = 300$ are reported in Tables 2, 13 and 14 except NequIP and Allegro. Their results in Appendix J.3 **(w/ normalization)** are reported Table 2.
- The performance comparison for COLL is in Table 23, and results with $d = 300$ are reported in Table 3.
- The performance comparison for LBA & LEP is in Tables 24 and 25, and results with $d = 300$ are reported in Table 4.

Table 18: Ablation studies of latent dimension d on QM9. 110K for training, 10K for validation, and 11K for testing. The evaluation metric is the mean absolute error (MAE).

Model	d	$\alpha \downarrow$	$\nabla\mathcal{E} \downarrow$	$\mathcal{E}_{\text{HOMO}} \downarrow$	$\mathcal{E}_{\text{LUMO}} \downarrow$	$\mu \downarrow$	$C_v \downarrow$	$G \downarrow$	$H \downarrow$	$R^2 \downarrow$	$U \downarrow$	$U_0 \downarrow$	ZPVE $\downarrow$
SchNet	128	0.068	49.66	31.91	26.09	0.030	0.032	14.17	14.16	0.126	14.11	14.27	1.684
	300	0.060	44.13	27.64	22.55	0.028	0.031	14.19	14.05	0.133	13.93	13.27	1.749
DimeNet++	128	0.046	37.93	20.99	17.50	0.028	0.022	7.33	6.72	0.299	6.38	7.26	1.260
	300	0.044	36.22	20.01	16.66	0.028	0.022	7.45	6.14	0.323	6.33	7.18	1.118
SE(3)-Trans	128	0.144	55.36	34.59	34.05	0.051	0.064	64.85	76.32	1.763	69.73	68.22	5.448
	300	0.137	56.52	34.65	34.41	0.050	0.063	65.28	70.70	1.747	68.92	68.88	5.428
EGNN	128	0.065	49.07	29.19	25.00	0.028	0.031	11.61	10.52	0.074	10.51	10.61	1.544
	300	0.062	49.56	30.08	24.98	0.029	0.030	10.01	9.14	0.089	9.28	9.08	1.519
PaiNN	128	0.049	44.02	25.92	20.87	0.016	0.025	10.32	7.30	0.126	7.60	7.51	1.295
	300	0.049	42.73	24.46	20.16	0.016	0.025	8.43	7.88	0.169	8.18	7.63	1.419
GemNet-T	128	0.042	34.49	17.82	14.80	0.020	0.021	8.48	7.05	0.246	6.94	6.97	1.201
	300	0.041	35.46	17.85	15.86	0.021	0.023	7.61	7.08	0.271	6.42	5.88	1.232
SphereNet	128	0.050	40.36	22.49	19.29	0.026	0.026	9.06	7.49	0.248	7.53	7.79	1.560
	300	0.047	38.93	21.45	18.25	0.027	0.025	8.16	13.68	0.288	6.77	7.43	1.295
SEGNN	128	0.056	41.40	22.40	20.77	0.024	0.029	13.11	12.99	0.481	13.82	13.71	1.596
	300	0.048	33.61	17.66	17.01	0.021	0.026	11.60	12.45	0.404	11.29	12.20	1.590
Equiformer	128	0.051	33.52	17.58	16.83	0.015	0.023	17.13	13.14	0.408	15.23	13.63	2.182
	300	0.051	33.46	17.93	16.85	0.015	0.023	14.49	14.60	0.433	14.88	13.78	2.342

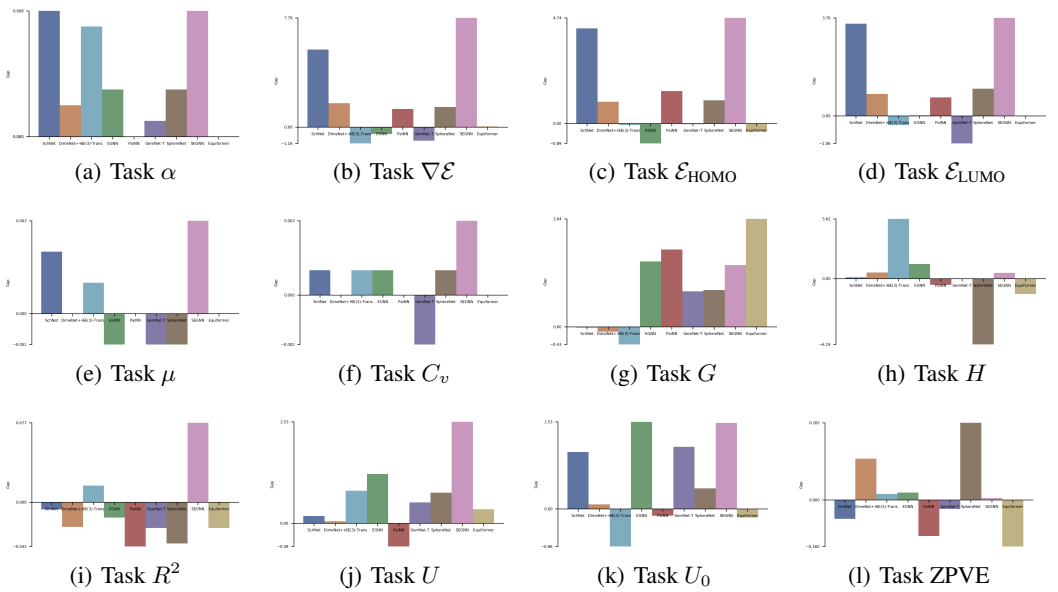

(a) Task α (b) Task $\nabla\mathcal{E}$ (c) Task $\mathcal{E}_{\text{HOMO}}$ (d) Task $\mathcal{E}_{\text{LUMO}}$

(e) Task μ (f) Task C_v (g) Task G (h) Task H

(i) Task R^2 (j) Task U (k) Task U_0 (l) Task ZPVE

Figure 9: Performance gap of MAE($d = 128$) - MAE($d = 300$) in QM9.

Table 19: Ablation studies of latent dimension ($d = 128$) on MD17. The evaluation is the mean absolute error. No data normalization is used.

Model	Energy / Force	Aspirin ↓	Benzene ↓	Ethanol ↓	Malonaldehyde ↓	Naphthalene ↓	Salicylic ↓	Toluene ↓	Uracil ↓
SchNet	Energy	0.695	0.118	0.182	0.338	0.210	0.232	0.157	0.192
	Force	1.500	0.399	0.663	1.157	0.759	0.896	0.594	0.906
DimeNet++	Energy	2.104	1.053	0.971	1.180	1.472	1.901	1.988	1.754
	Force	2.209	0.476	0.636	1.420	1.293	1.071	0.924	1.070
EGNN	Energy	91.490	0.663	1.439	1.385	17.064	31.006	7.190	1.409
	Force	19.211	1.049	1.983	2.380	2.185	3.957	2.453	2.172
PaiNN	Energy	0.209	0.097	0.070	0.093	0.235	0.127	0.133	0.107
	Force	0.549	0.053	0.198	0.328	0.134	0.284	0.146	0.180
GemNet-T	Energy	1.299	0.096	8.418	0.101	0.116	0.141	0.095	11.270
	Force	0.518	0.050	0.226	0.380	0.107	0.259	0.118	542.330
SphereNet	Energy	0.235	0.104	0.327	0.136	0.183	0.771	0.116	0.147
	Force	0.500	0.114	0.199	0.377	0.416	2.033	0.198	0.303
SEGNN	Energy	10.030	0.081	0.088	0.191	0.678	1.699	0.541	0.260
	Force	6.793	0.193	0.456	0.832	0.734	1.828	0.957	0.654
Allegro	Energy	2.380	0.278	0.386	0.583	0.732	1.131	0.615	1.357
	Force	6.537	1.777	1.916	2.572	3.359	5.063	3.022	6.974
Equiformer	Energy	0.708	0.076	0.056	0.102	0.097	0.191	0.094	0.103
	Force	0.282	0.044	0.142	0.229	0.068	0.202	0.080	0.140

Table 20: Ablation studies of latent dimension ($d = 300$) on MD17. The evaluation is the mean absolute error. No data normalization is used.

Model	Energy/Force	Aspirin ↓	Benzene ↓	Ethanol ↓	Malonaldehyde ↓	Naphthalene ↓	Salicylic ↓	Toluene ↓	Uracil ↓
SchNet	Energy	0.475	0.117	0.109	0.300	0.167	0.212	0.149	0.170
	Force	1.203	0.380	0.386	0.794	0.587	0.826	0.568	0.773
DimeNet++	Energy	4.168	0.893	1.238	1.385	1.846	2.445	1.484	1.522
	Force	7.212	0.603	0.753	1.842	8.515	1.752	1.037	1.632
EGNN	Energy	17.892	1.142	0.436	0.896	12.177	6.964	4.051	0.854
	Force	3.042	0.736	0.924	1.566	1.136	1.177	1.202	1.367
PaiNN	Energy	27.626	0.095	0.063	0.102	0.622	0.371	0.165	0.111
	Force	0.572	0.053	0.230	0.338	0.132	0.288	0.141	0.201
GemNet-T	Energy	0.684	0.097	4.598	4.966	0.482	0.128	0.098	1.349
	Force	0.558	0.089	0.219	0.433	0.212	0.326	0.174	486.612
SphereNet	Energy	0.244	0.107	1.603	1.559	0.167	0.188	0.113	7.115
	Force	0.546	0.135	0.168	0.667	0.315	0.479	0.194	0.442
SEGNN	Energy	17.774	0.086	0.151	0.247	0.655	2.173	0.624	0.259
	Force	9.003	0.265	0.893	1.249	0.895	2.220	1.138	0.948
Allegro	Energy	1.577	0.117	0.308	0.481	0.899	1.088	0.406	0.490
	Force	4.328	0.358	1.613	2.185	3.841	4.731	1.866	2.627
Equiformer	Energy	0.308	0.075	0.096	0.183	0.097	0.189	0.209	0.106
	Force	0.286	0.045	0.142	0.230	0.068	0.200	0.080	0.141

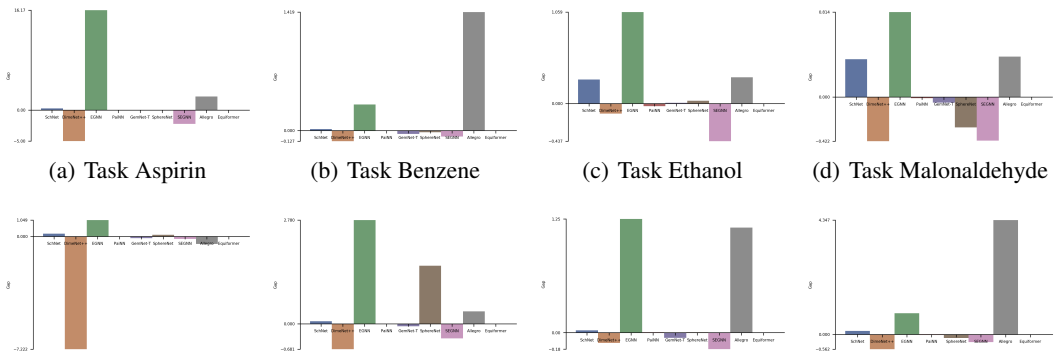

(a) Task Aspirin (b) Task Benzene (c) Task Ethanol (d) Task Malonaldehyde

(e) Task Naphthalene (f) Task Salicylic (g) Task Toluene (h) Task Uracil

Figure 10: Performance gap of MAE($d = 128$) - MAE($d = 300$) in MD17.

Table 21: Ablation studies of latent dimension (dim=128) on rMD17. The evaluation is the mean absolute error. No data normalization is used.

model	Energy / Force	Aspirin ↓	Azobenzene ↓	Benzene ↓	Ethanol ↓	Malonaldehyde ↓	Naphthalene ↓	Paracetamol ↓	Salicylic ↓	Toluene ↓	Uracil ↓
SchNet	Energy	0.764	1.332	0.388	0.226	0.380	0.205	1.298	1.759	0.166	0.173
	Force	1.662	3.071	0.318	0.782	1.109	0.805	2.344	0.950	0.693	0.943
DimeNet++	Energy	1.719	4.806	0.506	10.867	0.845	1.209	10.876	2.020	1.519	4227.668
	Force	1.253	1.033	0.307	20.860	0.632	0.602	1.123	1.022	0.991	33549.676
EGNN	Energy	89.661	51.554	4.893	1.065	9.339	32.901	77.996	27.114	12.766	4.519
	Force	20.531	4.436	0.912	2.305	3.056	2.287	9.484	13.117	2.567	2.482
PaiNN	Energy	1.949	5.733	0.036	0.606	1.626	2.610	0.541	0.831	0.158	0.181
	Force	3.189	0.940	0.143	0.727	1.158	0.851	1.636	1.450	0.682	0.875
GemNet-T	Energy	1.546	0.073	0.006	1.060	6.610	0.025	1.972	14.837	0.023	36.966
	Force	0.555	0.265	0.026	0.211	0.425	0.112	0.368	0.308	0.120	0.233
SphereNet	Energy	21.142	0.542	0.678	1.226	0.423	0.176	0.255	6.218	0.119	0.143
	Force	0.666	0.781	0.102	0.313	0.419	0.500	0.659	2.244	0.334	0.425
SEGNN	Energy	11.828	2.729	0.018	0.081	0.161	1.333	3.982	1.476	1.443	0.221
	Force	7.543	2.014	0.139	0.509	0.934	0.845	3.338	1.934	1.028	0.723
Allegro	Energy	6.142	2.221	0.094	0.465	0.592	1.320	2.196	1.239	0.584	1.739
	Force	4.891	5.727	0.960	2.166	2.630	3.546	4.571	5.949	2.885	6.610
Equiformer	Energy	0.480	0.119	0.031	0.085	0.098	0.065	0.848	0.261	0.082	0.214
	Force	0.303	0.132	0.020	0.163	0.242	0.069	0.260	0.217	0.077	0.150

Table 22: Ablation studies of latent dimension ($d = 300$) on rMD17. The evaluation is the mean absolute error. No data normalization is used.

Model	Energy/Force	Aspirin ↓	Azobenzene ↓	Benzene ↓	Ethanol ↓	Malonaldehyde ↓	Naphthalene ↓	Paracetamol ↓	Salicylic ↓	Toluene ↓	Uracil ↓
SchNet	Energy	0.534	1.818	0.111	1.757	0.260	0.124	8.138	2.618	0.119	7.029
	Force	1.243	3.596	0.233	0.449	0.862	0.587	2.320	0.878	0.574	0.762
DimeNet++	Energy	2.438	3.955	0.741	1.456	2.317	1.648	2.261	1.555	1.210	2.320
	Force	2.009	1.243	0.340	1.213	7.029	0.629	1.047	0.934	0.921	3.181
EGNN	Energy	17.350	21.333	0.315	0.402	0.534	12.164	26.902	7.794	15.021	1.669
	Force	3.825	2.330	0.529	0.989	1.334	1.183	2.313	1.571	1.165	1.323
PaiNN	Energy	30.156	0.107	0.010	1.170	0.070	5.297	0.117	5.219	0.045	2.478
	Force	0.573	0.326	0.032	0.316	0.377	0.161	0.440	0.321	0.231	0.235
GemNet-T	Energy	5.389	7.770	0.007	1.615	9.496	0.031	2.173	21.411	959.745	994.036
	Force	0.555	0.347	0.033	0.233	0.337	0.154	0.388	0.371	0.400	1.165
SphereNet	Energy	0.304	0.257	0.052	0.072	0.138	0.093	0.183	0.771	20.479	12.211
	Force	0.622	0.532	0.076	0.217	0.500	0.279	0.482	2.088	0.254	0.959
SEGNN	Energy	15.721	3.474	0.270	0.130	0.182	1.110	4.197	1.494	0.814	1.115
	Force	8.549	2.579	0.174	0.846	1.185	0.926	3.191	2.056	1.241	0.966
Allegro	Energy	1.339	2.441	0.049	0.339	0.651	3.781	0.978	1.356	0.451	2.497
	Force	3.861	4.609	0.467	1.579	1.816	3.428	3.693	5.086	2.241	5.183
Equiformer	Energy	0.375	0.127	0.027	0.064	0.085	0.069	0.215	0.143	0.104	0.200
	Force	0.305	0.132	0.020	0.162	0.240	0.070	0.258	0.218	0.077	0.149

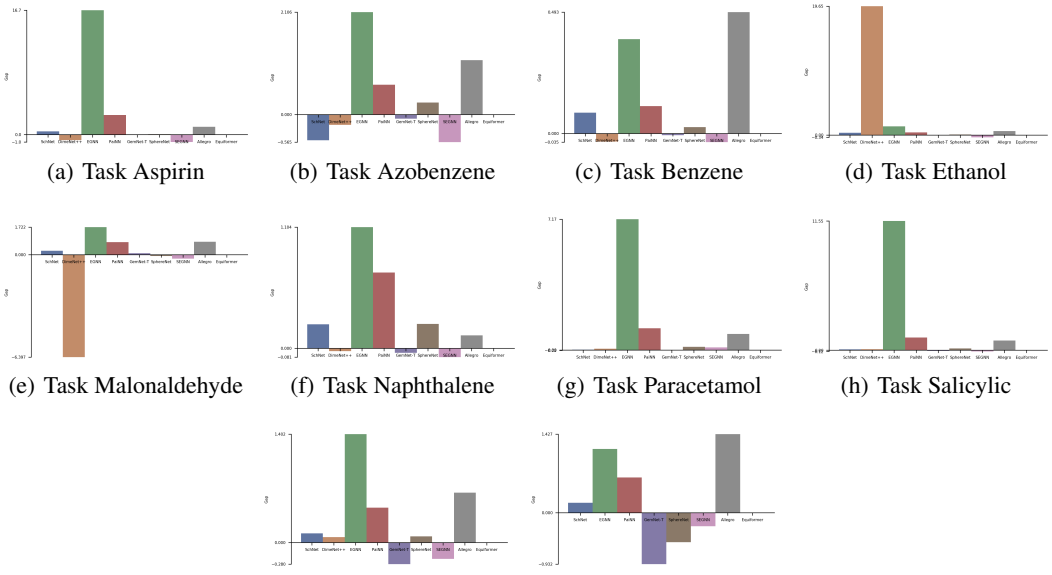

(a) Task Aspirin (b) Task Azobenzene (c) Task Benzene (d) Task Ethanol

(e) Task Malonaldehyde (f) Task Naphthalene (g) Task Paracetamol (h) Task Salicylic

(i) Task Toluene (j) Task Uracil

Figure 11: Performance gap of MAE($d = 128$) - MAE($d = 300$) in rMD17.

Table 23: Ablation studies of latent dimension on COLL. 120k for training, 10k for val, 9.48k for test. The evaluation metric is the mean absolute error (MAE).

Model	d	energy ↓	force ↓
SchNet	128	0.171	0.135
	300	0.178	0.130
DimeNet++	128	0.049	0.058
	300	0.036	0.049
EGNN	128	0.786	0.151
	300	1.808	0.234
PaiNN	128	0.047	0.066
	300	0.030	0.052
GemNet-T	128	0.022	0.035
	300	0.017	0.028
SphereNet	128	0.039	0.049
	300	0.032	0.047
SEGNN	128	7.054	0.511
	300	7.085	0.642
Equiformer	128	0.034	0.030
	300	0.036	0.030

Table 24: Ablation studies of latent dimension ($d = 128$) on 2 binding affinity prediction tasks. We select three evaluation metrics for LBA: the root mean squared error (RMSD), the Pearson correlation (R_p) and the Spearman correlation (R_S). LEP is a binary classification task, and we use the area under the curve for receiver operating characteristics (ROC) and precision-recall (PR) for evaluation. We run cross validation with 5 seeds and report the mean and std.

Model	LBA			LEP	
	RMSD ↓	R_P ↑	R_C ↑	ROC ↑	PR ↑
SchNet	1.509 ± 0.05	0.510 ± 0.02	0.487 ± 0.01	0.444 ± 0.03	0.391 ± 0.02
DimeNet++	1.808 ± 0.46	0.557 ± 0.01	0.566 ± 0.01	0.582 ± 0.06	0.494 ± 0.03
EGNN	1.531 ± 0.02	0.452 ± 0.01	0.419 ± 0.01	0.702 ± 0.05	0.603 ± 0.07
PaiNN	1.460 ± 0.03	0.569 ± 0.01	0.564 ± 0.01	0.627 ± 0.07	0.499 ± 0.09
GemNet	130.621 ± 13.90	-0.114 ± 0.54	-0.116 ± 0.55	0.623 ± 0.05	0.552 ± 0.05
SphereNet	1.605 ± 0.02	0.533 ± 0.00	0.527 ± 0.00	0.556 ± 0.05	0.471 ± 0.05
SEGNN	1.422 ± 0.04	0.560 ± 0.02	0.537 ± 0.03	0.582 ± 0.08	0.517 ± 0.09
Equiformer	1.490 ± 0.03	0.552 ± 0.01	0.543 ± 0.01	0.626 ± 0.08	0.530 ± 0.05

Table 25: Ablation studies of latent dimension ($d = 300$) on 2 binding affinity prediction tasks. We select three evaluation metrics for LBA: the root mean squared error (RMSD), the Pearson correlation (R_p) and the Spearman correlation (R_S). LEP is a binary classification task, and we use the area under the curve for receiver operating characteristics (ROC) and precision-recall (PR) for evaluation. We run cross validation with 5 seeds and report the mean and std.

Model	LBA			LEP	
	RMSD ↓	R_P ↑	R_C ↑	ROC ↑	PR ↑
SchNet	1.521 ± 0.02	0.474 ± 0.01	0.452 ± 0.01	0.450 ± 0.03	0.379 ± 0.03
DimeNet++	1.672 ± 0.09	0.550 ± 0.01	0.556 ± 0.01	0.590 ± 0.06	0.496 ± 0.05
EGNN	1.494 ± 0.04	0.503 ± 0.04	0.483 ± 0.05	0.657 ± 0.05	0.559 ± 0.05
PaiNN	1.434 ± 0.02	0.583 ± 0.02	0.580 ± 0.02	0.585 ± 0.02	0.432 ± 0.03
GemNet	269.427 ± 148.62	0.029 ± 0.50	0.036 ± 0.51	0.674 ± 0.04	0.565 ± 0.05
SphereNet	1.581 ± 0.02	0.538 ± 0.01	0.529 ± 0.01	0.523 ± 0.04	0.432 ± 0.05
SEGNN	1.416 ± 0.03	0.566 ± 0.02	0.550 ± 0.02	0.574 ± 0.03	0.485 ± 0.03
Equiformer	1.392 ± 0.03	0.598 ± 0.02	0.578 ± 0.02	0.618 ± 0.06	0.510 ± 0.05

J.2 Ablation Study on Data Normalization for Molecular Dynamics Prediction

Allegro [95] and NequIP [3] introduce a normalization strategy for molecular dynamics (energy and force) prediction on MD17 and rMD17 datasets:

$$\hat{y}_E = y_E * \text{Force Mean} + \text{Energy Mean} * \text{\# Atom}, \tag{28}$$

where y_E is the original predicted energy, and $\hat{y}_E$ is the normalized prediction. We find this trick important and would like to systematically test it here. Notice that as shown in Appendix J.1, the latent dimension is an important factor, and here we would like to conduct the ablation studies on both factors.

- MD17 w/o normalization and $d = 128$ in Table 19, $d = 300$ in Table 20. rMD17 w/o normalization and $d = 128$ in Table 21, $d = 300$ in Table 22.
- In the following tables, we test: MD17 w/ normalization and $d = 128$ in Table 26, $d = 300$ in Table 27. rMD17 w/ normalization and $d = 128$ in Table 28, $d = 300$ in Table 29.

Table 26: Ablation studies of latent dimension ($d = 128$) on MD17. The evaluation is the mean absolute error. Data normalization is used.

Model	Energy / Force	Aspirin ↓	Benzene ↓	Ethanol ↓	Malonaldehyde ↓	Naphthalene ↓	Salicylic ↓	Toluene ↓	Uracil ↓
SchNet	Energy	0.588	0.099	0.072	0.111	0.125	0.207	0.110	0.118
	Force	1.008	0.200	0.297	0.491	0.299	0.547	0.346	0.383
DimeNet++	Energy	0.370	0.154	28.604	57144.066	0.289	15.497	0.206	0.317
	Force	0.578	0.110	89.512	2119653.000	0.930	90.846	0.540	0.535
EGNN	Energy	0.668	0.144	0.470	0.238	0.481	0.462	0.234	0.429
	Force	1.249	0.461	1.042	0.827	0.913	0.927	0.631	1.227
PaiNN	Energy	0.146	0.095	0.057	0.083	0.113	0.110	0.095	0.104
	Force	0.315	0.034	0.157	0.244	0.074	0.177	0.093	0.120
GemNet-T	Energy	0.175	0.097	0.055	0.080	0.130	0.112	0.093	0.105
	Force	0.284	0.042	0.141	0.191	0.082	0.167	0.080	0.120
SphereNet	Energy	0.168	0.095	0.061	0.110	0.115	0.120	0.095	0.113
	Force	0.305	0.042	0.173	0.280	0.083	0.219	0.088	0.189
SEGNN	Energy	0.337	0.069	0.060	0.092	0.101	0.151	0.092	0.104
	Force	0.879	0.077	0.236	0.365	0.251	0.564	0.307	0.281
Allegro	Energy	0.290	0.096	0.064	0.105	0.143	0.151	0.123	0.112
	Force	0.646	0.073	0.228	0.346	0.285	0.407	0.265	0.245
Equiformer	Energy	0.140	0.072	0.056	0.085	0.090	0.112	0.078	0.101
	Force	0.315	0.057	0.159	0.250	0.069	0.204	0.083	0.156

Table 27: Ablation studies of latent dimension ($d = 300$) on MD17. The evaluation is the mean absolute error. Data normalization is used.

Model	Energy / Force	Aspirin ↓	Benzene ↓	Ethanol ↓	Malonaldehyde ↓	Naphthalene ↓	Salicylic ↓	Toluene ↓	Uracil ↓
SchNet	Energy	0.321	0.099	0.074	0.125	0.129	0.155	0.130	0.171
	Force	1.055	0.191	0.318	0.522	0.328	0.597	0.387	0.401
DimeNet++	Energy	0.628	56451512.000	0.192	0.480	14056.564	0.421	27644.078	7522.200
	Force	2.632	688219840.000	1.029	1.703	173932.344	0.621	972773.375	16002.980
EGNN	Energy	0.393	0.125	0.072	0.112	0.249	0.257	0.158	0.164
	Force	0.695	0.442	0.269	0.415	0.439	0.641	0.447	0.536
PaiNN	Energy	0.149	0.102	0.056	0.083	0.118	0.113	0.093	0.104
	Force	0.331	0.037	0.163	0.252	0.082	0.187	0.097	0.122
GemNet-T	Energy	0.162	0.142	0.068	0.089	0.136	0.115	0.095	0.106
	Force	0.329	0.052	0.206	0.262	0.101	0.234	0.091	0.146
SphereNet	Energy	0.212	0.096	0.081	0.101	0.116	0.145	0.099	0.120
	Force	0.334	0.047	0.177	0.309	0.087	0.238	0.097	0.212
SEGNN	Energy	0.345	0.069	0.072	0.097	0.096	0.354	0.093	0.110
	Force	1.023	0.080	0.331	0.452	0.227	0.803	0.314	0.327
Allegro	Energy	0.256	0.096	0.060	0.088	0.131	0.139	0.114	0.110
	Force	0.579	0.064	0.198	0.292	0.233	0.349	0.233	0.216
Equiformer	Energy	0.143	0.073	0.061	0.085	0.090	0.107	0.077	0.100
	Force	0.315	0.058	0.158	0.251	0.069	0.204	0.083	0.156

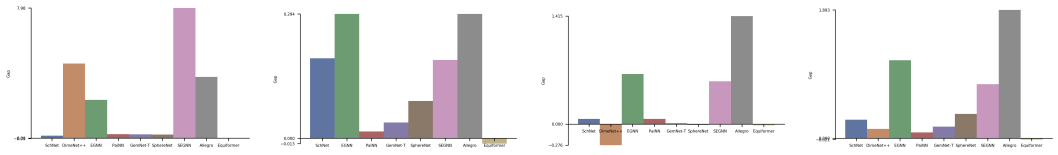

(a) Task Aspirin (b) Task Benzene (c) Task Ethanol (d) Task Malonaldehyde

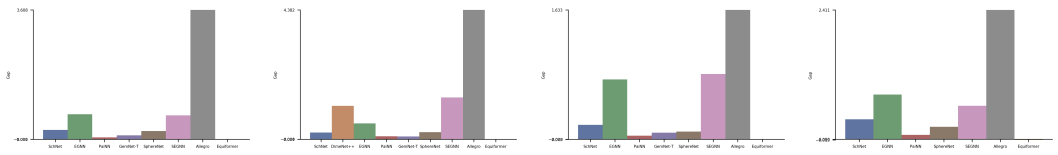

(e) Task Naphthalene (f) Task Salicylic (g) Task Toluene (h) Task Uracil

Figure 12: Performance gap of MAE(force prediction, $d = 300$ and w/o normalization) - MAE(force prediction, $d = 300$ and w/ normalization) in MD17.

Table 28: Ablation studies of latent dimension (dim=128) on rMD17. The evaluation is the mean absolute error. Data normalization is used.

Model	Energy / Force	Aspirin ↓	Azobenzene ↓	Benzene ↓	Ethanol ↓	Malonaldehyde ↓	Naphthalene ↓	Paracetamol ↓	Salicylic ↓	Toluene ↓	Uracil ↓
SchNet	Energy	0.702	0.583	0.013	0.055	0.079	0.058	0.179	0.103	0.064	0.054
	Force	1.028	0.780	0.137	0.311	0.488	0.314	0.757	0.578	0.371	0.373
DimeNet++	Energy	0.321	0.560	0.050	0.093	0.142	0.157	0.299	0.353	0.143	0.318
	Force	0.536	0.424	0.102	0.284	0.420	0.239	0.447	0.639	0.231	0.341
EGNN	Energy	0.653	0.684	0.056	0.275	0.238	0.440	0.476	0.514	0.233	0.395
	Force	1.102	1.003	0.275	0.939	0.955	0.826	0.971	0.911	0.560	1.031
PaiNN	Energy	0.187	0.076	0.006	0.046	0.076	0.048	0.109	0.063	0.033	0.040
	Force	0.551	0.260	0.035	0.282	0.396	0.151	0.407	0.328	0.177	0.238
GemNet-T	Energy	0.116	0.058	0.002	0.038	0.078	0.018	0.082	0.047	0.017	0.023
	Force	0.329	0.198	0.020	0.179	0.328	0.094	0.267	0.226	0.090	0.155
SphereNet	Energy	0.124	0.069	0.019	0.039	0.074	0.040	0.096	0.063	0.042	0.061
	Force	0.325	0.189	0.028	0.174	0.282	0.091	0.265	0.226	0.095	0.191
SEGNN	Energy	0.509	0.171	0.005	0.039	0.056	0.052	0.194	0.150	0.080	0.045
	Force	1.129	0.603	0.054	0.279	0.394	0.254	0.792	0.682	0.365	0.327
Allegro	Energy	0.348	0.183	0.005	0.046	0.081	0.094	0.190	0.131	0.080	0.046
	Force	0.673	0.385	0.039	0.249	0.371	0.289	0.476	0.430	0.270	0.254
Equiformer	Energy	0.106	0.044	0.002	0.030	0.038	0.016	0.112	0.050	0.021	0.025
	Force	0.321	0.134	0.026	0.183	0.264	0.070	0.284	0.222	0.079	0.164

Table 29: Ablation studies of latent dimension (dim=300) on rMD17. The evaluation is the mean absolute error. Data normalization is used.

Model	Energy / Force	Aspirin ↓	Azobenzene ↓	Benzene ↓	Ethanol ↓	Malonaldehyde ↓	Naphthalene ↓	Paracetamol ↓	Salicylic ↓	Toluene ↓	Uracil ↓
SchNet	Energy	0.556	0.482	0.013	0.059	0.107	0.067	0.218	0.122	0.119	0.064
	Force	1.115	0.824	0.094	0.338	0.536	0.349	0.783	0.636	0.397	0.391
DimeNet++	Energy	0.339	0.257	10.026	0.118	0.201	0.135	0.550	0.213	0.156	1.382
	Force	0.588	0.456	378.561	0.313	0.453	0.263	0.493	0.601	0.262	4.510
EGNN	Energy	0.455	0.522	0.048	0.070	0.068	0.212	0.313	0.233	0.359	0.150
	Force	0.738	0.720	0.234	0.314	0.391	0.515	0.684	0.618	0.682	0.603
PaiNN	Energy	0.127	0.056	0.002	0.037	0.056	0.017	0.078	0.044	0.022	0.024
	Force	0.443	0.183	0.019	0.237	0.331	0.095	0.331	0.248	0.126	0.171
GemNet-T	Energy	0.116	0.058	0.002	0.038	0.078	0.018	0.082	0.047	0.017	0.023
	Force	0.329	0.198	0.020	0.179	0.328	0.094	0.267	0.226	0.090	0.155
SphereNet	Energy	0.132	0.087	0.010	0.048	0.123	0.027	0.101	0.079	0.027	0.066
	Force	0.348	0.203	0.023	0.194	0.315	0.090	0.283	0.248	0.094	0.206
SEGNN	Energy	0.570	0.300	0.005	0.037	0.064	0.061	0.283	0.210	0.096	0.062
	Force	1.313	0.732	0.055	0.264	0.499	0.285	1.003	0.782	0.346	0.410
Allegro	Energy	0.294	0.167	0.004	0.043	0.056	0.070	0.170	0.093	0.063	0.037
	Force	0.597	0.347	0.034	0.212	0.312	0.237	0.435	0.367	0.233	0.217
Equiformer	Energy	0.101	0.044	0.002	0.030	0.041	0.016	0.090	0.045	0.020	0.024
	Force	0.321	0.134	0.026	0.180	0.265	0.070	0.284	0.223	0.079	0.164

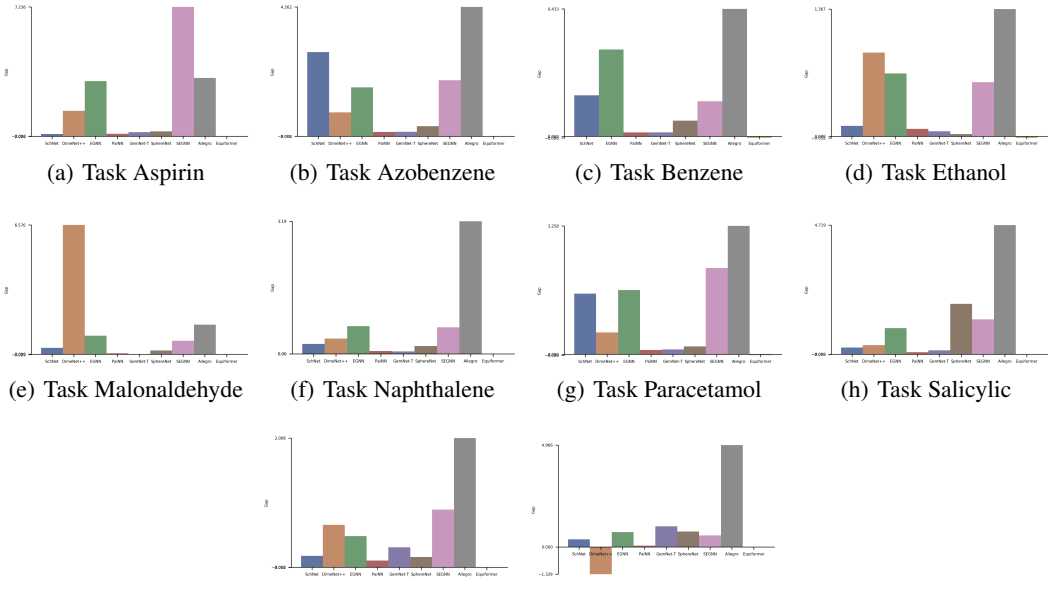

(a) Task Aspirin (b) Task Azobenzene (c) Task Benzene (d) Task Ethanol

(e) Task Malonaldehyde (f) Task Naphthalene (g) Task Paracetamol (h) Task Salicylic

(i) Task Toluene (j) Task Uracil

Figure 13: Performance gap of MAE(force prediction, $d = 300$ and w/o normalization) - MAE(force prediction, $d = 300$ and w/ normalization) in rMD17.

J.3 Ablation Studies on Reproduced Results of NequIP and Allegro

Here we would like to further discuss NequIP and Allegro.

- NequIP has no explicit molecule-level representation, and we directly put its results below.
- Allegro adopts $d = 512$ by default (by far we are mainly checking $d = 128$ and $d = 300$).
- We can reproduce NequIP and Allegro results w/ data normalization, as shown below.

Table 30: Ablation study of data normalization on NequIP and Allegro on MD17. The evaluation is the mean absolute error. Here Allegro uses $d = 512$, and both NequIP and Allegro can match the reported results [3, 95] w/ normalization.

Model	Normalization	Energy / Force	Aspirin ↓	Benzene ↓	Ethanol ↓	Malonaldehyde ↓	Naphthalene ↓	Salicylic ↓	Toluene ↓	Uracil ↓
NequIP	w/o Normalization	Energy	8.333	0.355	0.971	2.293	1.032	2.952	1.303	1.266
		Force	23.769	2.383	5.832	12.099	5.247	14.048	6.800	8.060
	w/ Normalization	Energy	0.175	0.095	0.058	0.089	0.114	0.114	0.094	0.105
		Force	0.383	0.039	0.195	0.294	0.091	0.212	0.106	0.136
Allegro	w/o Normalization	Energy	1.138	0.154	0.258	1.330	0.824	1.114	0.441	0.613
		Force	3.405	0.823	1.412	4.191	3.743	4.934	1.968	3.544
	w/ Normalization	Energy	0.240	0.096	0.058	0.085	0.128	0.130	0.107	0.107
		Force	0.553	0.058	0.179	0.259	0.207	0.311	0.203	0.184

Table 31: Ablation study of data normalization on NequIP and Allegro on rMD17. The evaluation is the mean absolute error. Here Allegro uses $d = 512$.

Model	Normalization	Energy / Force	Aspirin ↓	Azobenzene ↓	Benzene ↓	Ethanol ↓	Malonaldehyde ↓	Naphthalene ↓	Paracetamol ↓	Salicylic ↓	Toluene ↓	Uracil ↓
NequIP	w/o Normalization	Energy	9.618	1.993	3.048	0.936	2.313	2.089	5.136	3.302	1.306	1.738
		Force	22.904	6.406	1.523	6.027	12.372	5.529	17.574	15.693	7.094	10.220
	w/ Normalization	Energy	0.147	0.049	0.003	0.034	0.061	0.018	0.078	0.047	0.020	0.021
		Force	0.407	0.176	0.019	0.218	0.310	0.092	0.308	0.230	0.113	0.142
Allegro	w/o Normalization	Energy	1.366	0.872	0.029	1.002	0.417	1.756	0.944	1.035	0.437	0.387
		Force	3.186	2.763	0.237	2.799	2.125	3.815	3.081	4.781	2.048	1.939
	w/ Normalization	Energy	0.223	0.146	0.003	0.033	0.053	0.060	0.156	0.079	0.054	0.031
		Force	0.558	0.308	0.029	0.198	0.264	0.207	0.409	0.331	0.210	0.187

J.4 Ablation Study on the Data Split of Crystalline Material

In the main paper, we report the results on MatBench with 60%-20%-20% for train-valid-test split. To verify the reproducibility correctness of Geom3D, we carry on an ablation study with the same setting as MatBench [22]. Notice that MatBench adopts the setting in KGCNN [105]: with seed 18012019 and 80% for training and 20% for the test. The reproduced results are in Table 32.

The mean evaluation metrics of SchNet and DimeNet++ with cross-validation are reported in MatBench leaderboard and KGCNN leaderboard, and evaluation metrics of the PaiNN are reported in KGCNN leaderboard.

Table 32: Reproduced results on 8 MatBench tasks.

Model	Per. E_{form} ↓ 18,928	Dielectric ↓ 4,764	$log_{10}G$ ↓ 10,987	$log_{10}K$ ↓ 10,987	E_{exfo} ↓ 636	Phonons ↓ 1,265	Band Gap ↓ 106,113	E_{form} ↓ 132,752
SchNet (MatBench)	0.0342	0.3277	0.0796	0.0590	42.6637	38.9636	0.2352	0.0218
SchNet (KGCNN)	0.0347	0.3241	0.0798	0.0584	48.0629	40.2982	0.9351	0.0215
SchNet (Geom3D, ours)	0.035	0.334	0.080	0.060	49.363	35.172	0.226	0.023
DimeNet++ (MatBench)	0.0376	0.3400	0.0792	0.0572	49.0243	37.4619	0.1993	0.0235
DimeNet++ (KGCNN)	0.0373	0.3337	0.0805	0.0579	49.2113	36.7288	0.2089	0.0233
DimeNet++ (Geom3D, ours)	0.033	0.340	0.080	0.060	47.700	33.564	0.207	0.022
PaiNN (KGCNN)	0.0456	0.3587	0.0851	0.0646	50.5886	47.2212	0.2220	0.0244
PaiNN (Geom3D, ours)	0.033	0.323	0.081	0.053	42.325	38.859	0.192	0.022

J.5 Ablation Study on the Data Augmentation of Crystalline Material

The default latent dimension $d = 300$ for most of the models, except for EGNN and SEGNN, which lead to the out-of-memory exception.

Table 33: Ablation study on data augmentation (DA) on MatBench and QMOF.

Model	DA	MatBench								QMOF
		Per. $E_{\text{form}}\downarrow$ 18,928	Dielectric $\downarrow$ 4,764	$log_{10}G\downarrow$ 10,987	$log_{10}K\downarrow$ 10,987	$E_{\text{exfo}}\downarrow$ 636	Phonons $\downarrow$ 1,265	Band Gap $\downarrow$ 106,113	$E_{\text{form}}\downarrow$ 132,752	Band Gap $\downarrow$ 20,425
SchNet	gathered	0.040	0.334	0.081	0.060	65.201	42.586	0.327	0.026	0.236
	expanded	0.048	0.338	0.086	0.066	62.991	46.301	0.253	0.042	0.278
DimeNet++	gathered	0.037	0.357	0.081	0.058	68.685	38.339	0.208	0.025	0.234
	expanded	0.042	0.334	0.088	0.064	69.579	45.223	0.235	0.041	0.243
EGNN	gathered	0.407	0.329	0.128	0.088	76.247	87.201	0.304	0.097	0.483
	expanded	0.038	0.331	0.087	0.064	78.015	74.846	0.211	0.026	0.256
PaiNN	gathered	0.038	0.317	0.080	0.053	67.752	44.602	0.190	0.022	0.207
	expanded	0.038	0.327	0.083	0.056	73.224	59.930	0.203	0.029	0.229
GemNet-T	gathered	0.042	0.325	0.088	0.061	68.425	48.986	0.186	0.026	0.207
	expanded	0.042	0.364	0.090	0.063	68.376	57.316	0.195	0.036	0.230
SphereNet	gathered	0.043	0.388	0.087	0.061	72.987	36.300	0.217	0.029	0.251
	expanded	0.047	0.359	0.090	0.062	69.267	49.401	0.233	0.039	0.268
SEGNN	gathered	0.073	0.334	0.126	0.089	69.534	95.438	0.508	0.127	0.492
	expanded	0.046	0.360	0.087	0.059	65.052	43.638	0.330	0.047	0.330
Equiformer	gathered	0.046	0.280	0.087	0.057	62.977	37.381	0.202	0.027	0.234
	expanded	0.047	0.314	0.086	0.061	69.845	54.087	0.226	0.036	0.258

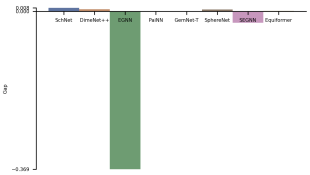

(a) MatBench Task Per. E_{form}

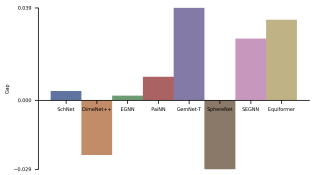

(b) MatBench Task Dielectric

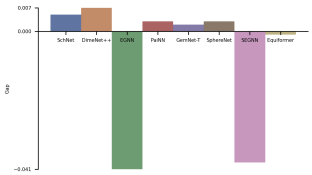

(c) MatBench Task $log_{10}G$

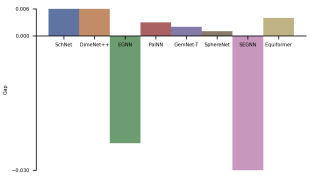

(d) MatBench Task $log_{10}K$

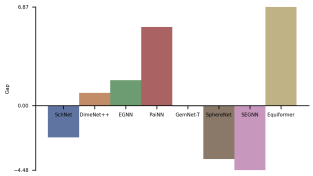

(e) MatBench Task E_{exfo}

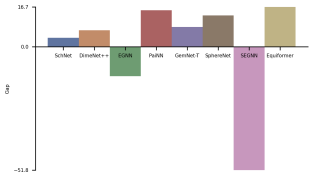

(f) MatBench Task Phonons

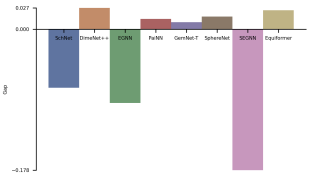

(g) MatBench Task Band Gap

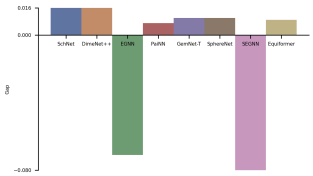

(h) MatBench Task E_{form}

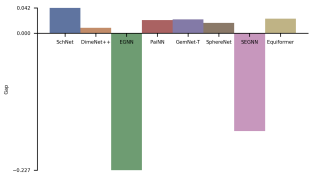

(i) QMOF Task Band Gap

Figure 14: Performance gap of DA: MAE(expanded DA) - MAE(gathered DA), in MatBench and QMOF.

J.6 An Evidence Example On The Importance of Atom Types and Atom Coordinates

First, it has been widely acknowledged [28] that the atom positions or molecule shapes are important factors to the quantum properties. Here we carry out an evidence example to empirically verify this. The goal here is to make predictions on 12 quantum properties in QM9.

The molecule geometric data includes two main components as input features: the atom types and atom coordinates. Other key information can be inferred accordingly, including the pairwise distances and torsion angles. We consider corruption on each of the component to empirically test their importance accordingly.

- Atom type corruption. There are in total 118 types of atom types, and the standard embedding option is to apply the one-hot encoding. In the corruption case, we replace all the atom types with a hold-out index, *i.e.*, index 119.
- Atom coordinate corruption. Originally QM9 includes atom coordinates that are in the stable state, and now we replace them with the coordinates generated with MMFF [42] from RDKit [72].

Table 34: An evidence example of molecular data. The goal is to predict 12 quantum properties (regression tasks) of 3D molecules (with 3D coordinates on each atom). The evaluation metric is MAE.

Model	Mode	$\alpha \downarrow$	$\nabla\mathcal{E} \downarrow$	$\mathcal{E}_{\text{HOMO}} \downarrow$	$\mathcal{E}_{\text{LUMO}} \downarrow$	$\mu \downarrow$	$C_v \downarrow$	$G \downarrow$	$H \downarrow$	$R^2 \downarrow$	$U \downarrow$	$U_0 \downarrow$	ZPVE $\downarrow$
SchNet	Stable Geometry	0.070	50.59	32.53	26.33	0.029	0.032	14.68	14.85	0.122	14.70	14.44	1.698
	Type Corruption	0.074	52.07	33.64	26.75	0.032	0.032	21.68	22.93	0.231	23.01	22.99	1.677
	Coordinate Corruption	0.265	110.59	79.92	78.59	0.422	0.113	57.07	58.92	18.649	60.71	59.32	5.151
DimeNet++	Stable Geometry	0.046	37.41	20.89	17.54	0.030	0.023	7.89	6.71	0.310	6.74	6.94	1.193
	Type Corruption	0.052	40.05	24.42	19.33	0.031	0.024	9.57	8.53	0.322	8.84	8.34	1.299
	Coordinate Corruption	0.257	202.34	88.33	167.63	0.514	0.115	77.95	628.73	19.923	72.92	804.56	5.950
SphereNet	Stable Geometry	0.048	39.98	22.69	18.98	0.026	0.027	8.94	6.95	0.234	7.33	7.34	1.620
	Type Corruption	0.049	41.09	23.56	20.08	0.028	0.028	13.21	14.63	0.287	16.35	13.74	2.063
	Coordinate Corruption	0.228	100.25	69.89	70.12	0.379	0.094	52.04	56.86	17.539	55.61	55.12	4.684
PaiNN	Stable Geometry	0.048	44.50	26.00	21.11	0.016	0.025	8.31	7.67	0.132	7.77	7.89	1.322
	Type Corruption	0.057	45.61	27.22	22.16	0.016	0.025	11.48	11.60	0.181	11.15	10.89	1.339
	Coordinate Corruption	0.223	108.31	73.43	72.35	0.391	0.095	48.40	51.82	16.828	51.43	48.95	4.395

We take SchNet and PaiNN as the backbone 3D GNN models, and the results are in Table 34. We can observe that (1) Both corruption examples lead to performance decrease. (2) The atom coordinate corruption may lead to more severe performance decrease than the atom type corruption. To put this into another way is that, when we corrupt the atom types with the same hold-out type, it is equivalently to removing the atom type information. Thus, this can be viewed as using the equilibrium atom coordinates alone, and the property prediction is comparatively robust. This observation can also be supported from the domain perspective. According to the valence bond theory, the atom type information can be implicitly and roughly inferred from the atom coordinates.

Therefore, by combining all the above observations and analysis, one can draw the conclusion that, *for molecule geometry data, the atom coordinates reveal more fundamental information for representation learning*.

J.7 Ablation on the Effect of Residue Type

As discussed in Sec. 2 and appendix A, proteins have four levels of backbone structures. In Appendix J.6, we carefully check the effect of atom types and atom coordinates in small molecules, and here we would like to check the effect of side residue type in protein geometry-related tasks.

For experiments, we take one of the most recent works, CDConv [29], as the backbone geometric model. The ablation study results are as in Table 35. We observe that the performance drops on all the tasks, and the performance drops on Sup and Fam are much more significant. This reveals that the effect of residue type may differ for different tasks, yet it is preferred to have them encoded for geometric modeling.

Table 35: The effect of residue type on the performance of CDConv.

Model	Residue Type	EC	Fold			
			Fold	Sup	Fam	Avg
CDConv	w/ residue type	86.887	60.028	79.904	99.528	79.820
CDConv	w/o residue type	86.144	41.783	61.164	95.598	66.182

K Resources

We use a single GPU (V100 or A100) for each task. Note that we try to run all the models with the same epoch numbers, yet some models are too large in terms of computational memory and time, so we have to reduce the computational time. Thus, we list the running time for the main tasks below for readers to check.

As shown in Tables 36 to 38, in total, it takes over 652 GPU days (without any hyperparameter tuning, random seeds, or ablation studies). It takes at least 1,384 GPU days if we include ablation studies discussed in Appendix J.

We would also like to acknowledge the following nice implementations and tutorials of geometric models:

- e3nn: Euclidean Neural Networks, by Tess [37]
- TFN [112]
- MaterialProject [55] and MatBench [21]
- Keras Graph Convolution Neural Networks (KGCNN) [105]
- DIG [105]
- TorchDrug [145]

Table 36: Running time for each (model, task, epoch) per epoch on small molecules and crystal materials. There are eight tasks in MatBench with various dataset sizes, and we take 2 times E_{form} for illustration here. For NequIP and Allegro, as you can find in the GitHub repository, we do tune their hyperparameters on QM9, yet not being able to reproduce the results. So we may as well report their numbers here.

Model		QM9	MD17	rMD17	COLL	LBA	LEP	MatBench	QMOF	Total
SchNet [109]	epochs	1,000	1,000	1,000	1000	300	300	1000	300	9.3 days
	time	36s	9s	8s	46s	7s	5s	77s	53s	
DimeNet++ [68]	epochs	500	800	800	1000	300	300	300	300	53.3 days
	time	185s	200s	200s	288s	58s	52s	470s	45s	
SE(3)-Trans [35]	epochs	100	–	–	–	–	–	–	–	24.2 days
	time	1740s	–	–	–	–	–	–	–	
EGNN [108]	epochs	1000	1000	1000	1000	300	300	800	300	22.5 days
	time	85s	12s	12s	100s	18s	14s	319s	300s	
PaiNN [110]	epochs	1000	1000	1000	1000	300	300	1000	300	13.3 days
	time	46s	8s	7s	61s	12s	8s	176s	150s	
GemNet-T [67]	epochs	1000	1000	1000	1000s	300	300	150	200	56.8 days
	time	273s	52s	48s	412s	75s	82s	600s	480s	
SphereNet [89]	epochs	1000	1000	1000	300	300	300	300	300	78.7 days
	time	250s	185s	180s	418s	14s	14s	480s	340s	
SEGNN [4]	epochs	500	800	800	100	300	300	40	60	81.7 days
	time	470s	245s	234s	1450s	370s	324s	3500s	2750s	
NequIP [3]	epochs	1000	1000	1000	300	300	300	–	–	21.2 days
	time	106s	29s	27s	147s	25s	15s	–	–	
Allegro [95]	epochs	1000	1000	1000	300	300	300	–	–	22.6 days
	time	133s	17s	17s	131s	25s	22s	–	–	
Equiformer [73]	epochs	300	1000	1000	100	300	300	100	150	58.6 days
	time	739s	87s	126s	660s	193s	109s	1130s	936s	

Table 37: Running time for each (model, task, epoch) per epoch on proteins.

Model		ECSingle	ECMultiple	Fold	GO-MF	GO-BP	GO-CC	MSP	PSR	Total
IEConv [45]	epochs	–	–	200	–	–	–	–	–	0.85 days
	time	–	–	368s	–	–	–	–	–	
GVP-GNN [62]	epochs	300	200	400	200	200	200	300	300	3.38 days
	time	150s	86s	21s	160s	133s	116s	241s	224s	
GearNet [142]	epochs	300	200	400	200	200	200	–	–	2.12 days
	time	61s	62s	21s	88s	239s	217s	–	–	
ProNet [122]	epochs	400	300	1000	300	300	300	300	300	2.85 days
	time	60s	33s	19s	57s	62s	57s	217s	256s	
CDConv [29]	epochs	150	200	400	200	200	200	300	300	4.86 days
	time	175s	138s	104s	249s	253s	251s	259s	325s	

Table 38: Running time for each (pretraining algorithm, dataset, backbone model) per epoch.

Dataset		PCQM4Mv2 (w/ SchNet)	PCQM4Mv2 (w/ PaiNN)	Total
Supervised	epochs time	100 426s	100 560s	13.4 days
Type Prediction	epochs time	100 433s	100 572s	13.5 days
Distance Prediction	epochs time	100 403s	100 530s	13.4 days
Angle Prediction	epochs time	100 479s	– –	6.4 days
3D InfoGraph [81]	epochs time	100 448s	100 592s	13.5 days
GraphMVP [86]	epochs time	100 701s	100 754s	14.0 days
3D InfoMax [86, 114]	epochs time	100 493s	100 584s	13.5 days
GeoSSL-RR [81]	epochs time	100 680s	100 924s	14.2 days
GeoSSL-EBM-NCE [81]	epochs time	100 630s	100 980s	14.2 days
GeoSSL-InfoNCE [81]	epochs time	100 598s	100 952s	14.1 days
GeoSSL-DDM [81]	epochs time	100 1100s	100 1200s	15.0 days
GeoSSL-DDM-1L [136]	epochs time	100 780s	100 1010s	14.4 days
3D-EMGP [59]	epochs time	– –	100 980s	7.6 days
MoleculeSDE-VE [79]	epochs time	50 1906s	50 1933s	14.5 days
MoleculeSDE-VP [79]	epochs time	50 1906s	50 1933s	14.5 days